Natural product discovery through heterologous expression in *Streptomyces*

Dissertation zur Erlangung des Grades
des Doktors der Naturwissenschaft
der Naturwissenschaftlich-technischen Fakultät
der Universität des Saarlandes

Von Sebastian Greif

Saarbrücken

2025

Tag des Kolloquiums:	12. Dezember 2025
Dekan:	Prof. Dr.-Ing. Dirk Bähre
Berichterstatter:	Prof. Dr. Andriy Luzhetskyy
	Prof. Dr. Christoph Wittmann
Vorsitz:	Prof. Dr. Marc Schneider
Akademisches Mitglied:	Dr. Daniel Krug

Diese Arbeit entstand unter der Anleitung von Prof. Dr. Andriy Luzhetskyy in der Fachrichtung 8.2, Pharmazeutische Biotechnologie der Naturwissenschaftlich-Technischen Fakultät der Universität des Saarlandes von Januar 2020 bis Juli 2025.

Acknowledgements

First of all, I want to thank Prof. Dr. Andriy Luzhetskyy for giving me the opportunity to do my PhD in his working group pharmaceutical biotechnology/Actinobacteria Metabolic Engineering Group (AMEG) at the Saarland University. I am thankful for the interesting projects I got to work on as well as for the support and great insights into the matter. I also thank him for his emotional support, kindness and for allowing me the freedom to finalize this work in Rostock.

I want to thank Prof. Dr. Christoph Wittmann for agreeing to be my second supervisor.

I am also grateful for my mentor Dr. Maksym Myronovskyi, who oversaw my experiments and taught me the things I was not familiar with. With his vast knowledge in biotechnology and microbiology he helped me navigate my way through my PhD years. A big thank you goes to Birgit Rosenkränzer and Anja Palusczak had an important influence on my work. Birgit provided most of the biological protocols and plasmids I work with. Anja introduced me to and took care of the analytical devices like HPLCs and mass spectrometers.

Thanks also go to Dr. Nikolas Eckert, Dr. Marta Rodríguez Estévez, Dr. Constanze Lasch, Dr. Mariia Lopatniuk, Patrick Oberhäuser, Dr. Constanze Paulus, Christopher Ruf, Dr. Hui Shuai and Dr. Marc Stierhof-Wißgott for showing me how to handle and solve different problems that occurred. I thank them and all the other members of AMEG for the enjoyable time in the lab and the office. I also thank Marta, Patrick, Constanze P. and Dmytro Bratiichuk for the wonderful time teaching/supervising the practical course 'Morphologie und Anatomie der Pflanzen'. Special thanks go to Constanze P. and Marc who solved the structures of my compounds via NMR. Thank you to Alexandra Amann from the HIPS who performed the biological assays, as well as thanks to Stephan Tistechok for forwarding them.

Besides that I will thank Dr. Pedro Dinis. He gave me insights into methyltransferases and also tried to crystalize OxaC for a better understanding of its function.

Last but not least I will thank my loving wife Dr. Amanda Wiesenthal for always supporting me and encouraging me especially during the writing process and making my life better and easier. Furthermore I want to thank my parents and my family, friends and all other supporters during my PhD years.

Zusammenfassung

In dieser Arbeit wurde die heterologe Expression als Teil der weiteren Analytik von Cyclohuinilsopeptin A, einem zyklischen Peptid, welches von Dr. Hui Shuai, entdeckt wurde, genutzt. Der Cyclohuinilsopeptin A Gencluster wurde in zehn heterologe Wirtsstämme konjugiert. Dadurch konnte ein zweiter Stamm, der Cyclohuinilsopeptin A produziert, hergestellt werden.

Weiterhin wurde die heterologe Expression zur Identifizierung des Oxanthromicin Genclusters aus *Streptomyces acidiscabies* LU19992 verwendet. Während dieser Experimente wurde der Gencluster Desmethylmensacarcin B entdeckt. Der Biosyntheseweg von Desmethylmensacarcin wurde mit Hilfe von Sequenzanalysen und dem Vergleich mit der Mensacarcin Biosynthese analysiert.

Der Oxanthromicin Biosyntheseweg wurde durch Oxanthromicin Derivate aus Knockout Experimenten, Sequenzanalyse von Gene und Vergleich von Enzymen mit denen in der Actinorhodin Biosynthese aufgeklärt. Ein stärkerer Fokus lag hierbei auf den drei Enzymen , die als SAM-abhängige Methyltransferasen annotiert waren, da von den drei Methylgruppen in der Oxanthromicin Monomerstruktur vorhandenen Methylgruppen nur zwei durch einen Methylgruppentransfer entstehen. Das dritte der SAM-abhängigen Enzyme OxaC scheint an der Dimerisierungsreaktion der Oxanthromicin Biosynthese beteiligt zu sein.

Abstract

In this work heterologous expression was used for further analysis of cyclohuinilsopeptin A, a cyclopeptide discovered by Dr. Hui Shuai. The cyclohuinilsopeptin A biosynthetic gene cluster was transferred to ten different heterologous host strains, leading to a second host strain that produced cyclohuinilsopeptin A.

Furthermore, heterologous expression was used for the discovery of the oxanthromicin biosynthetic gene cluster from *Streptomyces acidiscabies* LU19992. During these expression experiments the biosynthetic gene cluster of desmethylmensacarcin B was also detected. The biosynthetic pathway of desmethylmensacarcin B was analyzed through sequence analysis and comparison with mensacarcin biosynthesis.

The oxanthromicin biosynthetic pathway was analyzed through sequence analysis and gene deletion experiments. The biosynthesis was solved via oxanthromicin derivatives that were produced during knockout experiments and via the comparison with actinorhodin biosynthesis. The focus was on the three putative SAM-dependent methyltransferases encoded in the biosynthetic gene cluster. These were interesting because only two of the methyl groups in oxanthromicin monomeric structure originate from methyl group transfer. The third putative SAM-dependent methyltransferase instead seemed to be part of the dimerization reaction during oxanthromicin biosynthesis.

Publications

Greif, S.; Myronovskyi, M.; Paulus, C.; Luzhetskyy, A.; Biosynthesis of oxanthromicin in *Streptomyces acidiscabies*, (in preparation)

Conference contributions

Greif, S.; Myronovskyi, M; Paulus, C.; Luzhetskyy, A.; Insights on the biosynthetic pathway of Oxanthromicin, **PhD students` day 2023, Saarbrücken, Germany, 2023** (poster presentation)

Greif, S.; Myronovskyi, M.; Luzhetskyy, A.; Insights on the biosynthetic pathway of Oxanthromicin, **VAAM Section Meeting "Biology of Bacterial Natural Product Producers", Saarbrücken, Germany, 2023** (oral presentation)

Table of contents

List of figures

List of tables

List of abbreviations

ACP	acyl carrier protein
ADP	adenosine diphosphate
ARO	Aromatase
AT	acyl transferase
ATP	adenosine triphosphate
BAC	bacterial artificial chromosome
B.C.	Before Christ
BGC	biosynthetic gene cluster
BVMO	Bayer-Villiger Monooxygenase
CoA	coenzyme A
CYC	Cyclase
DH	Dehydratase
DNA	deoxyribonucleic acid
DO	Dioxygenase
e.g.	*exempli gratia*
E. coli	*Escherichia coli*
et al.	*et alii*
ER	enoyl reductase
FAS	fatty acid synthase
FAD(H_2)	flavin adenine dinucleotide (reduced)
FAD-OOH	C4a-hydroperoxy flavin
FDH	flavin dependent halogenase
GT	glycosyl transferase
HPLC	high performance liquid chromatography
Hyg	Hygromycin
K. albida	*Kutzneria albida*
KR	keto reductase
KSα/KS	Ketosynthase
KSβ/CLF	chain length factor
LC	liquid chromatography
MCAT	malonyl coenzyme A:acyl carrier protein transacylase
MCCAP	Microbial Culture Collection of Antibiotic Producers
MO	Monooxygenase
MS	mass spectrometer
MT	methyl transferase
NAD(P)H	nicotineamide dinucleotide (phosphate)
NDP	nucleotide diphosphate
NMP	nucleotide monophosphate
NMR	nucleare magnetic resonance
NRPs	nonribosomal peptides
NRPS	NRP synthase
NTF2	nuclear transport factor 2
ORF	open reading frame
OSMAC	one strain many compounds
P. luminescens	*Photorhabdus luminescens*
P450	cytochrome P450
PCP	peptide carrier protein
PCR	polymerase chain reaction
PKS	polyketide synthase
Ppant	4′-phosphopantetheine
RiPPs	ribosomal natural products

S. acidiscabies	*Streptomyces acidiscabies*
S. albus	*Streptomyces albus*
S. coelicolor	*Streptomyces coelicolor*
S. erythraea	*Saccharopolyspora erythraea*
S. lividans	*Streptomyces lividans*
SAH	*S*-adenosyl-L-homocysteine
SAM	*S*-adenosyl-L-methionin
SDR family	short chain dehydrogenasese/reductases family
SI	Supplementary Information
T1PKS	Type I polyketide synthase
T2PKS	Type II polyketide synthase
T3PKS	Type III polyketide synthase
TE	thioesterase
UV	Ultra violette

1 Introduction

1.1 Using heterologous expression of biosynthetic gene clusters for natural product discovery and development

Based on the remarkable diversity of bioactive properties, natural products have played a pivotal role in shaping healthcare management in recent years. One of the earliest historical records on the use of plant-based natural products is the Egyptian Ebers Papyrus that is dated to 2900 B.C.. Itdocuments the use of over 700 medicinal substances [1, 2]. Similarly, in ancient Mesopotamia, China, Greece, and Arabia, medicinal herbs were extensively studied and utilized [1, 2]. Between the 16th and 19th century, scientific exploration shifted towards isolating the compounds responsible for the medicinal properties of these plants [1]. During this period, volatile substances were commonly identified through the distillation of plant extracts [1]. However, natural products are not exclusive to plants; they are also produced by animals, fungi, and bacteria [3, 4]. Among these, bacteria—particularly Actinomycetes—are exceptionally prolific producers of natural products [3, 4]. In the mid-20th century, following the discovery of penicillin, the "golden age of antibiotic discovery" began, bringing bacterial natural products to the forefront of research [1, 2]. The immense diversity of bioactivity exhibited by natural products—regardless of the producing organism—can be attributed to their wide range of compound classes, including polyketides, ribosomal natural products (RiPPs), nonribosomal peptides (NRPs), fatty acids, and more [5-7].

Actinomycetes, in particular, have proven to be one of the richest sources for antibiotic discoveries [8]. They produce a variety of clinically important antimicrobial classes, such as aminoglycosides, β-lactams, glycopeptides, macrolides, and tetracyclines [8]. These compounds constitute some of the most widely used drugs in antimicrobial therapy [8]. However, the widespread use of antibiotics has led to the natural evolution of antibiotic resistance [9]. The pace of antibiotic discovery did not keep up with the rapid emergence of resistance, marking the end of the "golden age of antibiotic discovery" and the rise of multidrug-resistant bacteria [9, 10]. This prompted a shift in research to focus on modifying existing antibiotics. In recent years, however, there has been a renewed interest in the active search for novel natural products [9, 10].

The search for metabolites is still the most direct way for the discovery of new compounds [9, 10]. With new technical methods, engineered biosynthesis emerges as a new approach for rationally designed natural products [3]. In nature, different environmental conditions lead to differences in transcriptomes, proteomes and metabolomes [11]. These differences lead to natural products [11]. Based on variations in cultivation conditions this effect can be recreated in the lab [11]. A strain is treated with several cultivation conditions to trigger production of different natural products [11]. The one strain – many compounds (OSMAC) approach developed by Fuchser *et al*. is based on this feature of changed conditions [12]. Over the years, the discovery of new metabolites through secondary metabolite screenings became difficult, since many produced compounds were already known [13]. An alternative way to reach new natural products – that are not produced under lab conditions, but discovered in the genome of a target strain – is the heterologous expression. For this method a cryptic or silent cluster – a cluster that is not expressed under lab conditions – gets transferred to a host strain that is able to express such clusters [13-15]. The challenging part of developing these systems are: (1) generation of suitable vectors (e.g. plasmids, cosmids or bacterial artificial chromosomes (BACs)); (2) posessing viable working protocols; (3) the presence of possible precursor molecules in the host and (4) the host's ability to perform post-translational modifications [15]. For practicabillity in most cases a DNA manipulation is performed in *Escherichia coli* (*E. coli*) strains. With an *E. coli-Streptomyces* shuttle vector, the gene cluster is transferred to the host strain [15]. This transfer is accomplished by intergenomic conjugation or transformation [15]. The following requirements should be considered when choosing a heterologous host: a rapid growth, genetic availability, low background in HPLC analysis and it should provide all precursor molecules as well as enable all parts of the needed protein machinery [15]. Often, a closely related producer strain is used as the heterologous host [15]. To reduce the background noise during analysis in a chassis strain the secondary metabolome is reduced through gene cluster eliminations [15-17].

As typical hosts, *Streptomyces albus* J1074, *Streptomyces coelicolor* A3(2) and *Streptomyces lividans* TK24 are used [13-15]. All three have gene deletions compared to their respective ancestor strains [13-15].

Streptomyces coelicolor A3(2) – a model organism for actinomycetes – was used as an early heterologous host [13]. In 2012, Zhou *et al*. described the optimized host strain *S. coelicolor* ZM12 derivatized from *S. coelicolor* M145 [18, 19]. *S. coelicolor* M145 is a prototrophic derivative of *S. coelicolor* A3(2) [18, 19]. In the strain *S. coelicolor* ZM12, ten biosynthetic gene clusters were deleted [13, 18]. This increased the production of actinorhodin [13].

S. lividans is phylogenetically closely related to *S. coelicolor*, but differs in secondary metabolite expression levels [13, 14]. The restriction enzymes of *S. lividans* are not methylation-dependent [20]. This means that *S. lividans* is more transformable by foreign DNA than *S. coelicolor* [20].

S. albus J1074 has a defect in the *Sal*I endonuclease synthesis leading to it being a better host for bacteriophages than *S. albus* G [21]. Therefore, *S. albus* J1074 is used as a transformation host for cloning and expression of genes from Streptomycetes [13]. *S. albus* J1074 has one of the smallest genomes of heterologous hosts currently in use [22]. In 2006, it was discovered that non-Streptomyces Actinomycete gene clusters are also expressed in heterologous hosts [14, 23]. This was discovered when thiocoraline biosynthetic gene cluster (BGC) from a marine *Micromonospora* strain was successfully expressed in *S. albus* J1074–after *tioA* was activated with the *ermEp** promoter [14, 23]. Over the years, *S. albus* has become one of the most frequently used heterologous hosts [13, 14].

The Luzhetskyy group generated the chassis strain *S. albus* Del14 with fifteen gene cluster deletions compared to *S. albus* J1074 [16] as well as the strain *S. lividans* ΔYA9 with nine gene cluster deletions compared to *S. lividans* TK24 [17]. In both new strains, a simplified spectrum of metabolites is produced, leading to a lesser background in analysis and easier purification of target metabolites [13, 16, 17]. An additional improvement in these strains is the higher yield of produced natural products compared with the parental strains. Also, more foreign clusters are successfully expressed in *S. albus* Del14 and *S. lividans* ΔYA9 than in *S. albus* J1074 and *S. lividans* TK24 respectively [13, 16, 17].

Other host strains currently in use are *Streptomyces ambofaciens*, *Streptomyces avermitilis*, *Streptomyces cinnamonensis*, *Streptomyces fradiae*, *Streptomyces griseofuscus*, *Streptomyces roseosporus*, *Streptomyces toyocaensis* *Streptomyces venezueale*, *Amycolatopsis japonicum* and *Saccharopolyspora erythraea* [13, 14]. Ideally, as many strains as possible should be tested as heterologous hosts to raise the chance for production of a desired compound.

1.2 Brief introduction to the biosynthesis of nonribosomal peptides

Nonribosomal peptides (NRPs) are a major group of natural products, mostly derived from bacterial or fungal organisms [24]. Their antibiotic, immunosuppressive, cytostatic and toxic activity makes NRPs interesting compounds in pharmacology and medicine [24]. NRPs are built by a chain of amino acids that form a polymer through consecutive condensation [25]. Based on that NRPs show a high similarity to each other yet based on the variety of amino acids a great structurally diversity with a broad spectrum of bioactive properties [25]. Besides proteinogenic L-amino acids, D-amino acids and unnatural amino acids as well as other molecules can be incorporated into NRPs [7, 26]. The incorporation of non protogenenic amino acids and other increases the diversity even more [7, 26].

Nonribosomal peptides are produced by multi enzyme complexes called nonribosomal peptide synthases (NRPS) [7]. The NRPSs mega enzymes are structured into modules [26, 27]. Each adds a single amino acid to the growing peptide chain [26, 27]. The modules each consist of specific domains that perform the biosynthesis in their catalytic centers [26, 27]. First the adenylation domain (A-domain) selects and activates an amino acid by adding ATP to produce the acyl-adenylate [7, 27, 28]. The activated amino acyl adenylate is loaded to the thiolation domain (T-domain) that also called peptide carrier protein (PCP) [7, 27, 28]. The PCP transfers an amino acid to the condensation domain (C-domain) [7, 27, 28]. Subsequently, a nascent peptide chain is coupled with the new amino acid [7, 27, 28]. When attached to the T-domain, modifications of the amino acid can be performed by optional domains within the respective module, e.g. cyclization domain, epimerization domain, formylation domain, methylation domain, oxidation domain, reduction domain or by tailoring enzymes for additional modifications [27]. The final step in NRP biosynthesis is performed by the thioesterase-domain (TE) that disconnects the peptide chain from the NPRS-complex [27].

1.3 Recent developments in the analysis of type II polyketide synthases

A considerable group of natural products is the family of polyketides. Polyketides are produced by animals, bacteria, fungi and plants and display a great diversity in design and biological activity [5]. Polyketides are synthesized by a consecutive decarboxylative condensation of acyl-coenzyme A units by polyketide synthases (PKSs) [5]. PKSs are categorized into three different types based on the mechanism their enzymes perform the biosynthetic pathway.

Type I PKS (T1PKS) enzymes primarily function in a non-iterative manner but can also exhibit iterative activity in certain cases [5, 29]. Type I PKSs are multifunctional enzymes with different catalytic modules [5]. Each module consists of an acyltransferase (AT), a ketosynthase (KS) and an acyl carrier protein (ACP) [3, 5, 30]. This so called minimal PKS produces a β-keto ester intermediate which is elongated in the subsequent steps until the synthesis is completed [5, 30]. In a non-iterative PKS system, each elongation step is carried out by a new module [3, 5, 30]. Each module can also contain domains for keto group modifications [3, 30]. These domains decorate the nascent polyketide chain and show various activities, e.g. as dehydratase (DH), enoyl reductase (ER) or ketoreductase (KR) [3, 30]. After completion of the polyketide chain expansion, the chain is released by a thioesterase domain [5, 30]. The biological activity of the polyketide is often acquired through post-PKS processing by oxidations, methylation or incorporation of deoxysugar molecules [5]. In comparison to non-iterative T1PKS, the KS domain of an iterative T1PKS can recapture the prolonged polyketide chain after each cycle of elongation and termination [3, 5]. Products of T1PKSs are often macrocyclic polyketides (macrolides) or linear polyketides [30].

Unlike type I PKSs, type II PKSs' (T2PKS) biosynthesis is ensured by multiple individual enzymes with distinctive functions. Products of a type II PKS are typically polycyclic aromatic compounds [5, 29]. In the first step of the T2PKS biosynthesis a polyketide chain with a specific chain length is produced by the minimal PKS [3, 5]. The minimal PKS consists of a ketosynthase (KSα), a chain length factor (CLF or KSβ) and an acyl carrier protein (ACP) [3, 5]. Subsequently the poly-β-keto chain is cyclized, aromatized and modified by tailoring enzymes such as oxygenases and transferases [3].

In the third group of PKSs–the type III PKSs–the enzyme consists of a homodimer of identical KS analogue subunits. This simple structure helps by enzyme analysis and manipulation [31]. The main products of type III PKS are mono- and dicyclic aromatic polyketides [29]. The PKS III enzyme performs a number of iterative condensations on diverse starter units [31]. The enzyme is able to independently fulfill all the roles of the essential domains of type I/II PKSs, e.g. starter unit selection, chain assembly and folding [32, 33]. It does not contain an ACP and uses SCoA activated substrates [6, 32, 33].

Within the following, this work will focus on the biosynthesis as well as recent developments in the field of type II polyketide synthases. In the past, the field of bacterial aromatic polyketides was focused on Actinobacteria due to the fact that actinobacterial T2PKS clusters were the only identified clusters until 2015 [34]. Since then, genomic and metagenomic studies have shown that T2PKSs are widely distributed across fourteen bacterial phyla [34-36]. The structure of polyketides produced by a T2PKS is difficult to predict since polyketide biosynthesis does not follow a strict sequence-to-structure pathway [35].

1.3.1 PKS II core and starter units

KSα and KSβ (CLF) show high similarities in their sequences. The main difference is the cysteine of the active site of KSα that is mutated to glutamine in KSβ [6]. This cysteine in KSα is essential in C-C bond formations [6]. Together KSα and KSβ build a heterodimer [37] that, combined with the ACP (Figure 1), produces a β-ester chain by Claisen condensation (Figure 5) [6]. Chain length is mainly controlled by KSβ which provides a water-exclusive pocket of specific sizes for different chain lengths [34, 38]. This cavity protects the highly reactive emerging polyketide [34, 39]. Typically polyketides synthesized by T2PKSs have a chain length of 16 (octaketides), 20 (decaketides) or 24 (dodecaketides) carbon atoms, but longer chains can also be formed [6]. In a computer simulation Hillenmeyer *et al*. studied the KS-CLF amphipathic cavity that houses the growing polyketide chain [34]. They discovered a stronger size increase of the cavity between C16 and C24 (347 Å^3) than the one between C24-C30 (84 Å^3) [34]. Hillenmeyer *et al*. discovered that longer polyketide chains can end outside the KSα/KSβ dimer [34]. This discovery explains why the cavity does not increase as much in KS-dimers for C24-C30 polyketides as in the shorter polyketides [34].

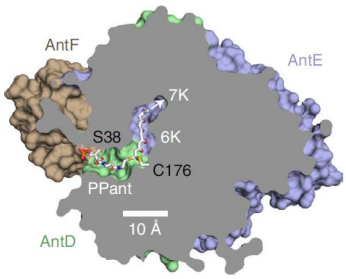

Figure 1. Cross section of the AntDE with the holo-AntF bound with Ppant and hexaketide intermediate within the elongation channel with space for heptaketide [39].

KSα and KSβ most likely evolved from duplication of an ancient KS homolog (initial ancestor) of the fatty acid synthase (FAS) pathway [35, 40]. In the last few years, three studies [34-36] focused on the evolution of T2PKS BGC based on the gene sequences of CLF as well as on the coevolution KS and CLF. In their experiments, the authors screened genomic sequences from the GenBank database [41] for genes encoding for KS homologs and CLF homologs that are located near to each other in the genome (up to 2000 bp) [34-36]. In their studies 544 (2015; [34]), 3421 (2022; [35]) and 6352 (2023; [36]) putative T2PKS BGCs were identified respectively. Of the 6352 clusters only 167 were characterized in 2023, emphasizing

the great unused potential of T2PKS [36]. Hillenmeyer *et al*. demonstrated that KS and CLF coevolved from the initial ancestor mentioned above, with hardly any changes through gene swaps (Figure 2A-C) [34]. They also discovered that the architectures of the accessory genes are consistent within the CLF clade. Because of this discovery the gene cluster as well as the starter units can be predicted with the CLFs protein sequence [34].

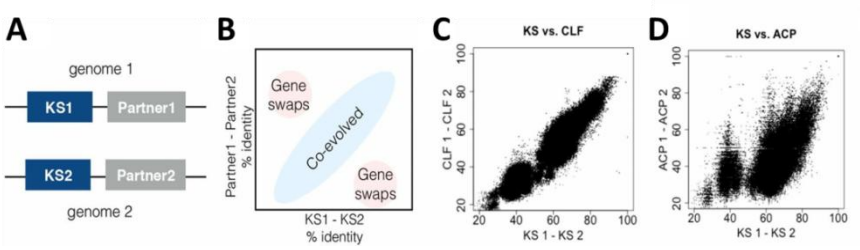

Figure 2. Coevolution of T2PKS KS with partner genes [34]; (A) – scheme of two different BGCs KS with compared partner; (B) – scheme for plot, KS1-KS2 identity plotted against partner1-partner2 identity; (C/D) – evolutionary history plotted of KS vs CLF/ACP.

ACPs are small (~9 kDa), flexible proteins with a conserved structural feature of 4 helices (Figure 3A) [42]. The ACP in its inactive form ("*apo*"-ACP) needs to be modified to transform into its active form ("*holo*"-ACP). To activate the apo-ACP a phosphopantetheinyl transferase (PPTase) attaches 4'-phosphopantetheine (Ppant) to ACP (Figure 3C). Ppant derives from coenzyme A (CoA) through a CoA ligase reaction (Figure 3B) [43]. The Ppant is bound to a serine at the N-terminus of helix II or the loop region between helices I and II respectively (Figure 3A) [39, 42]. The PPTase as well as the CoA ligase are essential for conversion of apo-ACP to holo-ACP, but are not necessarily part of the biosynthetic gene cluster of polyketides [43].

In the T2PKS system ACP seems to have coevolved (Figure 2D) within the evolution of KS/CLF because T2PKS ACPs' clade is distinct from other secondary ACPs as well as primary fatty acid synthase (FAS) ACPs [34]. Some clusters lack the ACP completely. These are situated within an older clade than the presumed initial ancestor for aromatic polyketides in the phylogenetic tree [34].

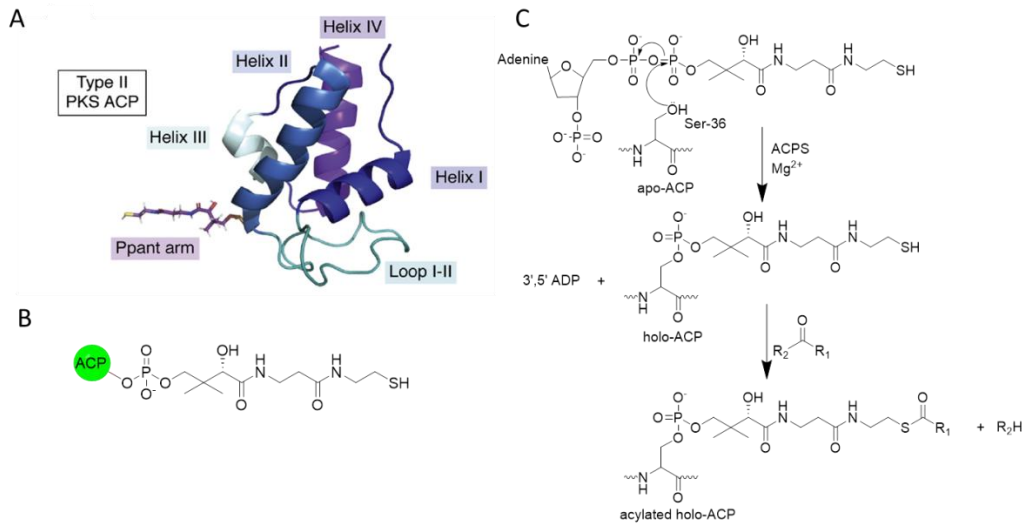

Figure 3. Structure and activation of ACP; A: ACP structure coupled with Ppant [42], B: chemical structure of Ppant bound to ACP, C: reactions leading from apo-ACP to holo-ACP by holo-ACP synthase (ACPS) and production of acetyl-ACP.

The starter units of type II PKSs are generally acyl-CoAs. Besides malonyl-CoA, which is the main extender unit but often also acts as the starter, acetyl-CoA functions as the main starter unit. Genes responsible for extender and starter-unit synthesis are often located outside the PKSs biosynthetic gene cluster (BGC) [38]. Fatty acyl-CoAs, benzoyl-CoA, 2-methylbutyryl-CoA or T1PKS products can also act as starter units [3, 6, 44, 45]. In tetracyclines synthesis malonamate, in rishirilide B synthesis isobutyl-CoA and in lomaiviticin synthesis methylmalonyl-CoA are used as special starter units [44-47]. Malonyl-CoA as the main extender unit is synthesized by carboxylation of acetyl-CoA performed by biotin dependent acetyl-CoA carboxylases (Figure 4) [48].

The transfer of the malonyl group from a malonyl-CoA to holo-ACP is performed by MCAT (malonyl coenzyme A:acyl carrier protein transacylase) generating the free CoA-SH and the activated malonyl-ACP (Figure 3C) [49]. MCAT is a promiscuous enzyme that can transacylate various holo-ACPs. Hence, even if MCAT is essential for the synthesis PKS clusters do not necessarily need this enzyme – as long as another suitable MCAT is available in the host strain [39]. Up to today the *in vivo* relevance of self-malonylation of ACP remains unclear [42].

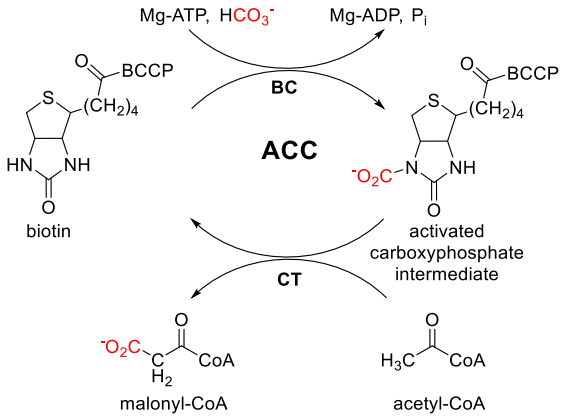

Figure 4. Malonyl-CoA synthesis through the carboxytransferase-unit (CT) actvity in acetyl coenzyme-A carboxylase (ACC) and biotin as cofactor which is activated by the biotincarboxylase-unit (BC).

Polyketide biosynthesis is started by the priming process [50]. The dedicated starter unit attaches to the ACP's thiol group of Ppant, is then decarboxylated and transferred to the cysteine thiol of KSα (Figure 5A) [50]. After priming the elongation beginns and a malonyl group attaches to ACP. The malonyl group is decarboxylated and attached to the polyketo chain through Claisen condensation [50]. The elongated chain is transferred to KSα for another elongation cycle or the elongation is terminated when the polyketo chain has the correct length, which is controlled by KSβ [34, 38, 50]. ACP and the polyketide chain bound to it detach from the KS/CLF heterodimer for tailoring steps (Figure 5B-C) [50].

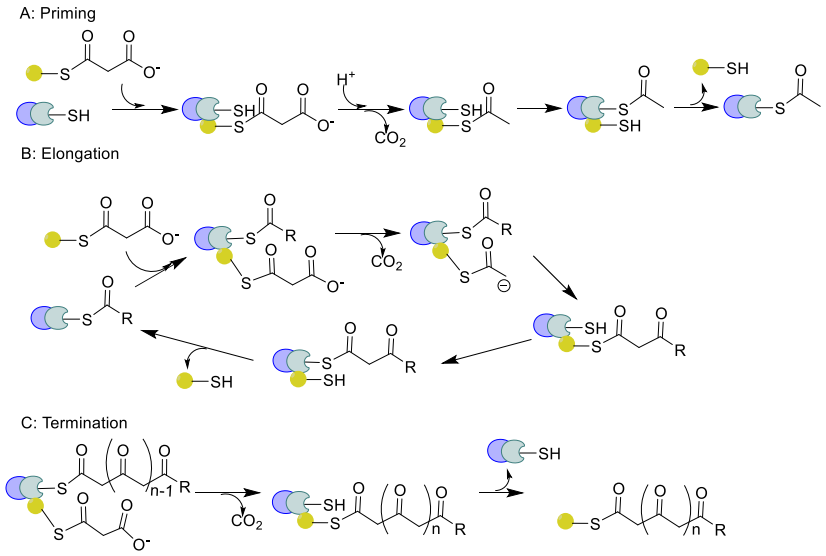

Figure 5. Biosynthesis of the polyketo chain performed by KS, CLF and ACP with the 3 steps of the pathway, i.e. A: priming, B: chain elongation and C: termination. Ketosynthase (KS) with active site cysteine shown in green, chain length factor (CLF) in blue and acyl carrier protein (ACP) with the pantetheine arms thiol in yellow.

In studies concerning the minimal PKS, Bräuer *et al*. investigated the *ant* gene cluster (*antA–antI*) from *Photorhabdus luminescens*, which is responsible for producing the anthraquinone AQ256 [39]. The authors successfully expressed the genes in *E. coli* and produced the AQ256 [39]. Through crystallization experiments, they demonstrated that the polyketide-binding channel of AntDE has a length of 20 Å, which accommodates only a heptaketide, despite the system ultimately producing an octaketide (Figure 1) [39]. Once the heptaketide is formed, the binding channel becomes filled [39]. The lastly added acetyl group is tilted and AntDE:AntF undergo structural changes to avoid steric clashes [39]. The last added malonate unit is not stabilized, leading to the cleavage of the bond between AntDE and holo-AntF [39]. Consequently, the produced octaketide is released [39]. It is stated that AntDE:apo-AntF is structurally identical to AntDE:holo-AntF [39]. Within the system, AntDE:holo-AntF are more interactions of holo-AntF to AntE than to AntD [39]. This supports the current knowledge that within the minimal PKS the interaction of CLF and ACP is the main factor in the production of variable polyketides [34]. The CLF:ACP interaction is based on a few polar interactions [34, 39]. The KS:CLF heterodimer AntDE is more stable [34, 39]. The Ppant increases the contact area of AntDE:holo-AntF by 30%, which stabilizes the enzyme complex and in turn leads to a possible explanation on how holo-AntF is recognized [39].

Qian *et al*. solved the biosynthesis of a cryptic T2PKS gene cluster of *Streptomyces* sp. Tü6314–that produces new streptoketides–called *skt*. The authors discovered three enzymes (Skt17-19) that produce a propionyl-CoA starter unit. In the absence of these enzymes however, the minimal PKS (Skt1-3) will use acetyl-CoA as a starter unit [51]. The use of acetyl-CoA as the starter unit resulted in production of three new streptoketides which led to the conclusion that some PKSs might also use alternate starter units [51]. This generates an even wider spectrum of possible products [51]. Deng *et al*. were also able to switch the starter unit in their *in vitro* experiments with derivatives of the natural product youssoufene from acetyl-CoA to butyryl-CoA showing the substrate promiscuity of the ketosynthases YsfB/C as well [52]. Both actyl-CoA and butyryl-CoA YsfB/C produced a C16 chain, confirming that rather than the starter unit the size of the polyketide chain restricts the number of further elongation steps [52].

In an *in vitro* experiment Zhang *et al*. worked with the highly reducing (HR) T2PKS gene cluster *mbg*. It contained eight ketosynthases that potentially formed four KS-CLF heterodimers (Mbg7-Mbg3, Mbg6-Mbg5, Mbg16-Mbg15 and Mbg21-Mbg22) as well as three ACPs (Mbg8, Mgb10 and Mgb14) [53]. The main products of this cluster were the two (to date unnamed) compounds mbg-A (1) and mbg-B (2) with a rare *o*-dialkylbenzene moiety (green) and a 2-amino-3-hydroxycyclopent-2-enone ring (C_5N-ring) (blue) (Figure 6) [53]. In an Mbg8 elusive *in vitro* experiment, the *o*-tolyl group was missing in the compounds and resulted in the production of mbg-G (7) and mbg-H (8). Thus, it was assumed that Mbg8 is responsible for the formation of the *o*-tolyl-group, while the enzymes Mbg10/14 appeared to be responsible for chain elongation [53]. To analyze the activity of the ketosynthases, single KS-CLF pairs were excluded within the *in vitro* experiments. The experiments showed that Mbg21/22 elongates compound mbg-C (3) and produces compound mbg-D (4). Mbg-D in turn is elongated by Mbg16/15 and produces mbg-E (5) (Figure 6) [53]. Compounds mbg-G (7) and mbg-H (8) were produced in any of the experiments where Mbg8, Mbg7/3 or Mbg6/5 were deleted. These results indicated that these mentioned enzymes produce the *o*-tolyl group of the compound mbg-C (3) and use mbg-F (6) as a precursor (Figure 6) [53]. The genes responsible for C_5N-ring (Figure 6 blue) synthesis were found to be located in the *Streptomyces* sp. SANK60404 genome outside the *mbg*-cluster [54]. The C_5N-ring was synthesized and then added to the intermediates mbg-D (4) and mbg-E (5) by the activity of C_5N-1 (an amide synthase), C_5N-2 (a 5-aminolevulinate synthase) and C_5N-3 (an acyl-CoA ligase) (Figure 6) [53]. The findings of Zhang *et al*. showed that within one cluster–e.g. the *mbg*-cluster–various ketosynthases and ACPs can work together by pointing out the large variety in PKS biosynthesis (Figure 6) [53]. Even the universal conserved KS and CLF showed a high specificity towards their respective substrates in these experiments [53].

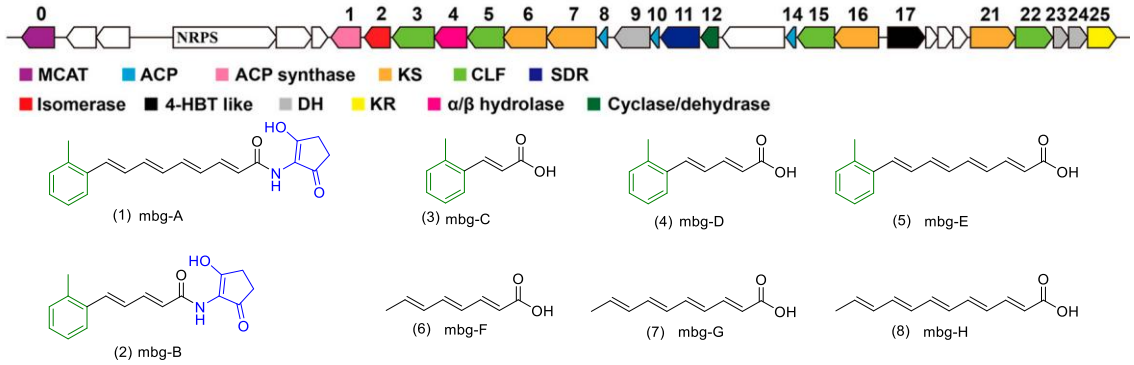

Figure 6. Schematic visualization of the *mbg* cluster with the main products (mbg-A and mbg-B) and six side products received after knockout experiments (mbg-C to mbg-H). The *o*-dialkylbenzene moiety is depicted in green and the 2-amino-3-hydroxycyclopent-2-enone-ring (C5N-ring) in blue

In T2PKS the release mechanism of the nascent polyketide is not well investigated [55]. Typically, T2PKS BGCs contain no genes encoding for thioesterases which are responsible for the release in T1PKSs. But a few type II thioesterases (TEII) such as ZhuC (R1128 PKS; [56]) and EncL (enterocin PKS; [57]) have been identified [55]. Hua *et al*. discovered that AlpS is essential for kanamycin biosynthesis because it is responsible for the hydrolysis of the thioester bond in the aromatic polyketide-ACP complex [55]. AlpS was the first thioesterase described as a chain-releasing enzyme in T2PKS biosynthesis [55]. Since most T2PKS clusters do not contain thioesterases, other release mechanisms are needed. In the actinorhodin biosynthesis the second ring cyclase ActIV is a bifunctional enzyme which is also responsible for the release of the polyketide chain from ACP [55, 58]. Thus no specific thioesterase is required in actinorhodin biosynthesis [55, 58]. In most type II polyketide biosynthesis systems ACP is released during the cyclization steps [6].

Following the production of the nascent polyketide chain, several types of enzymes convert the polyketide precursor into the functional polyketide. These enzymes are belong to two groups, namely 1) auxiliary PKS enzymes, e.g. ketoreductases (KR), cyclases (CYC) and aromatases (ARO) that alter ACP-bound substrates [59] and 2) tailoring enzymes, e.g. transferases and oxygenases that modify free substrates [59].

1.3.2 Auxiliary polyketide enzymes

1.3.2.1 Ketoreductases

In the biosynthesis of reducing aromatic polyketides the first reaction performed on the nascent polyketide chain is often the reduction of a keto group [6]. This reaction performed by a ketoreductase. Ketoreductases belong to the family of short chain dehydrogenases and contain a Rossmann fold [3]. The Rossmann fold is a secondary protein structure, built up by alternating β-strands and α-helices [60]. The β-strands form a β-sheet that is surrounded by the helices [60, 61]. The Rossmann fold structure harbors a binding site for adenosine diphosphate (ADP), that's part of cofactors like flavin adenine dinucleotide (FAD), nicotinamide adenine dinucleotide (phosphate) (NAD(P)H) or *S*-adenosyl-L-methionine (SAM) [60, 61].

A ketoreductase stereo specifically reduces a keto group of the nascent polyketide chain through hydrogen transfer from NAD(P)H to form a secondary alcohol (Figure 7B) [6]. This reduction leads to a conformational change of the polyketide chain putting it into a favorable orientation for subsequent cyclization steps [6]. Ketoreductases show stereospecificity dependent on the supposed cyclization through the geometry of their active site [62, 63]. Next, the reduction of a C9 keto group leads to C7/C12 cyclization with a C7 reduction leading to C5/C10 cyclization [62]. Depending on the regio selectivity as well as the cyclization pattern, ketoreductases are divided into four groups: clade I (C19-KRs for pentangular polyketides), clade II (C17-KRs for anthracyclines), clade III (C15-KRs for angucyclines) and clade IV (C9-KRs for bezoisochromane quinones) [64].

Research on the reduction mechanism is highly difficult since the polyketide chain is very reactive and is likely to a spontaneous cyclization [3, 6]. This cyclization leads to nonfunctional side products [6, 65]. Nevertheless, Zhao *et al*. were able to form co-crystals of *act*KR (ActIII) with a stable isoxazole-based polyketide mimic bound to (P)pant (Figure 7A) [65]. By means of crystal structures, the binding of the polyketides to the ketoreductase was modelled [65]. Zhao *et al*. discovered two polyketide binding sites. The front patch consists of arginine residues R38, R65, R93 and the back patch of amidic residues Q149, R220, N260 (Figure 7C) [65]. Both binding sites formed opposite entrances into a long channel that harbored the active site with the catalytic residues N114, S144, Y157 and K161 (Figure 7D)

[65]. In the model, longer polyketide chains (C16, octaketides) attached to the front pocket while shorter polyketides (C8, tetraketides) attached to the back pocket [65]. Normally ketoreductases are present in a tetramer form [65]. In the *act*KR the back pocket was covered by the other tetramer units, which explains the high affinity of *act*KR to octaketides [65]. Simulations showed that both pantetheine and phosphopantetheine also play an essential role in stabilizing the KR-ligand binding at an arginine-rich binding site [62]. This is even the case when binding is mainly based on the van der Waals interaction and hydrophobic effects between the binding pocket and uncharged polyketide chain [65].

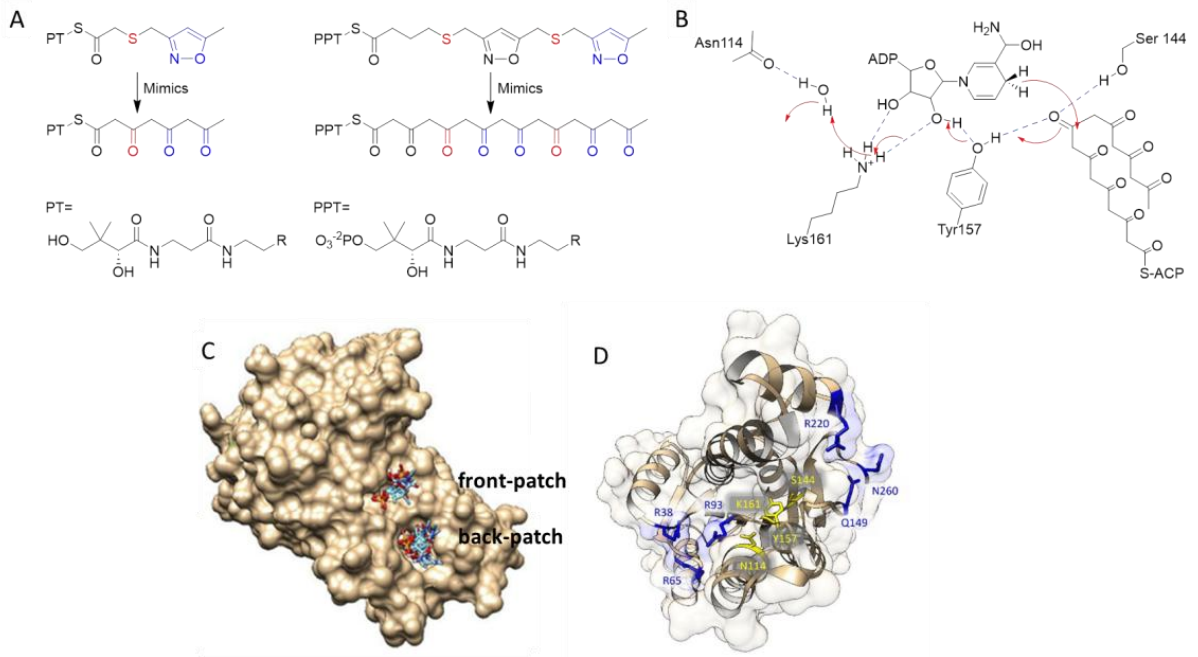

Figure 7. Isoxazole-based linear poly-β-ketone mimics (keto groups are substituted with sulfurs and isoxazoles) bound to *act*KR. (A) Panthetheinylated (PT) tetraketide and phosphopantetheinylated (PPT) octaketide mimics. Isoxazole (blue) and sulfur (red) substitutions replace the native carbonyls. (B) Proposed proton-relay mechanism for ketoreduction with NADPH and catalytic center. (C) *Act*KR monomer conformation with isoxazole mimics bound to front-patch (top) and back-patch [65]. (D) *Act*KR monomer conformation displaying the positions of residues responsible for building the front-patch (R38, R65, R93), the back-patch (Q149, R220, N260) and the catalytic center (N114, S144, Y157, K161) [65].

Ketoreduction as seen in the enterocin biosynthesis can also be performed during chain elongation [6]. There are only few polyketide biosynthetic pathways in which an additional ketoreductase is active in later stages as well, e.g. in pradimicin A biosynthesis [3, 6]. In the doxorubicin biosynthesis a chiral carbon center is produced by a ketoreductase [3, 6]. In 2020 Husain *et al*. proposed that in the case of longer polyketide chains and in deoxygenated aromatic polyketides a cyclization occurs that produces a non-aromatic ring, beore the ketoreadution reaction [66]. The reduction is performed on this non-aromatic ring and later the ring is aromatized [66].

1.3.2.2 Cyclases and aromatases

The aromatic polyketides are formed through cyclization and aromatization of the nascent polyketide chain [6]. The spontaneous cyclization of the highly reactive polyketide chain is prevented through chaperone-like enzymes (so called cyclases) that are produced by the BGC [6]. Cyclases stabilize the polyketide intermediates and help with the correct folding by forming a C-C-bond [6]. Cyclization takes place after ketoreduction in reducing PKSs or immediately after the polyketide chain is produced in non-reducing PKSs [67]. The structural motif with the amino acid sequence HxGTHxDxPxH, shared by different cyclases, forms the active site [6]. The enzymes often occur as didomain enzymes containing two identical domains or as monodomain enzymes [6, 67]. But they can also appear coupled with other enzymes e.g. with aromatases (ARO/CYC) or ketoreductases (CYC/KR) [6, 67]. Aromatases often support the cyclization process by dehydration of alcohols in ACP-bound substrate that yield to an aromatic ring system [6]. In general, cyclases are specific for each ring closure of their final polyketide and are not interchangeable [6]. Nevertheless, in a few biosynthesis routes specific 2,3-cyclases are present, e.g. TxnC3 in the trioxacarcin biosynthesis or Gra-ORF33 in the granaticin biosynthesis [68, 69]. In some polyketides, the last ring cyclization may also form spontaneously [58, 70]. In these cases the structure is fairly stable and only a select few cyclization patterns are possible [58, 70]. After complete cyclization, nearly all polyketides are present as “linear” or “angular” structures with a U-shaped cyclization pattern (Figure 8) [3, 6, 71]. However, a “discoid” structure in an S-shaped pattern is rare, yet possible (Figure 8) [3, 6, 71].

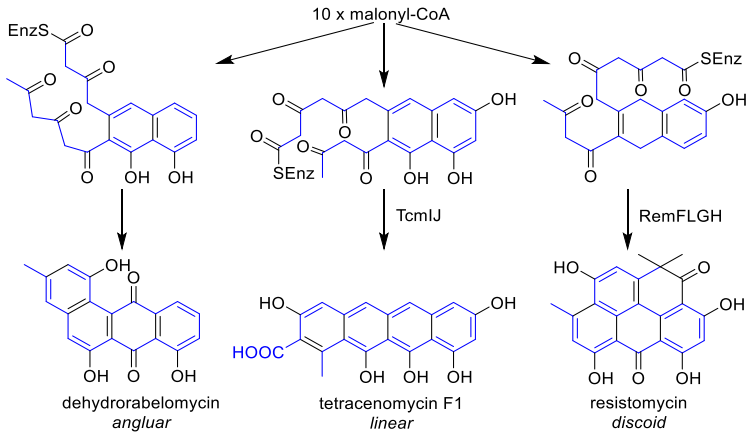

Figure 8. U-shape and S-shape folding leading to angular, linear and discoid polyketides.

Xu *et al*. discovered a type II PKS cluster (*als* with 29 open reading frames (ORFs)) from *Streptomyces sundarbansensis* SCSIO NS01 that – after heterologous expression into *Streptomyces coelicolor* M1152 – after six different cyclization patterns, produced eight different compounds (Figure 9) [70]. The *als*-BGC only harbored *als*Q as a cyclase encoding gene and *als*R as an aromatase encoding gene [70]. In the biosynthesis, the main product is prealnumycin B which is cyclized with pattern I (C7/C12; C5/C14; C15OH/C3) by AlsQR and spontaneous cyclization of the C-ring (Figure 9) [70]. The cyclization pattern II (C7/C12; C5/C14; C2/C15) is also performed by AlsQR, but with a different spontaneous cyclization of the C-ring (Figure 9) [70]. Cyclization patterns III (C7/C12; C6/C15) and IV (C7/C12, C11OH/C15) are based on spontaneous cyclization of the second ring after cyclase induced cyclization of the first ring (Figure 9) [70]. The last two cyclization patterns are based on a modified polyketide chain. In pattern V the first ring is cyclized by AlsR at C7/C12 and then spontaneously C4/C13 cyclization occurs (Figure 9) [70]. In pattern VI a spontaneous C8/C3 cyclization followed by another spontaneous C7OH/C11 cyclization is performed (Figure 9) [70]. This example shows that more than one cyclization pattern can be achieved with two cyclases [70]. It also demonstrated that unwanted side products may occur when cyclization is not properly controlled [70].

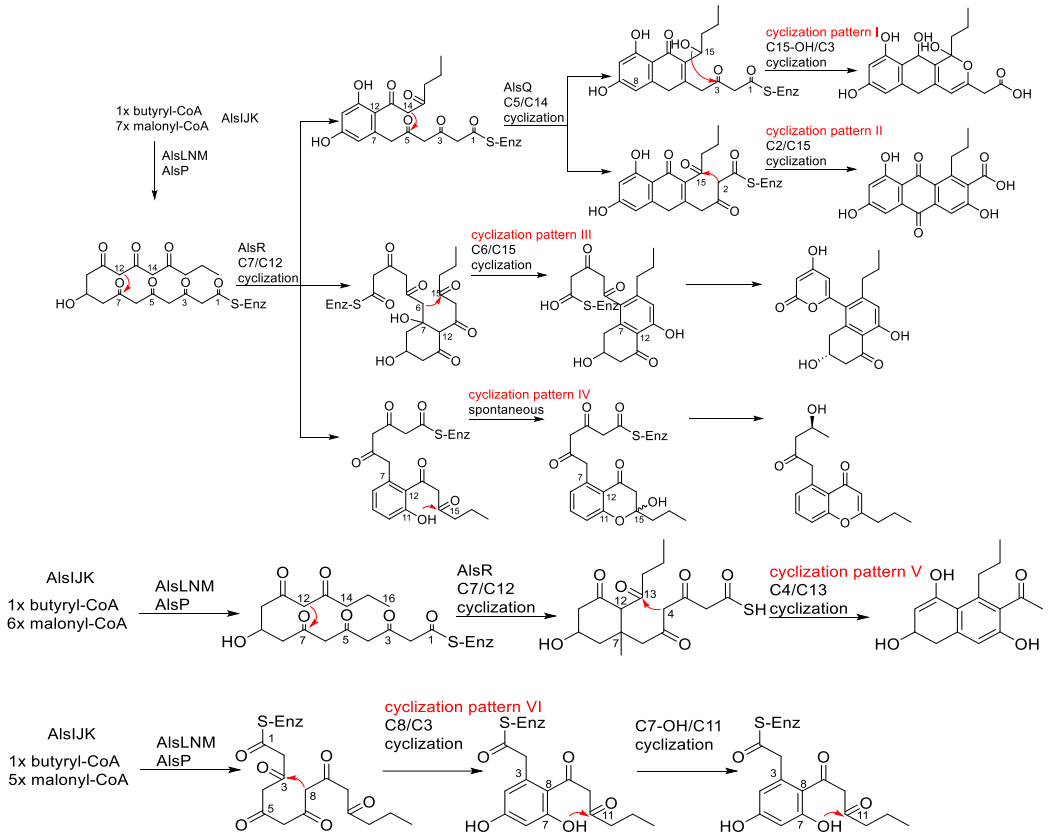

Figure 9. Proposed biosynthetic pathways of compounds produced by the *als* BGC of *Streptomyces sundarbansensis* SCSIO NS01 after heterologous expression into *Streptomyces coelicolor* M1152 [70].

Taguchi *et al*. discovered that the actinorhodin second-ring cyclase ActIV has a zinc metal-binding motif as found in the metallo-hydrolase superfamily [58]. This feature supports the release of the bicyclic intermediate from ACP [58]. This release is similar to the one performed by thioesterases in T1PKS' TE-domain [58]. The released actinorhodin precursor is reduced at C3 by ActVI-1 which leads to the formation of the C-ring (Figure 10) [3, 58].

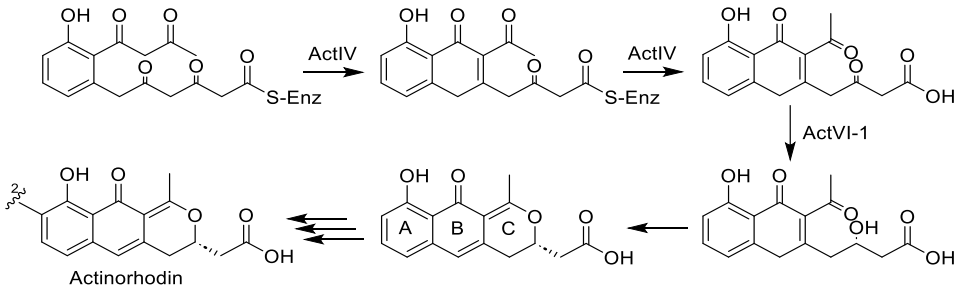

Figure 10. Cyclization of the second and third ring in actinorhodin biosynthesis.

1.3.3 Polyketide tailoring enzymes

The main reason for the diversity of aromatic polyketides is the activity of tailoring enzymes that modify the nascent polyketide through e.g. oxidation reactions, halogenation or transferase activity [3, 6]. The genes encoding for these tailoring enzymes are mostly part of the biosynthetic gene cluster [72].

1.3.3.1 Oxygenases

Tailoring steps involving oxygenases are present in most polyketide biosynthetic pathways [3, 6]. The main function of oxygenases is the incorporation of oxygen atoms from molecular oxygen into the substrate [3, 6]. All oxygenases are composed of subunits with an alpha/beta barrel with a hydrophobic cavity for substrate binding [73]. Despite large differences in their quaternary structures as well as the amino acids of their active site, oxygenases show a high similarity to cyclases in their respective subunits [73]. This observation led to the assumption that both oxygenases and cyclases may have evolved from a common ancestor [3]. Depending on the number of oxygen atoms inserted into the substrate oxygenases are divided into mono- and dioxygenases [6, 72]. Monooxygenases (MO) incorporate one of the two oxygen atoms into the substrate and reduce the other oxygen atom to water [6]. Dioxygenases (DO) can insert both oxygen atoms into the substrate [6].

Mono- and dioxygenases present in type II polyketide biosynthesis were differentiated by their oxidation mechanism into anthrone monooxygenases, cytochrome P-450 monooxygenases and flavin-dependent mono- and dioxygenases (Figure 11) [6]. In the following is a short overview of the oxygenase types:

Anthrone-type oxygenases are responsible for the oxidation of naphtacenone- and anthrone-precursors resulting in the quinone derivative (Figure 11 A) [6]. Anthrone oxygenases are classified as internal monooxygenases. These oxygenases oxidize the substrate and reduce oxygen to water without the need of cofactors [6, 74, 75]. The substrate is deprotonated at C10 through a Trp residue [76]. The C10 carbanion reacts with molecular oxygen and a C10 peroxy-intermediate is created [76]. The peroxy-intermediate is protonated and then dehydrated to form the oxidized polyketide [76].

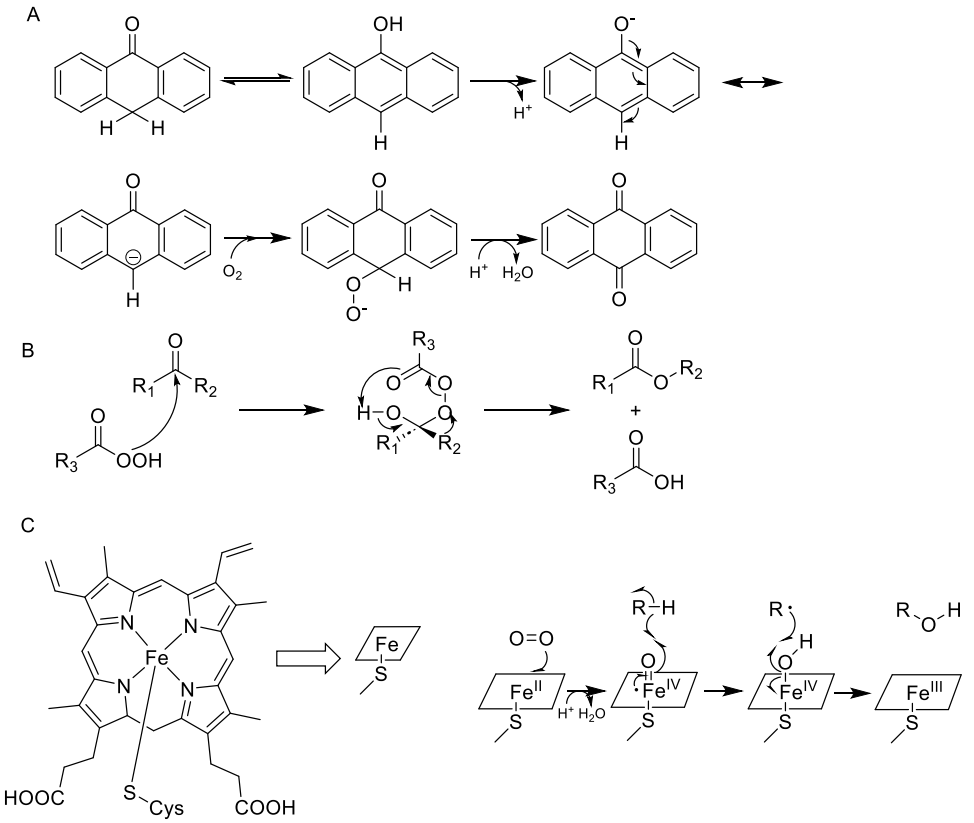

Figure 11. Scheme of the reactions catalyzed by different types of oxygenases. (A) anthrone-type oxygenase; (B) Baeyer-Villiger monooxygenase; (C) hydroxylation reaction of P450 monooxygenases;

Flavin-dependent oxygenases use FAD as a cofactor [6]. The adenosine part of FAD is bound to a region near the N-terminus, whereas the flavin part is bound to a second region within the enzyme with a high homology to the N-terminal region [6]. FAD-dependent oxygenases perform epoxidations, hydroxylations, Favorskii and most prominently Baeyer-Villinger rearrangements [6, 72]. Baeyer-Villinger-monooxygenases (BVMOs) contain FAD and utilize NADPH as a cofactor. The BVMO supports the reaction of a nucleophilic peroxy acid with a ketone group which leads to an insertion of one oxygen atom into a C-C-bond of the substrate (Figure 11 B) [77, 78].

Because of their complex chemical reaction mechanisms cytochrome P450-dependent monooxygenases are of great interest to researchers around the world [79]. Furthermore, they play a role in primary and secondary metabolisms as well as in drug degradation [79]. The heme group in the active center of a P450 monooxygenase breaks and activates a normally inert C-H-bond (Figure 11 C), epoxidates C=C-double bonds, cleaves C-C-bonds or oxidizes sulfur or nitrogen [79, 80]. Most P450 monooxygenases use NAD(P)H as an

additional cofactor for electron transfer [79]. P450 monooxygenases catalyze the oxidations regio- and stereospecifically and under mild reaction conditions [79]. This cannot be replicated by a pure chemical reaction [79].

As an example for polyketides where in their biosynthesis a cytochrome P450 monooxygenases performs a biaryl C-C coupling are julichromes. [81]. In recent years, these compounds were analyzed by Jianhua Ju and his co-workers. In the reaction of julichrome Q_6 (9) to julichrom $Q_{6\text{-}6}$ (10) the monooxygenase JuiI is responsible for the dimerization (Figure 12) [81]. Ju *et al*. analyzed the tailoring steps in the biosynthesis route of julichrome $Q_{6\text{-}6}$ (10) and its derivatives and examined two enzymes JuiN and JuiO [82, 83]. JuiN is a flavin monooxygenase that catalyzes the tailoring steps that lead from julichrome $Q_{6\text{-}6}$ (10) to the intermediate julichrome $Q_{6\text{-}8}$ (11) and the product julichrome $Q_{8\text{-}8}$ (12) (Figure 12) [82, 83]. Investigations showed that the monomer julichrome Q_6 (9) is not converted by JuiN [83]. JuiO supports the epoxidation and ketoreduction steps leading from julichrome $Q_{8\text{-}8}$ (12) to julichrome $Q_{3\text{-}8}$ (intermediate) (13) and julichrome $Q_{3\text{-}3}$ (product)(14) (Figure 12) [83]. JuiO is a dehydrogenase/reductase of the SDR family (short-chain dehydrogenases/reductases family), therefore, it only uses NAD(P)H as a cofactor [83]. JuiO belongs to the group of cofactor-independent oxygenases described within the last decades [76, 83]. Both JuiN and JuiO iteratively perform their reactions, but the mechanism how they perform hydroxylation and epoxidation on both sides of the dimeric intermediates remains unclear [83].

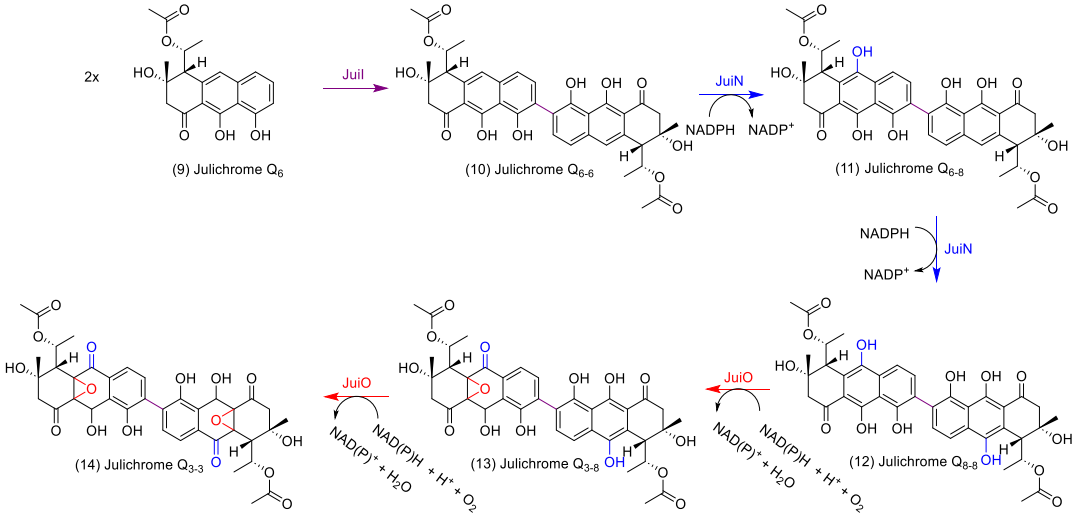

Figure 12. Proposed biosynthetic pathway of tailoring steps with dimerization by JuiI and oxygenase activity of JuiN and JuiO.

1.3.3.2 Halogenases

The incorporation of halogens (F, Cl, Br and I) into compounds is called halogenation. Halogenated natural products are mostly brominated or chlorinated [84]. Through halogenation the diversity and range of biological activities of polyketides increases [84-86]. Therefore, this modification step is of great scientific interest, especially for pharmaceutical research [84-86]. Typically, a flavin-dependent ($FADH_2$-dependent) halogenase (FDH) is used for halogenation of natural products [87]. Enzymes of the FDH family share a conserved Rossmann fold as well as two tryptophan residues within the active site to prevent monooxygenase activity [88]. FDHs can halogenate both, substrates that are free and those that are bound to a carrier protein [88]. In the case of a chlorination the FDH requires $FADH_2$, NaCl and molecular oxygen [89]. The oxygen binds to the flavin to form C4a-hydroperoxy flavin (FAD-OOH) [89]. FAD-OOH is attacked by the chloride anion to form a hydroxychloride with one oxygen atom leaving the FAD in form of a water molecule [89]. The hydroxychloride diffuses and binds to a Lys-binding site in the active center of the FDH [89, 90]. The resulting aminochloride forms a Wheland complex with the substrate and the halogenated product is formed by deprotonation (Figure 13) [89, 91].

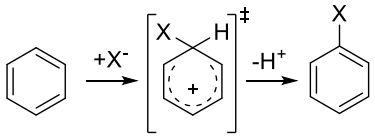

Figure 13: Reaction to the halogenation of an aromatic compound with the Wheland complex as an intermediate.

Polycyclic xanthones are a family of aromatic angular polyketides that tend to be halogenated e.g. xantholpin (17) (Figure 14) [88]. Halogenation of such xanthones increases their cytotoxicity against cancer cells, yet the role halogen atoms play in cytotoxic mechanism has not been discovered [88]. Kong *et al*. started to investigate the post-PKS tailoring steps in xantholpin (17) biosynthesis [88, 92, 93]. Inactivation of the halogenase XanH abolished xantholpin (17) production, but resulted in production of the intermediate (15) [92]. XanH is a flavin-dependent halogenase that can be supported by a flavin reductase for better chlorination of the C12 in intermediate (15) to generate intermediate (16) in xantholpin biosynthesis (Figure 14) [88]. $FADH_2$ in XanH needs to be regenerated by NADH [88].

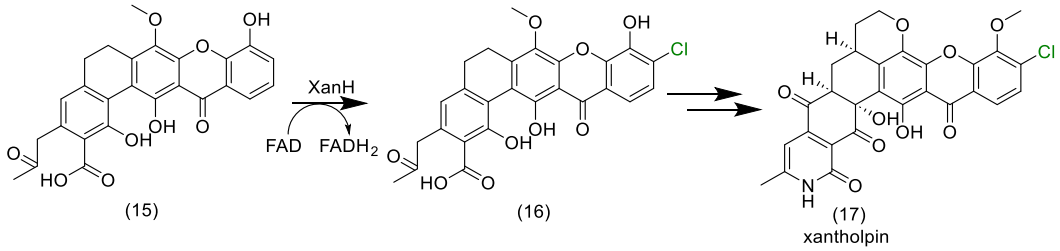

Figure 14. Reaction performed by halogenase XanH as part of the xantholpin biosynthesis.

1.3.3.3 Transferases

Aditionally to the abovementioned tailoring steps, aminotransferases, glycosyltransferases (GT) and methyltransferases (MT) increase the structural diversity and activity of aromatic polyketides [3, 45]. These transferases transmit methyl or amino groups from a donor to the substrate or a specially built activated sugar to the aglycone [3, 6, 45, 94].

Glycosyltransferases are categorized into two superfamilies GT-A and GT-B [6, 94]. The glycosyltransferases found in polyketide BGCs belong to the superfamily GT-B [6, 94]. Depending on their acceptor atom (carbon, nitrogen, oxygen and sulfur) there are four types of glycosyltransferases [95, 96]. O-GTs are the most frequent, N-GTs and C-GTs are less frequent, while S-GTs are the rarest [95, 96]. C-GTs are quite interesting because their sugars are more stably bound to the natural product substrate compared with *N*-glycosylated compounds [95, 97]. *C*-glycosyl-bonds are less affected by enzymatic or hydrolytic cleavage [95, 97]. This stability makes the *C*-glycosylated polyketide interesting for usage in medical applications [95, 97]. Glycosyltransferases are also specific for their substrates, transferred sugars and catalyzed reactions [6, 94]. The sugar moieties that are added to the substrate through glycosyltransferases are mostly produced and activated through enzymes encoded within the biosynthetic gene cluster [6, 95]. Attached sugars can be mono- or polysaccharides and exist either modified or unmodified [98]. The above mentionend activation of the sugars is results in the nucleoside mono- or diphosphate sugar derivatives (NMP/NDP-sugar) [98].

Medermycin is a *C*-glycosylated pyranonaphthoquinone (PNQ) with a strong antitumor activity by inhibition of the serine-threonine-kinase AKT [96, 99]. Cai *et al*. analyzed the biosynthetic pathway of medermycin (lactoquinomycin) (Figure 15). The first steps in medermycin biosynthesis are identical to the early actinorhodin biosynthetic pathway (Figure 10) leading to a trihydroxynapththalene derivative (Figure 15) [96]. This intermediate is converted to kalafungin and is then *C*-glycosylated with the rare sugar D-angolosamine by the enzyme Med-8 (Figure 15) [96]. The activated sugar NDP-D-angolosamine is produced by the six enzymes Med-14 - 18 and Med-20 (Figure 15) [96]. In their study Cai *et al*. performed heterologous expressions of the *med*-BGC–with and without the *med*-8 gene–into *S. coelicolor* CH999 lacking the *act*-gene cluster. After cultivation, it was shown that the Δ*med*-8-knockout strain did not produce medermycin anymore, but complementation of the *med*-8 gene

restored the production [96]. As a side product in the knockout strain, kalafungin was discovered in an amount that is comparable to medermycin in the wildtype strain [96]. Thus, Med-8 is the second known tailoring enzyme after ActVA-ORF4 that can modify the C10 position of PNQ compounds [96]. The experiments of Cai *et al*. showed a new possibility to produce unusual glycosylated polyketides with high pharmaceutical potential.

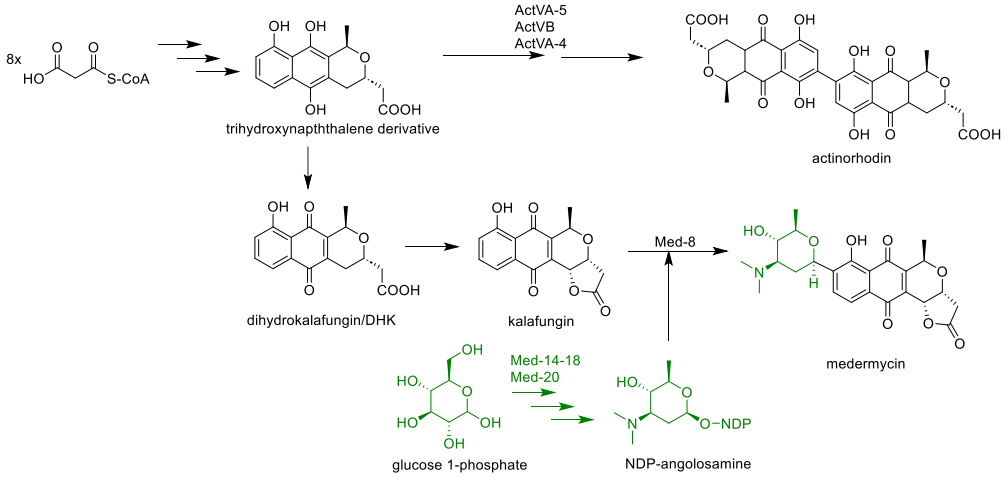

Figure 15. Biosynthesis of medermycin with *C*-glycosylation performed by Med-8. Early biosynthetic steps are identical to actinorhodin biosynthesis.

Despite their selectivity, some glycosyltransferases can also act as N-GT and O-GT [100]. Gutacker *et al*. identified Sace_3599 as such a promiscuous glycosyltransferase from *Saccharopolyspora erythraea* NRRL2338 [100]. Depending on the substrate, Sace_3599 is able to build an *N*- or *O*-, mono- or di-glycosylated product [100]. In an attempt to discover new glycosyltransferases Gutacker *et al*. later screened *S. erythraea* NRRL2338 with different sugar acceptor molecules [100]. The strain was able to convert the substrate 1,4-diamino-anthrachinone (U3) [100]. Hence the genome was screened for glycosyltransferases and three suitable candidates were found and heterologously expressed in *S. albus* Gluc [100]. In the presence of UDP-α-D-glucose the host strain harboring Sace_3599 was able to convert U3 to the N_1-α- and N_1-β-glycosylated derivative (U3G) as well as the N_1,N_4-diglucosylated derivative (U3DG) (Figure 16 A) [100]. To test if Sace_5399 was also able to produce *O*-glycosidic derivatives, Gutacker *et al*. used 1,4-dihydroxyanthraquinone (U2) as the substrate [100]. In the presence of UDP-α-D-glucose the substrate U2 in low amounts was converted to O_1-glucosyl-1,4-dihydroxyanthraquinone (U2G) and O_1,O_4-diglucosyl-1,4-dihydroxyanthraquinone (U2DG) (Figure 16 B) [100].

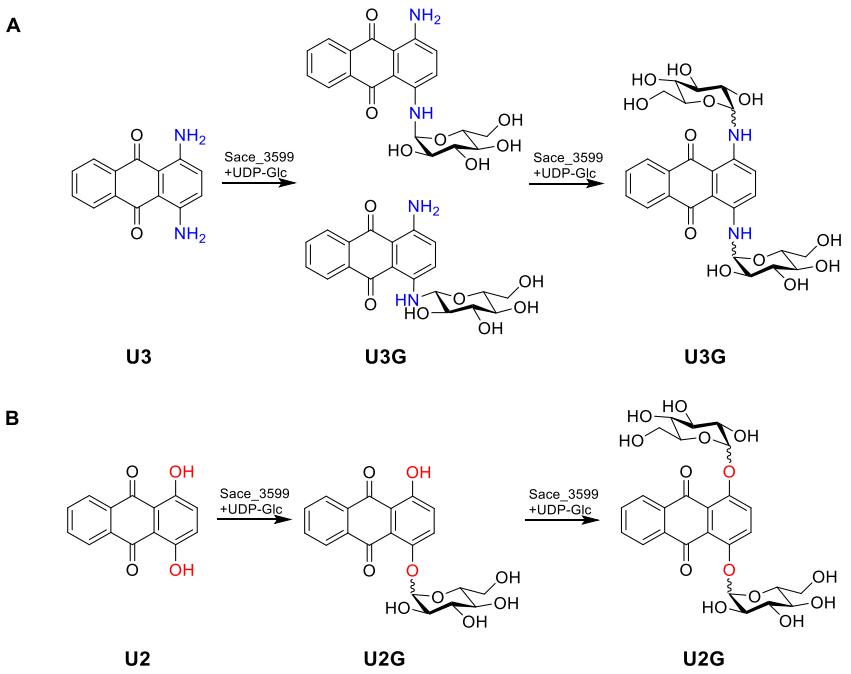

Figure 16. Glycosylation reactions catalyzed by Sace_3599. (A) *N*-glycosylation of U3 resulting in the products U3G and U3DG.; (B) *O*-glycosylation of U2 resulting in the products U2G and U2DG.

Normally glycosylation is performed as a tailoring step in polyketide biosynthesis [6]. However, there are some rare cases in which glycosylation is performed during the formation of the polyketide core structure, e.g. in biosynthesis of mitomycin and pactamycin [101-104]. Pactamycin is a strong antitumor agent of *Streptomyces pactum* ATCC 27456 that consists of an aminocyclopentiol core (blue), a 3-aminoactophenone unit (red), a 6-methylsalicylic acid (dark yellow) and an *N*,*N*-dimethylurea moiety (purple) (Figure 17) [101, 104]. The biosynthetic pathway of pactamycin was studied *in vitro* with focus on the glycosylation by Eida *et al*. in 2019. The 3-aminoacetaophenone moiety derives from dehydroshikimic acid with 3-aminobenzoic acid as an intermediate (Figure 17) [101]. The 6-mathylsalicylic acid is produced by PtmQ an iterative T1PKS and the *N*,*N*-dimethylurea moiety is added as part of the tailoring steps (Figure 17) [101, 104]. The 3-aminobenzoic acid functions as a starter unit for the polyketide synthase machinery with a maloyl-CoA as an extender unit (Figure 17) [101]. Bound to PtmI, the ACP, starter and extender units are connected by KSβ PtmK to enable the production of 3-(3-aminophenyl)3-oxopropionyl-ACP which is then N-glycosylated by PtmJ (Figure 17) [101].

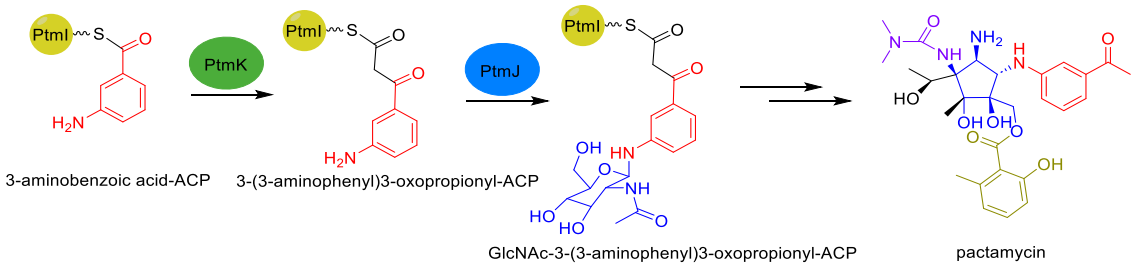

Figure 17. Proposed pathway for pactamycin biosynthesis that shows the glycosylation of the ACP-bound intermediate 3-(3-aminophenyl)3-oxopropionyl.

Methyltransferases transfer a methyl group from a donor like *S*-adenosyl-L-methionine (SAM) to the acceptor atom of the substrate [6]. Through the methyl group transfer, SAM is converted to *S*-adenosyl-L-homocysteine (SAH) [105, 106]. Most methyltransferases have the same SAM binding site and a Rossmann fold [6, 106]. SAM is bound by hydrogen bonds and van der Waals interactions of the first and last thirds of the methyltransferases protein sequence [106, 107]. Catalytic activity can depend on coordinated cations like Ca^{2+}, Mg^{2+} (stabilized by an acidic tryad DD(D/N)) or Zn^{2+} (stabilized by four Cys residues) [106]. Metal-independent, homodimeric MTs show an open conformation through which both the SAM cofactor and the substrate can enter [106, 108]. In these homodimeric MTs the SAM binding site is C-terminal [106]. In the closed conformation, substrate and SAM are positioned in a way that immediately leads to substrate methylation [106].

Depending on the acceptor, atom methyltransferases are characterized into C-MTs, N-MTs and O-MTs, with O-MTs showing the broadest spectrum of substrates out of those three [45, 106]. The phylogenetic tree of methyltransferases shows that methyltransferases cluster based on the methylation site not the type of methylation (Figure 18) [71]. The transmethylation reaction follows an S_N2-like nucleophilic substitution [6, 109, 110]. The activated acceptor atom attacks the nucleophilic methyl group of SAM and after the methyl group transfer is completed, SAH is released (Figure 19) [6, 109, 110]. The active site of methyltransferases needs to position the substrate and the cofactor in a way that acceptor atom and sulfonium moiety of SAM are about 4 Å apart (Figure 19) [106]. The acceptor also has to be the most reactive agent available for the electron deficient methyl group [106].

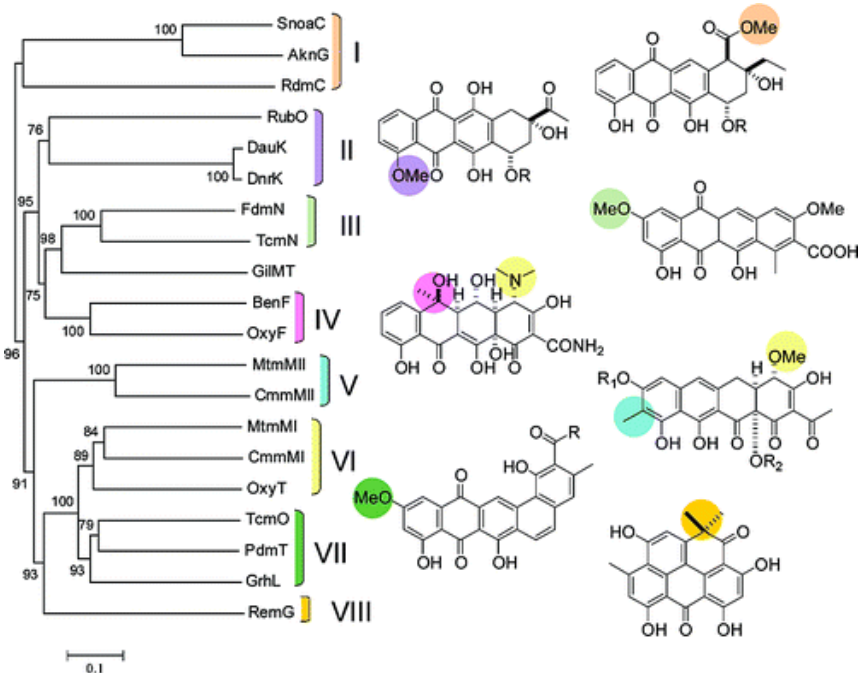

Figure 18. Phylogenetic tree of methyltransferases with their different target areas and methylation function [71].

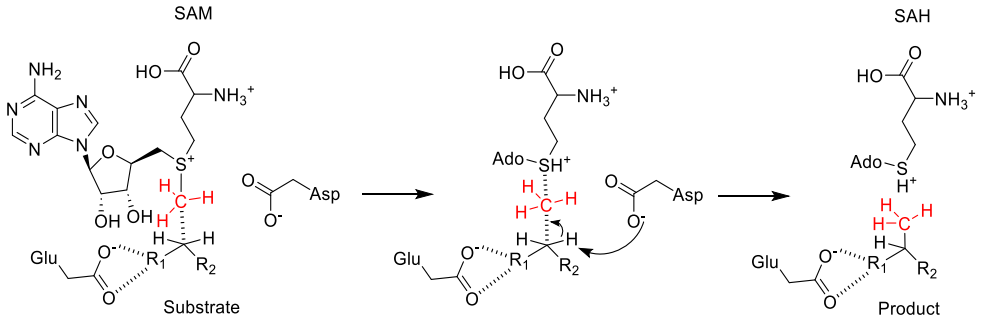

Figure 19. Schematic mechanism of a methyl group transfer.

In the biosynthesis of pentagumycin (22), an unusual angucyclinone polyketide from *Saccharothrix espanaensis*, an O-MT was discovered that can act on diverse intermediates [111]. Gummerlich *et al*. showed that methylation of C1-OH in pentagumycin (22) was performed by PenD (Figure 20). Intermediates discovered in knockout experiments with *penD* and other genes involved in pentagumycin biosynthesis suggested that methylation as well as the other modifications of the A-ring can be sequenced differently (Figure 20) [111]. Methylation by PenD can be the both the first and the last tailoring step in pentagumycin biosynthesis (Figure 20) [111].

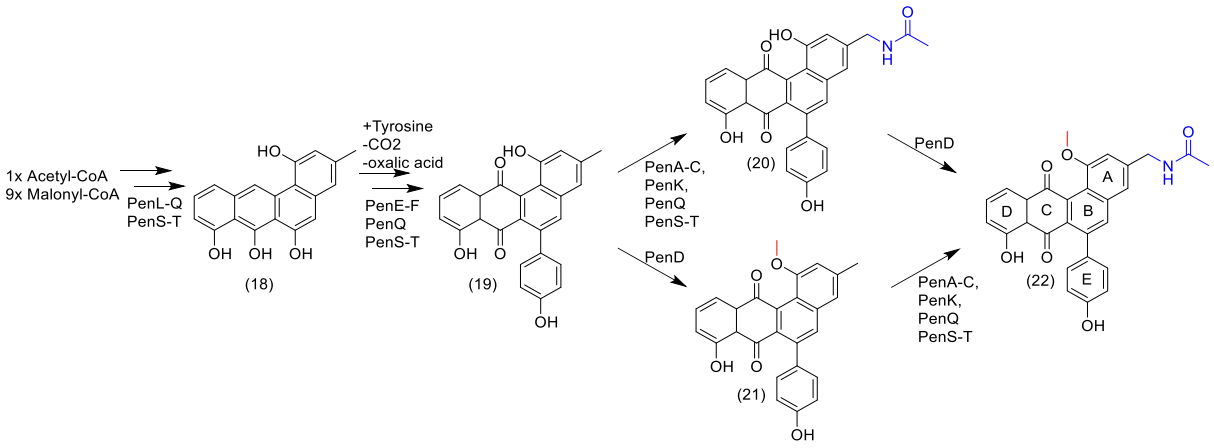

Figure 20. Biosynthesis of pentagumycin with the methylation as first (top) or last tailoring step (bottom).

During screening for aromatic polyketides in marine Actinobacteria from the Persian gulf, Matroodi *et al*. discovered persiamycin A (25) a tetracenomycin type polyketide that shows moderate antimicrobial activity [112]. The biosynthetic pathway was predicted in comparison to tetracenomycin biosynthesis (Figure 21) [112]. The polyketide core structure produced by the minimal PKS (Per1-3) is cyclized by PerB, PerD and PerC (Figure 21) [112]. The unique C9 decarboxylation by PerE differs from tetracenomycin biosynthesis (Figure 21 marked in blue) [112]. The following quinone syntehsis by the cofactor independent PerF, however, is again similar to tetracenomycin biosynthesis [112]. Unlike tetracenomycins, persiamycin A (25) is not *O*-methylated (Figure 21 marked in red) [112]. Instead PerG performs *C*-methylation at the C2 position (Figure 21 marked in red) [112].

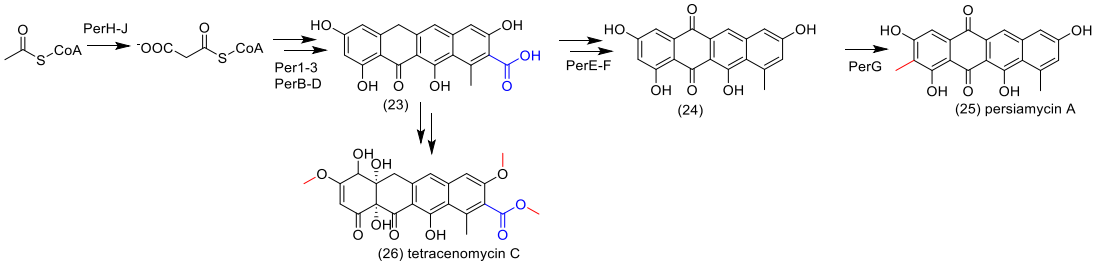

Figure 21. Proposed biosynthetic pathway of persiamycin A with tetracenomycin C as an example for tetracenomycins.

Huang *et al*. identified a T2PKS from a metagenomics library that, after expression in *S. albus* J1074, produced three new benz[*h*]isquinoline derivatives (32)-(34) (Figure 22). Having malonyl-CoA as the extender unit in a T2PKSs suggests that the methyl group at C1a (see Figure 22 compound 28 red) is derived from the tailoring step by a methyltransferase [113]. The putative methyltransferase gene *amdA* was identified in the so called *amd*-BGC [113]. The knockout experiments clarified the role of AmdA in the biosynthesis of the amodsemycins (32)/(33) [113]. The amodesmycin production was abolished and the demethylated side product compound (35) occurred (Figure 22) [113]. The methylation by AmdA is the first tailoring step in the amodsemycin biosynthesis [113]. The C1 carbon is oxidized by AmdP1-3 to form a formyl group[113]. This formyl group is nucleophilicly attacked by the amino group of desferrioamine B (31), followed by spontaneous dehydration and the third ring cyclization (Figure 22) [113]. These steps lead to the production of amodesmycin B (32) and later amodesmycin A (33) (Figure 22) [113].

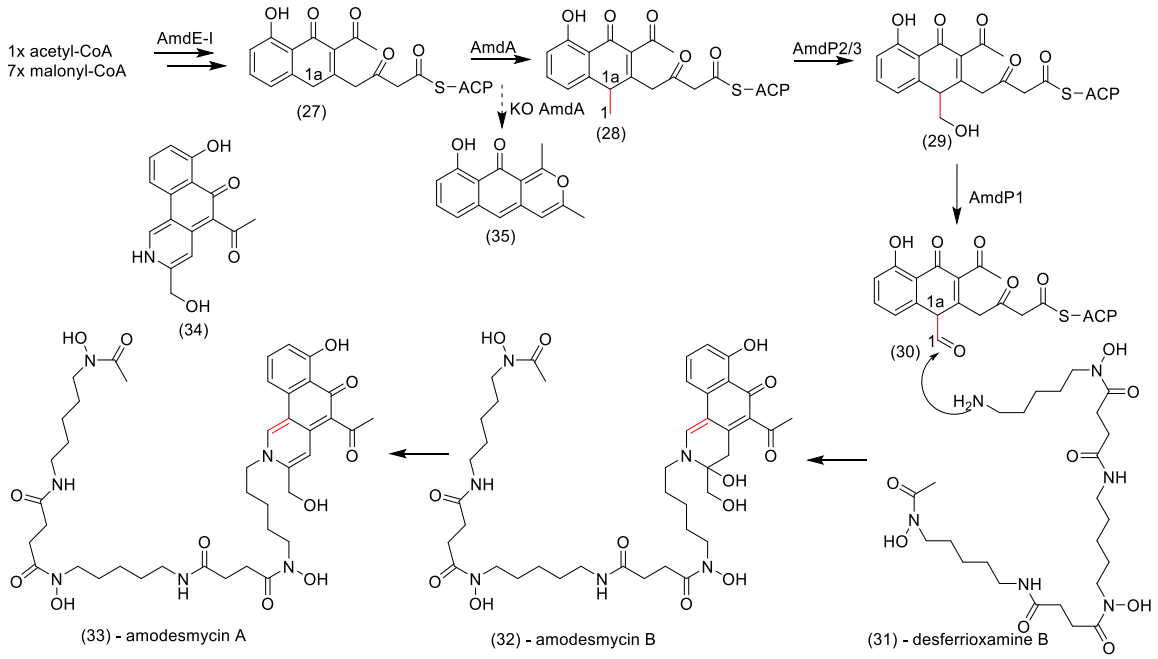

Figure 22. Proposed biosynthesis of amodesmycin A.

Up until now only three type II polyketide biosynthetic gene clusters have been discovered in gram negative bacteria [114-116]. A product of one of these BGCs is the anthraquinone AQ-256 from *Photorhabdus luminescens* that was discovered in 2007 [114]. Interestingly, the octaketide produced by the minimal PKS in AQ-256 biosynthesis is shortened by AntI to obtain a heptaketide (Figure 23) [117-119]. The heptaketide is cyclized and modified by oxidation to generate AQ-256 [114, 117]. In the wildtype strain *P. luminescens*, methylated derivatives were detected, but no methyltransferase encoding genes were found within the AQ-256 BGC (*ant*-BGC) [114]. Cummings *et al*. were able to express the *ant*-BGC in *E. coli* BL21 (DE3) resulting in production of AQ-256. For the methylation, the gene *ifmt* encoding an O-MT from *Medicago truncatula* was expressed in the *E. coli* host and the C8 methoxy compound, 1,3-dihydroxy-8-methoxyanthraquinone (neomedicamycin, AQ-270c) was identified [120]. In 2023, Huber *et al*. screened the genome of *P. luminescens* for methyltransferase genes using tBLAST (protein to translated nucleotides) [41]. They detected five *O*-methyltransferases encoding genes (*plu4890*, *plu4891*, *plu4892*, *plu4894* and *plu4895*) 0.8 Mb apart from the *ant* cluster [118]. Huber *et al*. tested the *in vitro* conversion of AQ-256 with all five methyltransferases separately. Plu4892 and Plu4894 did not show any activity regarding conversion of AQ-256 [118]. In the methylation experiments with Plu4890, Plu4891 and Plu4895, the monomethylated derivatives AQ-270a, AQ-270b and AQ-270c were discovered [118]. Plu4890 methylated the C8-OH group regiospecific, Plu4891 methylated the C3-OH group and Plu4895 methylated the C1-OH group, but the C3-OH group with a low efficiency as well (Figure 23) [118]. In further experiments the dimethylated derivatives AQ-284a-b were also observed (Figure 23) [118]. In the derivatives AQ-284a C1-OH and C3-OH and in AQ-284b C3-OH and C8-OH are methylated [118]. No C1-OH and C8-OH dimethylated compound was detected [118]. The low methylation rates in the experiments may be caused by strong regulation or by the missing optimization if the enzymes originate from another gene cluster that was perhaps lost in evolution [118].

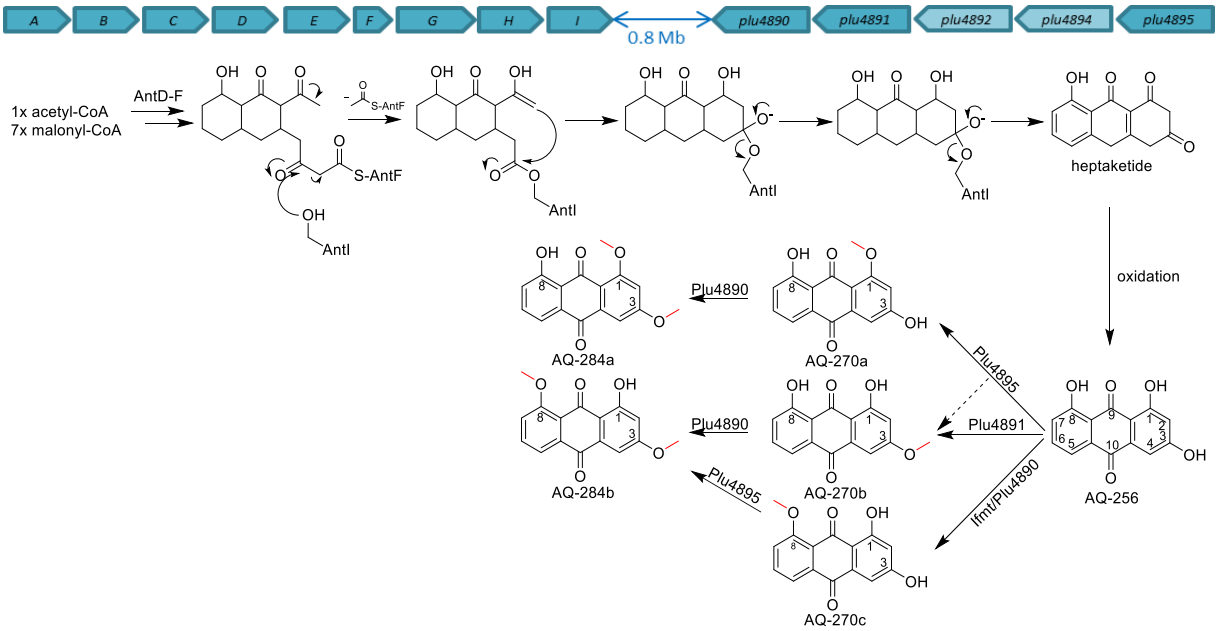

Figure 23. Schematic depiction of *ant*BGC with methyltransferase encoding genes 0.8 Mb apart of cluster responsible for tailoring of AQ-256 and biosynthesis of AQ-256 and its methylated derivatives.

In recent years SAM dependent methyltransferase-like proteins that show methylation activity as well as decarboxylation or hydroxylation activity were described in more detail [121]. Dinis *et al*. compared the *O*-methyltransferase DnrK with homologs that show site reactions or have lost their methyltransferase activity completely. The authors defined four regions that are important for the methyltransferase activity as well as the mutations in these regions that are responsible for the change of the methyltransferase activity towards decarboxylation or hydroxylation activity [121]. These regions are named R1, the N-terminal half of the α16 helix and its following loop, R2, the loop region between the β8 and β9 folds, R3, the loop region between the α11 and α12 helices, and R4, the SAM binding site (Figure 24) [121].

The helix of the R1 region is positioned parallel to the anthracycline-substrate near the C10 carboxyl group. An insertion of S298 triggers a rotation of F297 resulting in a solvent free active site [121, 122]. The mutation of highly conserved Y299 also leads to a solvent free active site [121]. A solvent free active site supports the 10-hydroxylation reaction instead of methylation and decarboxylation [121, 122]. The loop regions R2 and R3 are responsible for sugar binding [121]. A change within the orientation of the two loop regions to each other shifts the specificity towards more or less glycosylated substrates [121]. The SAM binding

site (R4 region) is conserved in the methyltransferase family [121]. The enzymes that favorably perform the 10-decarboxylation present an exception [121]. In these enzymes, two mutations of G189A/K190P are found [121]. This modification leads to a 1.8 Å shift in SAM positioning and the loss of methyltransferase activity [121]. Dinis *et al*. discovered 9,10-elimination activity caused by an interaction of highly conserved R285 (DnrK) with the substrate [121]. Dinis *et al*. presented events in the evolution of SAM-dependent methyltransferases that allowed these enzymes to diversify their catalytic spectra. They showed point mutations in four regions that are responsible for the change in the enzymes activity from methyltransferase to hydroxylase, decarboxylase or elimination activity [121].

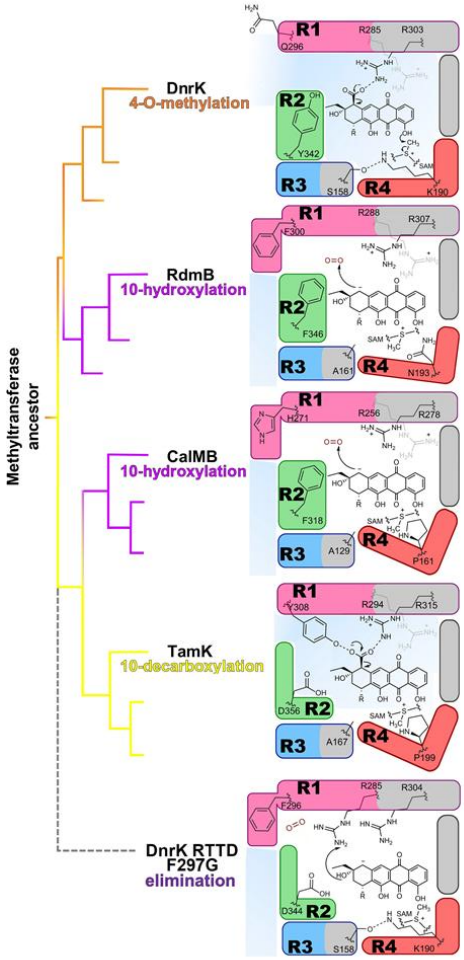

Figure 24. Schematic presentation of different activities harbored by SAM-dependent enzymes [121].

2 Outline of this study

Natural products are key elements in medical treatments. For the discovery and isolation of a vast majority of natural products *Streptomyces* and Actinomycetes continue to be a great source, because the natural products produced by these bacteria show a broad structural and bioactive range. A commonly used method for natural product discovery is the heterologous expression of biosynthetic gene clusters. Therefore in this work heterologous expression was used to discover and analyze biosynthetic gene clusters of Actinomycetes.

In the first project shown in this work, the known NRPS gene cluster 2D19, responsible for cyclohuinilsopeptin A synthesis, from the genome of *Kutzneria albida* DSM43870 was heterologously expressed in several new host strains. These experiments were performed in order to clarify the main product of this biosynthetic gene cluster. Furthermore, a wildtype knockout in the cyclohuinilsopeptin A biosynthetic gene cluster was performed to search for other compounds synthesized by this cluster.

In the second project the genome of *Streptomyces acidiscabies* LU19992 was screened for T2PKS BGCs to identify the cluster responsible for the antifungal agent oxanthromicin that was discovered in 1984 and rediscovered in the biomass extract of *S. acidiscabies* LU19992 in 2019. The oxanthromicin biosynthetic gene cluster was detected through heterologous expression of possible gene clusters in *S. albus* Del14 and *S. lividans* ΔYA8 as heterologous hosts. Through sequence analysis and gene deletion experiments the biosynthesis of oxanthromicin was solved. Intermediates and side products were isolated and analyzed through structure elucidation.

3 Material and Methods

3.1 General biological procedures

3.1.1 Media

Media for bacteria cultivation were mixed as shown in Table 1 and autoclaved before use.

Table 1. Media compositions.

Medium	Compounds	Contributor
DNPM [123]	40 g/L dextrin	Merck KGaA
	7.5 g/L bacto soytone	Sigma-Aldrich
	5 g/L fresh yeast	Dr.Oetker GmbH
	21 g/L MOPS (4-morpholinepropanesulfonic acid) adjusted to pH 6.8	Carl Roth GmbH & Co. KG
Lysogeny broth medium LB-medium	10 g/L tryptone	Sigma-Aldrich
	5 g/L yeast extract	Sigma-Aldrich
	5 g/L NaCl	Grüssing GmbH
	20 g/L agar for LB-Agar	Sigma-Aldrich
	1 L H_2O	
minimal medium	0.5 g K_2HPO_4	Th. Geyer GmbH & Co. KG
	0.2 g $MgSO_4$ x 7 H_2O	Grüssing GmbH
	0.01 g $FeSO_4$ x 7 H_2O	Carl Roth GmbH & Co. KG
	5 g/L mannitol	Sigma-Aldrich
	0.5 g NH_4SO_4	Merck KGaA
MS-Agar [124]	20 g/L mannitol	Sigma-Aldrich
	20 g/L low-fat soy	Sigma-Aldrich
	20 g/L agar	Sigma-Aldrich
	1 L H_2O	
SOC-medium (SOB-medium (super optimized broth) with glucose [125])	20 g/L Tryptone	Sigma-Aldrich
	5 g/L Yeast Extract	Sigma-Aldrich
	1 mL 5M NaCl	Grüssing GmbH
	1.25 mL 1M KCl	VWR international
	5 mL 1M $MgCl_2$	Grüssing GmbH
	5 mL 1M $MgSO_4$	Grüssing GmbH
	0.5 L H_2O	
	After autoclaving	
	add 10 mL 1M sterile glucose	Sigma-Aldrich
tryptic soy broth [123]	30 g/L tryptic soy broth	Sigma-Aldrich

3.1.2 Bacteria strains and cultivation

3.1.2.1 Cultivation of bacteria cultures

All strains used in this work are listed in Table 3 to Table 7. *Escherichia coli* strains were grown on LB-Agar (Table 1) at 37 °C and cultivated in LB-Medium at 37 °C and 180 rpm (Infors HT Multitron Humidity/CO2 Tripple Incubator Shaker, Infors HT, Bottmingen, CH) [126]. For transformation experiments with *E. coli,* SOC-Medium was used instead of LB-medium [125]. Actinomycete strains were grown on MS-Agar (Table 1) at 28 °C [124] except for LV1-625 which was grown on minimal medium agar (Table 1) at 28 °C. Overnight cultures of actinomycetes were prepared with 1 cm² mycelium of an agar plate on 15 mL in liquid tryptic soy broth (TSB) (Table 1) at 28 °C and 180 rpm [123]. DNPM was used as a production medium (Table 1) for 7 days at 28 °C and 180 rpm [123]. The flasks were induced with 1 mL of overnight culture. The cultivation for isolation and structure analysis of the compounds was performed as 10 L cultivation with 100 flasks with 100 mL DNPM medium each for 7 days at 28 °C and 180 rpm. As the preculture 5 flasks with 25 mL TSB each were used.

When required, the media were supplemented with antibiotics with working concentrations shown in Table 2. Production medium did not contain antibiotics.

Table 2. Antibiotics with stock solution and working concentration used in this work.

Antibiotic	Solvent	Stock solution [mg/mL]	Working concentration [mg/mL]	Contributor	Target
Ampicillin	H_2O	100	100	Carl Roth GmbH & Co. KG	*E. coli*
Apramycin	H_2O	100	50	AppliChem GmbH	*E. coli* and *Streptomycetes*
Chloramphenicol	Ethanol	25	50	Carl Roth GmbH & Co. KG	*E. coli*
Hygromycin	H_2O	50	100	Carl Roth GmbH & Co. KG	*E. coli* and *Streptomycetes*
Kanamycin	H_2O	100	50	Carl Roth GmbH & Co. KG	*E. coli*
Nalidixic Acid	1 N NaOH	100	50	Carl Roth GmbH & Co. KG	*E. coli*
Lincomycin	H_2O	100	100	Toronto Research Chemicals Inc.	*Streptomycetes*

3.1.2.2 Strains used in this work

The Actinomycetes strains of the LV strain collection were provided by the Microbial Culture Collection of Antibiotic Producers (MCCAP) of Ivan Franko National University of Lviv, Ukraine.

Table 3. General strains used in this work.

Strain	Description	Reference or source
Escherichia coli DH10β	General cloning strain	[127]
Escherichia coli ET12567 pUB307	Donor strain for intergeneric conjugation	[128]
Escherichia coli GB2005	*E. coli* DH10β with deletion of *fhuA*, *ybcC* and *recET*	[129]
Escherichia coli GB05 redCC	*E. coli* GB2005 with insertion of P_{BAD}-*gbaA* at *ybcC* locus	[129]
Kutzneria albida DSM 43870	A wild type strain; the source of the cyclohuinilsopeptin A cluster	[130]
LV1-4	A heterologous host strain;	MCCAP
LV1-18.2	A heterologous host strain;	MCCAP
LV1-22	A heterologous host strain;	MCCAP
LV1-144	A heterologous host strain;	MCCAP
LV1-166	A heterologous host strain;	MCCAP
LV1-208	A heterologous host strain;	MCCAP
LV1-209 notched (gekerbt)	A heterologous host strain;	MCCAP
LV1-209 smooth (glatt)	A heterologous host strain;	MCCAP
LV1-213	A heterologous host strain;	MCCAP
LV1-625	A heterologous host strain;	MCCAP
Streptomyces acidiscabies LU19992	A wild type strain; the source of the oxanthromicin cluster	[131]
Streptomyces albus Del14	A heterologous host strain; cluster-free derivative of the *S. albus* J1074	[16]
Streptomyces lividans ΔYA8	A heterologous host strain; cluster-free derivative of the *S. lividans* TK24	[17]

Table 4. Strains produced in the cyclohuinilsopeptin project.

Strain	Description
E. coli GB05 redCC 2D19	Derivative of *E. coli* GB05 redCC harboring the BAC 2D19 (containing the cyclohuinilsopeptin A cluster)
E. coli GB05 redCC 2D19 KO4	Derivative of *E. coli* GB05 redCC harboring the BAC 2D19 KO4
E. coli GB05 redCC 2D19 KO4 Int/Amp	Derivative of *E. coli* GB05 redCC harboring the BAC 2D19 KO4 Int/Amp
E. coli GB05 redCC 2D19 KO5	Derivative of *E. coli* GB05 redCC harboring the BAC 2D19 KO5
E. coli ET12567 pUB307 2D19	Derivative of *E. coli* ET12567 pUB307 harboring the BAC 2D19
E. coli ET12567 pUB307 2D19 KO4 Int/Amp	Derivative of *E. coli* ET12567 pUB307 harboring the BAC 2D19 KO4 Int/Amp
E. coli ET12567 pUB307 2D19 KO5	Derivative of *E. coli* ET12567 pUB307 harboring the BAC 2D19 KO5
S. albus Del14 2D19	Derivative of *S. albus* Del14 harboring the BAC 2D19
LV1-4 2D19	Derivative of LV1-4 harboring the BAC 2D19
LV1-18.2 2D19	Derivative of LV1-18.2 harboring the BAC 2D19
LV1-22 2D19	Derivative of LV1-22 harboring the BAC 2D19
LV1-144 2D19	Derivative of LV1-144 harboring the BAC 2D19
LV1-166 2D19	Derivative of LV1-166 harboring the BAC 2D19
LV1-208 2D19	Derivative of LV1-208 harboring the BAC 2D19
LV1-209 notched 2D19	Derivative of LV1-209 notched harboring the BAC 2D19
LV1-209 smooth 2D19	Derivative of LV1-209 smooth harboring the BAC 2D19
LV1-209 smooth 2D19 KO5	Derivative of LV1-209 smooth harboring the BAC 2D19 KO5
LV1-213 2D19	Derivative of LV1-213 harboring the BAC 2D19
LV1-625 2D19	Derivative of LV1-625 harboring the BAC 2D19
K. albida 2D19 KO4 Int/Amp	Derivative of *K. albida* harboring the BAC 2D19 KO4 Int
K. albida pKC1139	Derivative of *K. albida* harboring the plasmid pKC1139

Table 5. Strains produced in the *S. acidiscabies* project

Strain	Description
E. coli GB2005 1D11	Derivative of *E. coli* GB2005 harboring the cosmid 1D11
E. coli GB2005 2D04	Derivative of *E. coli* GB2005 harboring the cosmid 2D04
E. coli GB2005 9H08	Derivative of *E. coli* GB2005 harboring the cosmid 9H08
E. coli GB2005 18F05	Derivative of *E. coli* GB2005 harboring the cosmid 18F05
E. coli ET12567 pUB307 1D11	Derivative of *E. coli* ET12567 pUB307 harboring the cosmid 1D11
E. coli ET12567 pUB307 2D04	Derivative of *E. coli* ET12567 pUB307 harboring the cosmid 2D04
E. coli ET12567 pUB307 9H08	Derivative of *E. coli* ET12567 pUB307 harboring the cosmid 9H08
E. coli ET12567 pUB307 18F05	Derivative of *E. coli* ET12567 pUB307 harboring the cosmid 18F05
S. albus 1D11	Derivative of *S. albus* Del14 harboring the cosmid 1D11
S. albus 2D04	Derivative of *S. albus* Del14 harboring the cosmid 2D04
S. albus 9H08	Derivative of *S. albus* Del14 harboring the cosmid 9H08
S. albus 18F05	Derivative of *S. albus* Del14 harboring the cosmid 18F05
S. lividans 1D11	Derivative of *S. lividans* ΔYA8 harboring the cosmid 1D11
S. lividans 2D04	Derivative of *S. lividans* ΔYA8 harboring the cosmid 2D04
S. lividans 9H08	Derivative of *S. lividans* ΔYA8 harboring the cosmid 9H08
S. lividans 18F05	Derivative of *S. lividans* ΔYA8 harboring the cosmid 18F05

Table 6. *E. coli* strains produced in the oxanthromicin project.

Strain	Description
E. coli GB2005 1D11 LSHyg	Derivative of *E. coli* GB2005 harboring the cosmid 1D11 LSHyg
E. coli GB2005 1D11 RS1Hyg	Derivative of *E. coli* GB2005 harboring the cosmid 1D11 RS1Hyg
E. coli GB2005 1D11 RS1	Derivative of *E. coli* GB2005 harboring the cosmid 1D11 RS1
E. coli GB2005 1D11 RS2Hyg	Derivative of *E. coli* GB2005 harboring the cosmid 1D11 RS2Hyg
E. coli GB2005 1D11 KO0Hyg	Derivative of *E. coli* GB2005 harboring the cosmid 1D11 KO0Hyg
E. coli GB2005 1D11 KO0	Derivative of *E. coli* GB2005 harboring the cosmid 1D11 KO0
E. coli GB2005 1D11 KOCHyg	Derivative of *E. coli* GB2005 harboring the cosmid 1D11 KOC Hyg
E. coli GB2005 1D11 KOC	Derivative of *E. coli* GB2005 harboring the cosmid 1D11 KOC
E. coli GB2005 1D11 KODHyg	Derivative of *E. coli* GB2005 harboring the cosmid 1D11 KODHyg
E. coli GB2005 1D11 KOD	Derivative of *E. coli* GB2005 harboring the cosmid 1D11 KOD
E. coli GB2005 1D11 KOFHyg	Derivative of *E. coli* GB2005 harboring the cosmid 1D11 KOFHyg
E. coli GB2005 1D11 KOF	Derivative of *E. coli* GB2005 harboring the cosmid 1D11 KOF
E. coli GB2005 1D11 KOGHyg	Derivative of *E. coli* GB2005 harboring the cosmid 1D11 KOGHyg
E. coli GB2005 1D11 KOG	Derivative of *E. coli* GB2005 harboring the cosmid 1D11 KOG
E. coli GB2005 1D11 KOHHyg	Derivative of *E. coli* GB2005 harboring the cosmid 1D11 KOHHyg
E. coli GB2005 1D11 KOH	Derivative of *E. coli* GB2005 harboring the cosmid 1D11 KOH
E. coli GB2005 1D11 KOIHyg	Derivative of *E. coli* GB2005 harboring the cosmid 1D11 KOIHyg
E. coli GB2005 1D11 KOI	Derivative of *E. coli* GB2005 harboring the cosmid 1D11 KOI
E. coli GB2005 1D11 KOJHyg	Derivative of *E. coli* GB2005 harboring the cosmid 1D11 KOJHyg
E. coli GB2005 1D11 KOJ	Derivative of *E. coli* GB2005 harboring the cosmid 1D11 KOK
E. coli GB2005 1D11 KOKHyg	Derivative of *E. coli* GB2005 harboring the cosmid 1D11 KOKHyg
E. coli GB2005 1D11 KOK	Derivative of *E. coli* GB2005 harboring the cosmid 1D11 KOK
E. coli GB2005 1D11 KOLHyg	Derivative of *E. coli* GB2005 harboring the cosmid 1D11 KOLHyg
E. coli GB2005 1D11 KOL	Derivative of *E. coli* GB2005 harboring the cosmid 1D11 KOL
E. coli GB2005 1D11 KOMHyg	Derivative of *E. coli* GB2005 harboring the cosmid 1D11 KOMHyg
E. coli GB2005 1D11 KOM	Derivative of *E. coli* GB2005 harboring the cosmid 1D11 KOM
E. coli GB05 redCC 1D11 LSHyg	Derivative of *E. coli* GB05 redCC harboring the cosmid 1D11 LSHyg
E. coli GB05 redCC 1D11 RS1Hyg	Derivative of *E. coli* GB05 redCC harboring the cosmid 1D11 RS1Hyg
E. coli GB05 redCC 1D11 RS2Hyg	Derivative of *E. coli* GB05 redCC harboring the cosmid 1D11 RS2Hyg
E. coli GB05 redCC 1D11 RS1	Derivative of *E. coli* GB05 redCC harboring the cosmid 1D11 RS1
E. coli GB05 redCC 1D11	Derivative of *E. coli* GB05 redCC harboring the cosmid 1D11
E. coli GB05 redCC 1D11 KOC	Derivative of *E. coli* GB05 redCC harboring the cosmid 1D11 KOC
E. coli GB05 redCC 1D11 KOD	Derivative of *E. coli* GB05 redCC harboring the cosmid 1D11 KOD
E. coli GB05 redCC 1D11 KOF	Derivative of *E. coli* GB05 redCC harboring the cosmid 1D11 KOF
E. coli GB05 redCC 1D11 KOG	Derivative of *E. coli* GB05 redCC harboring the cosmid 1D11 KOG
E. coli GB05 redCC 1D11 KOH	Derivative of *E. coli* GB05 redCC harboring the cosmid 1D11 KOH
E. coli GB05 redCC 1D11 KOI	Derivative of *E. coli* GB05 redCC harboring the cosmid 1D11 KOI
E. coli GB05 redCC 1D11 KOJ	Derivative of *E. coli* GB05 redCC harboring the cosmid 1D11 KOJ
E. coli GB05 redCC 1D11 KOK	Derivative of *E. coli* GB05 redCC harboring the cosmid 1D11 KOK
E. coli GB05 redCC 1D11 KOL	Derivative of *E. coli* GB05 redCC harboring the cosmid 1D11 KOL
E. coli GB05 redCC 1D11 KOM	Derivative of *E. coli* GB05 redCC harboring the cosmid 1D11 KOM
E. coli ET12567 pUB307 1D11 LSHyg	Derivative of *E. coli* ET12567 pUB307 harboring the cosmid 1D11 LSHyg
E. coli ET12567 pUB307 1D11 RS1Hyg	Derivative of *E. coli* ET12567 pUB307 harboring the cosmid 1D11 RS1Hyg
E. coli ET12567 pUB307 1D11 RS2Hyg	Derivative of *E. coli* ET12567 pUB307 harboring the cosmid 1D11 RS2Hyg
E. coli ET12567 pUB307 1D11 KO0	Derivative of *E. coli* ET12567 pUB307 harboring the cosmid 1D11 KO0
E. coli ET12567 pUB307 1D11 KOC	Derivative of *E. coli* ET12567 pUB307 harboring the cosmid 1D11 KOC
E. coli ET12567 pUB307 1D11 KOD	Derivative of *E. coli* ET12567 pUB307 harboring the cosmid 1D11 KOD
E. coli ET12567 pUB307 1D11 KOF	Derivative of *E. coli* ET12567 pUB307 harboring the cosmid 1D11 KOF
E. coli ET12567 pUB307 1D11 KOG	Derivative of *E. coli* ET12567 pUB307 harboring the cosmid 1D11 KOG

E. coli ET12567 pUB307 1D11 KOH	Derivative of *E. coli* ET12567 pUB307 harboring the cosmid 1D11 KOH
E. coli ET12567 pUB307 1D11 KOI	Derivative of *E. coli* ET12567 pUB307 harboring the cosmid 1D11 KOI
E. coli ET12567 pUB307 1D11 KOJ	Derivative of *E. coli* ET12567 pUB307 harboring the cosmid 1D11 KOJ
E. coli ET12567 pUB307 1D11 KOK	Derivative of *E. coli* ET12567 pUB307 harboring the cosmid 1D11 KOK
E. coli ET12567 pUB307 1D11 KOL	Derivative of *E. coli* ET12567 pUB307 harboring the cosmid 1D11 KOL
E. coli ET12567 pUB307 1D11 KOM	Derivative of *E. coli* ET12567 pUB307 harboring the cosmid 1D11 KOM
E. coli GB2005 pRT801 1D11 KompC	Derivative of *E. coli* GB2005 harboring the plasmid pRT801 1D11 KompC
E. coli GB2005 pRT801 1D11 KompD	Derivative of *E. coli* GB2005 harboring the plasmid pRT801 1D11 KompD
E. coli GB2005 pRT801 1D11 KompF	Derivative of *E. coli* GB2005 harboring the plasmid pRT801 1D11 KompF
E. coli GB2005 pRT801 1D11 KompG	Derivative of *E. coli* GB2005 harboring the plasmid pRT801 1D11 KompG
E. coli GB2005 pRT801 1D11 KompH	Derivative of *E. coli* GB2005 harboring the plasmid pRT801 1D11 KompH
E. coli GB2005 pRT801 1D11 KompI	Derivative of *E. coli* GB2005 harboring the plasmid pRT801 1D11 KompI
E. coli GB2005 pRT801 1D11 KompJ	Derivative of *E. coli* GB2005 harboring the plasmid pRT801 1D11 KompJ
E. coli GB2005 pRT801 1D11 KompK	Derivative of *E. coli* GB2005 harboring the plasmid pRT801 1D11 KompK
E. coli GB2005 pRT801 1D11 KompL	Derivative of *E. coli* GB2005 harboring the plasmid pRT801 1D11 KompL
E. coli GB2005 pRT801 1D11 KompM	Derivative of *E. coli* GB2005 harboring the plasmid pRT801 1D11 KompM
E. coli ET12567 pUB307 pRT801 1D11 KompC	Derivative of *E. coli* ET12567 pUB307 harboring the plasmid pRT801 1D11 KompC
E. coli ET12567 pUB307 pRT801 1D11 KompD	Derivative of *E. coli* ET12567 pUB307 harboring the plasmid pRT801 1D11 KompD
E. coli ET12567 pUB307 pRT801 1D11 KompF	Derivative of *E. coli* ET12567 pUB307 harboring the plasmid pRT801 1D11 KompF
E. coli ET12567 pUB307 pRT801 1D11 KompH	Derivative of *E. coli* ET12567 pUB307 harboring the plasmid pRT801 1D11 KompH
E. coli ET12567 pUB307 pRT801 1D11 KompI	Derivative of *E. coli* ET12567 pUB307 harboring the plasmid pRT801 1D11 KompI
E. coli ET12567 pUB307 pRT801 1D11 KompK	Derivative of *E. coli* ET12567 pUB307 harboring the plasmid pRT801 1D11 KompK

Table 7. Actinomycete strains produced in the oxanthromicin project.

Strain	Description
S. albus 1D11 LSHyg	Derivative of *S. albus* Del14 harboring the cosmid 1D11 LSHyg
S. albus 1D11 RS1Hyg	Derivative of *S. albus* Del14 harboring the cosmid 1D11 RS1Hyg
S. albus 1D11 RS2Hyg	Derivative of *S. albus* Del14 harboring the cosmid 1D11 RS2Hyg
S. albus 1D11 KO0	Derivative of *S. albus* Del14 harboring the cosmid 1D11 KO0
S. albus 1D11 KOC	Derivative of *S. albus* Del14 harboring the cosmid 1D11 KOC
S. albus 1D11 KOD	Derivative of *S. albus* Del14 harboring the cosmid 1D11 KOD
S. albus 1D11 KOF	Derivative of *S. albus* Del14 harboring the cosmid 1D11 KOF
S. albus 1D11 KOG	Derivative of *S. albus* Del14 harboring the cosmid 1D11 KOG
S. albus 1D11 KOH	Derivative of *S. albus* Del14 harboring the cosmid 1D11 KOH
S. albus 1D11 KOI	Derivative of *S. albus* Del14 harboring the cosmid 1D11 KOI
S. albus 1D11 KOJ	Derivative of *S. albus* Del14 harboring the cosmid 1D11 KOJ
S. albus 1D11 KOK	Derivative of *S. albus* Del14 harboring the cosmid 1D11 KOK
S. albus 1D11 KOL	Derivative of *S. albus* Del14 harboring the cosmid 1D11 KOL
S. albus 1D11 KOM	Derivative of *S. albus* Del14 harboring the cosmid 1D11 KOM
S. albus 1D11 KOC KompC	Derivative of *S. albus* Del14 harboring the cosmid 1D11 KOC and the plasmid pRT801 1D11 KompC
S. albus 1D11 KOD KompD	Derivative of *S. albus* Del14 harboring the cosmid 1D11 KOD and the plasmid pRT801 1D11 KompD
S. albus 1D11 KOF KompF	Derivative of *S. albus* Del14 harboring the cosmid 1D11 KOF and the plasmid pRT801 1D11 KompF
S. albus 1D11 KOH KompH	Derivative of *S. albus* Del14 harboring the cosmid 1D11 KOH and the plasmid pRT801 1D11 KompH
S. albus 1D11 KOI KompI	Derivative of *S. albus* Del14 harboring the cosmid 1D11 KOI and the plasmid pRT801 1D11 KompI
S. albus 1D11 KOK KompK	Derivative of *S. albus* Del14 harboring the cosmid 1D11 KOK and the plasmid pRT801 1D11 KompK
LV1-4 1D11 KO0	Derivative of LV1-4 harboring the cosmid 1D11 KO0
LV1-18.2 1D11 KO0	Derivative of LV1-18.2 harboring the cosmid 1D11 KO0
LV1-22 1D11 KO0	Derivative of LV1-22 harboring the cosmid 1D11 KO0
LV1-144 1D11 KO0	Derivative of LV1-144 harboring the cosmid 1D11 KO0
LV1-166 1D11 KO0	Derivative of LV1-166 harboring the cosmid 1D11 KO0
LV1-208 1D11 KO0	Derivative of LV1-208 harboring the cosmid 1D11 KO0
LV1-209 notched 1D11 KO0	Derivative of LV1-209 notched harboring the cosmid 1D11 KO0
LV1-209 smooth 1D11 KO0	Derivative of LV1-209 smooth harboring the cosmid 1D11 KO0
LV1-213 1D11 KO0	Derivative of LV1-213 harboring the cosmid 1D11 KO0
LV1-625 1D11 KO0	Derivative of LV1-625 harboring the cosmid 1D11 KO0

3.1.2.3 Generation of competent cells

For the preparation of chemically competent cells three buffers were prepared: a 0.1 M $MgCl_2$ (magnesium chloride, Grüssing GmbH) buffer, a 0.1 M $CaCl_2$ (calcium chloride, Carl Roth GmbH & Co. KG) buffer and a 0.1 M $CaCl_2$ buffer with 15% glycerol (Merck KGaA). To prepare electrocompetent cells, water was used instead of the buffers.

Competent cells were resuspended in 900 µL LB medium. Dilutions of this solution were prepared and each dilution up to the 5^{th} was plated on a LB plate. After an overnight cultivation a single colony was picked and incubated in 100 mL LB (to *E. coli* ET12567 pUB307 50 µL kanamycin was added) overnight. 1 mL of the overnight culture was added to each of 8 flasks each with 100 mL LB (*E. coli* ET12567 pUB307 with 50 µL kanamycin added). These flasks were cultivated for about three hours to reach an OD_{600} of 0.6-0.8. The cells were separated from the culture broth by centrifugation (1 min, 4 °C, 6000 rcf). The cells were washed twice with the $MgCl_2$ buffer and then washed twice with the $CaCl_2$ buffer, once with the $CaCl_2$/glycerol buffer and subsequently the cells were resuspended in 5 mL $CaCl_2$/glycerol buffer. The resuspended competent cells were aliquoted to 80-100 µl. Electrocompetent cells were resuspended in 10% glycerol.

3.1.3 Genome mining and bioinformatics analysis

The *S. acidiscabies* LU19992 strain was screened for secondary metabolite biosynthetic gene clusters using the antiSMASH online tool V7.0 [132]. The NCBI BLAST analysis was used to assign functions to the genes [133]. For sequence analysis and primer generation the software Geneious 11.1.5 [134] was used.

3.1.4 DNA manipulation

3.1.4.1 Plasmids, cosmids and bacterial artificial chromosomes

All plasmids, cosmids and bacterial artificial chromosomes (BACs) used in this work are listed in Table 8. The cosmids 1D11, 2D04, 9H08 and 18F05 were isolated from a cosmid library comprising the genome of *Streptomyces acidiscabies* LU19992 [131]. The BAC 2D19 was isolated from a BAC library comprising the genome of *Kutzneria albida* DSM 43870 T [130].

Table 8. Plasmids, Cosmids and BACs used in this work.

Cosmid	Description	Reference or source
1D11	The cosmid containing 39 kb chromosomal fragment of *S. acidiscabies* LU19992; containing the oxanthromicin gene cluster	[131], BASF
1D11 LS1Hyg	The derivative of 1D11 with the deletion of the 20 kb DNA fragment upstream the *oxaA* gene and insertion of the hygromycin resistance gene	This work
1D11 RS1Hyg	The derivative of 1D11 with the deletion of the 6 kb DNA fragment downstream the *oxaM* gene and insertion of the hygromycin resistance gene	This work
1D11 RS1	The derivative of 1D11 RS1Hyg with the deletion of the hygromycin resistance gene	This work
1D11 RS2Hyg	The derivative of 1D11 with the deletion of the 7 kb DNA fragment downstream the *oxaL* gene and insertion of the hygromycin resistance gene	This work
1D11 LS1RS1Hyg	The derivative of 1D11 RS1 with the deletion of the 20 kb DNA fragment upstream the *oxaA* gene and insertion of the hygromycin resistance gene	This work
1D11 KO0	The derivative of 1D11 LS1RS1Hyg with the deletion hygromycin resistance gene	This work
1D11 KOC+Hyg	The derivative of 1D11 KO0 with insertion of the hygromycin resistance gene and the deletion of the *oxaC* gene	This work
1D11 KOC	The derivative of 1D11 KOC+Hyg with deletion of the hygromycin resistance gene	This work
1D11 KOD+Hyg	The derivative of 1D11 KO0 with insertion of the hygromycin resistance gene and the deletion of the *oxaD* gene	This work
1D11 KOD	The derivative of 1D11 KOD+Hyg with deletion of the hygromycin resistance gene	This work
1D11 KOF+Hyg	The derivative of 1D11 KO0 with insertion of the hygromycin resistance gene and the deletion of the *oxaF* gene	This work
1D11 KOF	The derivative of 1D11 KOF+Hyg with deletion of the hygromycin resistance gene	This work
1D11 KOG+Hyg	The derivative of 1D11 KO0 with insertion of the hygromycin resistance gene and the deletion of the *oxaG* gene	This work
1D11 KOG	The derivative of 1D11 KOG+Hyg with deletion of the hygromycin resistance gene	This work
1D11 KOH+Hyg	The derivative of 1D11 KO0 with insertion of the hygromycin resistance gene and the deletion of the *oxaH* gene	This work
1D11 KOH	The derivative of 1D11 K KOH+Hyg with deletion of the hygromycin resistance gene	This work
1D11 KOI+Hyg	The derivative of 1D11 KO0 with insertion of the hygromycin resistance gene and the deletion of the *oxaI* gene	This work

1D11 KOI	The derivative of 1D11 KOI+Hyg with deletion of the hygromycin resistance gene	This work
1D11 KOJ+Hyg	The derivative of 1D11 KO0 with insertion of the hygromycin resistance gene and the deletion of the *oxaJ* gene	This work
1D11 KOJ	The derivative of 1D11 KOJ+Hyg with deletion of the hygromycin resistance gene	This work
1D11 KOK+Hyg	The derivative of 1D11 KO0 with insertion of the hygromycin resistance gene and the deletion of the *oxaK* gene	This work
1D11 KOK	The derivative of 1D11 KOK+Hyg with deletion of the hygromycin resistance gene	This work
1D11 KOL+Hyg	The derivative of 1D11 KO0 with insertion of the hygromycin resistance gene and the deletion of the *oxaL* gene	This work
1D11 KOL	The derivative of 1D11 KOL+Hyg with deletion of the hygromycin resistance gene	This work
1D11 KOM+Hyg	The derivative of 1D11 KO0 with insertion of the hygromycin resistance gene and the deletion of the *oxaM* gene	This work
1D11 KOM	The derivative of 1D11 KOM+Hyg with deletion of the hygromycin resistance gene	This work
pACS-hyg	The plasmid containing hygromycin resistance gene	[135]
pUC19	The plasmid containing ampicillin resistance gene	[136]
pKC1139	The plasmid containing the temperature-sensitive origin of replication from pSG5	[137]
cos15A_gus	General cloning cosmid	[138]
pRT801_cat_ampery	Derivative of pRT801 ([139] BT1 integrative vector for Streptomyces strains with apramycin resistance), containing promotor TS81 and chloramphenicol resistance, Apramycin resistance was substituted with ampicillin-erythromicin resistance cassette.	[140]
pRT801 1D11 KompC	Derivative of pRT801_cat_ampery with insertion of the *oxaC* gene	This work
pRT801 1D11 KompD	Derivative of pRT801_cat_ampery with insertion of the *oxaD* gene	This work
pRT801 1D11 KompF	Derivative of pRT801_cat_ampery with insertion of the *oxaF* gene	This work
pRT801 1D11 KompG	Derivative of pRT801_cat_ampery with insertion of the *oxaG* gene	This work
pRT801 1D11 KompH	Derivative of pRT801_cat_ampery with insertion of the *oxaH* gene	This work
pRT801 1D11 KompI	Derivative of pRT801_cat_ampery with insertion of the *oxaI* gene	This work
pRT801 1D11 KompJ	Derivative of pRT801_cat_ampery with insertion of the *oxaJ* gene	This work
pRT801 1D11 KompK	Derivative of pRT801_cat_ampery with insertion of the *oxaK* gene	This work
pRT801 1D11 KompL	Derivative of pRT801_cat_ampery with insertion of the *oxaL* gene	This work
pRT801 1D11 KompM	Derivative of pRT801_cat_ampery with insertion of the *oxaM* gene	This work
2D04	The cosmid containing a 34 kb chromosomal fragment of *S. acidiscabies* LU19992.	[131], BASF
2D19	The BAC containing a 95.6 kb chromosomal fragment of *K. albida* DSM 43870 T. The BAC contains the cyclohuinilsopeptin gene cluster.	[130, 140]
2D19 KO4	Derivative of the BAC 2D19 with insertion of hygromycin resistance gene and deletion of KALB_5512 (NRPS gene)	[140]
2D19 KO4 Int/Amp	Derivative of the BAC 2D19 KO4 with insertion of ampicillin resistance and deletion of integrase gene	This work
2D19 KO5	Derivative of the BAC 2D19 with insertion of hygromycin resistance gene and deletion of KALB_5514 (gene encoding for a radical SAM protein)	[140]
9H08	The cosmid containing a 31 kb chromosomal fragment of *S. acidiscabies* LU19992.	[131], BASF
18F05	The cosmid containing a 31 kb chromosomal fragment of *S. acidiscabies* LU19992. The cosmid contains the desmethylmensacarcin B gene cluster.	[131], BASF

3.1.4.2 Primers

All primers used in this work are listed in Table 9.

Table 9. Primers used in this work.

Primer name	Primer sequence
KORS1F	ATGAGCGGCATCCTCGGAACGCGCCCGGCCGTGGCCCACCCCGCCACCCCGTAT ACAATACTTGACATATCACTGT
KORS1R	GCCAGCGCGAGCGGCTCAGGACCGAGGGGCCGGCCGACGCGCAGGTCTCCGTTT AAACTCAGGCGCCGGGGGCGGTGT
KORS2F	ATGACGATCCAGGAAAAGGACATCACCGATCACGGTGCGATCATCGGGGTGTAT ACAATACTTGACATATCACTGT
KORS1chkR	CCCGACAGCAGGTTCTTCAT
KORS2chkR	CCTTTCCACCGTGTCCTTGA
CosmidchkFW	GATCTCCATCGACTAAACGT
KOLS1F	CCACCCGGTCTGGACGGTGCGCCCGGAACACGCCGACGCCTACGCGGCCTGTAT ACAATACTTGACATATCACTGT
KOLS1R	TCAGGAAGAACCGGATTCTCCGGTGCGCAGCAGTGCCTGTACCCGGAAACGTTT AAACTCAGGCGCCGGGGGCGGTGT
KOLS1chkF	CATTGCCGCCGGATTGAAAT
CosmidchkRev	GTTAACTGCGGTCAAGATAT
KOCF	ATGAGCCAGGGAACAGACGTCAGCTACATGAAGGAACTGCACAGCGATTCAGT ATACAATACTTGACATATCACTGT
KOCR	TCAGGCCGGTTCCGCGATGACCACGCTCGACGGGAGCGCCCGCCCGATCGGTTT AAACTCAGGCGCCGGGGGCGGTGT
KOCchkF	CCAGGTGGACGTGGTCTTC
KOCchkR	GATGCCGATCTCCGCTATCG
KODF	ATGACCGATCAGACAGCGGGTGCCCCGGCCGACAGCGGTCGCGATGAAGCCGTA TACAATACTTGACATATCACTGT
KODR	TCACTGGGCCGGGGCGGCGATGACCACGCTCGACGGCGCGTTCAGGCCGAGTTT AAACTCAGGCGCCGGGGGCGGTGT
KODchkF	CCGACGAAGATCCTGGACAG
KODchkR	TGTTCATCGTGCCTCCAGTC
KOFF	ATGAACACGCCCGAGATCCACGCGCGCCACGAGACCGAGATCGACTCCCCGGTA TACAATACTTGACATATCACTGT
KOFR	TCACGGGGCACCGACCGACGCGGAGTACCGGTCCGCGTGCTGCATCGTGAGTTT AAACTCAGGCGCCGGGGGCGGTGT
KOFchkF	GTGACGAAACGAGCAGAGGA
KOFchkR	CGCAGGTAGCTCTCCATCTG
KOGF	GTGAGCACCGAGGTACGCGCACCGCTCGGCCGCCTGCGCGAACTGGCGGACGTA TACAATACTTGACATATCACTGT
KOGR	CTAGGCCAGGCACGTCGGCAGGCGGCCGTCGTTGAACTGGACCATCTCGTGTTTA AACTCAGGCGCCGGGGGCGGTGT
KOGchkF	TGGTCCTCGAACACAGCTTC
KOGchkR	GGGTGAAGGTGAATCCCTGG
KOHF	ATGACGATGCCGGCCGAGGGGACAACGGTGTCCCCCGAGACCTTCTACGAGGTA TACAATACTTGACATATCACTGT
KOHR	TCAACCTAGGGGAACGCTCTGTTTTCCGGTGTCCAGGCGGCCGAGGTCGTGTTTA AACTCAGGCGCCGGGGGCGGTGT
KOHchkF	GTGACGTTCACCGAGACCAT
KOHchkR	TTGTCGGAGCTGACCAGTTC
KOIF	ATGGACAACACGGTCACCACCGGCAAAGGAACCGCTCCGGCCGAAGTGTGCGT ATACAATACTTGACATATCACTGT

KOIR	TCATGTGCCGCTCCCCCGCTGCGCGACCGCGAGGAGGTCGTCGCGGGTGAGTTTA AACTCAGGCGCCGGGGGCGGTGT
KOIchkF	GGTACCCAAGTCGGAGTTCG
KOIchkR	ATCGGTGTCGTGTCGATCAG
KOJF	ATGACGTCCCTGCGAGGCAGCCTGGGCGGGGCCGTGCTGGGCCCCGGGGACGTA TACAATACTTGACATATCACTGT
KOJR	TCAGCGGTGCGTGACGATCTCATTCCCCTGATCGTCTTTGCCGTGCGGGCGTTTAA ACTCAGGCGCCGGGGGCGGTGT
KOJchkF	GACGGCACTTCGTGTTCAAC
KOJchkR	GAGCGTGGTCTGTACACTCC
KOKF	GTGGACATTCATATACTCGGGTCGTTGTCGTTATCGGAGCACGGTCGCGACGTAT ACAATACTTGACATATCACTGT
KOKR	TCAGGCCCCGCGGGCGGTGACTCCGTCGAGGGCGGGGTCCCCGTCCAGGAGTTT AAACTCAGGCGCCGGGGGCGGTGT
KOKchkF	GGCAAAGACGATCAGGGGAA
KOKchkR	CAACACCAACCTGAACAGCG
KOLF	ATGGCACAGGAAAACGCCCGGGCAGCTCTTGTCACGGGTGCCACGAGCGGTGTA TACAATACTTGACATATCACTGT
KOLR	CTAGTAGTTGCCCAGCCCCCCGCACACGTTCATCGCCTGGGCCGTCACCAGTTTA AACTCAGGCGCCGGGGGCGGTGT
KOLchkF	ATGAAGAACCTGCTGTCGGG
KOLchkR	AGACCACGCTCCAGACCTAT
KOMF	ATGACGATCCAGGAAAAGGACATCACCGATCACGGTGCGATCATCGGGGTGGTA TACAATACTTGACATATCACTGT
KOMR	TCATGTCGAGGGTGCCGCCTCCAGGAGATGCAGGTACGAGTTCACGGGCCGGTTT AAACTCAGGCGCCGGGGGCGGTGT
KOMchkR	CCTTTCCACCGTGTCCTTGA
IntAmpF	ATGACACAAGGGGTTGTGACCGGGGTGGACACGTACGCGGGTGCTTACGACGTC AGGTGGCACTTTTCG
IntAmpR	CTACGCCGCTACGTCTTCCGTGCCGTCCTGGGCGTCGTCTTCGTCGTCGTTTACCA ATGCTTAATCAGTG
IntChkF	GTTTGGCCTCCGACTAACGA
IntChkR	TGGGAGAGATCAGGGGAGTG
pRT801F	GCCACCCTGAGACGAAGAAA
pRT801R	TACCGCCTTTGAGTGAGCTG
KompCF	AAAAGAGCTCATTGGCACGACTGCCCGGAA
KompCR	AAAAGATATCTCAGGCCGGTTCCGCGATGA
KompDF	AAAAGAGCTCCGACATCCAGCGGGAGTGGA
KompDR	AAAAGATATCTCACTGGGCCGGGGCGGCGA
KompFF	AAAAGAGCTCAGCACAAGGGCGAACCGGAC
KompFR	AAAAGATATCTCACGGGGCACCGACCGACG
KompGF	AAAAGAGCTCGGACCGGTACTCCGCGTCGG
KompGR	AAAAGATATCCTAGGCCAGGCACGTCGGCA
KompHF	AAAAGAGCTCTGCCGACGTGCCTGGCCTAG
KompHR	AAAAGATATCTCAACCTAGGGGAACGCTCT
KompIF	AAAAGAGCTCGAGCGTTCCCCTAGGTTGAG
KompIR	AAAAGATATCTCATGTGCCGCTCCCCCGCT
KompJF	AAAACATATGCCTCGCGGTCGCGCAGCGGG
KompJR	AAAAGATATCTCAGCGGTGCGTGACGATCT
KompKF	AAAAGAGCTCCAAATTCCGAAAAAGATCGG

KompKR	AAAAGATATCTCAGGCCCCGCGGGCGGTGA
KompLF	AAAACATATGGACGATGGTGCTCTCATCCT
KompLR	AAAAGATATCCTAGTAGTTGCCCAGCCCCC
KompMF	AAAACATATGGAAAAACAAAGGTTGCGAAC
KompMR	AAAAGATATCTCATGTCGAGGGTGCCGCCT

3.1.4.3 Plasmid, Cosmid and BAC isolation

Plasmids and cosmids were isolated with the same protocol. The protocol for BAC isolation was slightly different. The isolation buffers were prepared as shown in Table 10.

Table 10. Buffers for plasmid, cosmid and BAC isolation.

Buffer	Compounds	Distributer
1M Tris-HCl	12.11 g Tris base (tris(hydroxymethyl)aminomethane) filled to 100 mL H_2O adjusted to pH 8 by HCl	Merck KGaA
0.5M EDTA	18.6 g Na_2EDTA x 2 H_2O (disodium ethylenediaminetetracetic acid) 5 mL 10N NaOH filled to 100 mL H_2O adjusted to pH 8	 Carl Roth GmbH & Co. KG Carl Roth GmbH & Co. KG
Buffer I / TE-buffer (plasmid isolation)	12.5 mL 1M Tris-HCl buffer 10 mL 0.5M EDTA 477.5 mL H_2O	Merck KGaA Carl Roth GmbH & Co. KG
Buffer I / TE-buffer (BAC isolation)	5 mL 1M glucose 2.5 mL 1M Tris 2 mL 0.5M EDTA 490.5 ml H_2O	Sigma-Aldrich Merck KGaA Carl Roth GmbH & Co. KG
Buffer II / lysis buffer	10 mL 10% SDS (sodium dodecyl sulfate) 20 mL 10N NaOH	Carl Roth GmbH & Co. KG Carl Roth GmbH & Co. KG
Buffer III / neutralization buffer	5M CHCOOK (29.5 g CHCOOK in 60 mL H_2O) (potassium acetate) 11.5 mL glacial acetic acid in 100 mL H_2O	Sigma-Aldrich Carl Roth GmbH & Co. KG

For the plasmid isolation, cells were scratched from a preculture plate and resuspended in 100 µL TE-buffer. to inactivate DNases. 200 µL lysis buffer were added, the solution was mixed carefully to break open the cells, 350 µL Buffer III were added and the solution was again mixed carefully to neutralize the lysis buffer and precipitate proteins and genomic DNA. The solution was centrifuged (10 min, 4 °C, 21300 rcf) to separate the DNA from the cell debris. The supernatant was mixed with 600 µL isopropanol to precipitate the DNA, centrifuged and the supernatant discarded. The DNA was washed twice with 500 µL ethanol, dried and dissolved in 30 µL H_2O.

For the BAC isolation, an overnight culture of the strain was prepared in 15 mL LB-medium with 3.75 µL apramycin and 15 µL 10% L-arabinose solution (Carl Roth GmbH & Co. KG). 6 mL of the culture were spun down and the cells were taken for BAC isolation. The cells were resuspended in 250 µL TE-buffer. To the solution 250 µL lysis buffer were added and the solution was mixed to lyse the cells. Then 350 µl neutralization buffer were added, the solution was mixed to precipitate genomic DNA and proteins and then centrifuged (4 min, 4 °C, 21300 rcf). The supernatant was mixed with 600 mL isopropanol, centrifuged, the supernatant discarded and the DNA washed twice with 500 µL ethanol, dried and dissolved in 30 µL H_2O.

3.1.4.4 Plasmid check through restriction mapping and sequencing

Plasmids, cosmids and BACs were tested after each manipulation step through restriction mapping and sequencing. For this purpose, the vectors were isolated as shown in chapter 3.1.4.3. The isolated vectors were digested with restriction enzymes to generate specific DNA fragmentation patterns that were compared with each other as well as compared to predictions from in silico fragmentation by Geneious 11.1.5 software [134].

For the digestion, 2 µL vector DNA were mixed with 2 µL enzyme specific Thermo Scientific™ 10x buffer, 1 µL RNase, 1 µL Thermo Scientific™ restriction enzyme (Table 11) and the solution filled up to 20 µL with MilliQ®-water (MQ) (Merck Millipore, Burlington, MA, USA). The digestion mixture was incubated at 37 °C for two hours. Afterwards restriction mapping was performed via gel electrophoresis (90 minutes at 110 V, 250 A and 15 W with a Consort EV series power supply). As a reference the Thermo Scientific™ GeneRuler 1 kb DNA was used. The gel was stained with ethidium bromide for five minutes and examined under UV-light in a Bio-Rad GelDoc Go System (Bio-Rad Laboratories, Inc., Hercules, CA, USA).

Table 11. Restriction enzymes of Thermo Fischer Scientific Inc., Waltham, MA, USA, with restriction site and corresponding buffer.

restriction enzyme	restriction site indicated by arrows	10x buffer
*Bam*HI	5' G↓G A T C C 3' 3' C C T A G↑G 5'	*Bam*HI
*Bst*1107I	5' G T A↓T A C 3' 3' C A T↑A T G 5'	orange
*Eco*RV	5' G A T↓A T C 3' 3' C T A↑T A G 5'	red
*Kpn*I	5' G G T A C↓C 3' 3' C↑C A T G G 5'	*Kpn*I
*Mss*I	5' G T T T↓A A A C 3' 3' C A A A↑T T T G 5'	blue
*Nde*I	5' C A↓T A T G 3' 3' G T A T↑A C 5'	orange
*Pvu*II	5' C A G↓C T G 3' 3' G T C↑G A C 5'	green
*Sac*I	5' G A G C T↓C 3' 3' C↑T C G A G 5'	*Sac*I

For sequencing, the genomic DNA on the verge to the vector's backbone was inspected. Therefore, a polymerase chain reaction (PCR) with the cosmid as the template and the primers CosmidchkFW and CosmidchkRev, respectively, was performed. The PCR was performed with a temperature gradient of 60±6 °C. A master mix for 12 reactions of 50 µL each was prepared as shown in Table 12. The PCR program was as follows:

- 3 min initial denaturation at 95 °C,
- 30 cycles: - 45 s denaturation at 95 °C,
  - 30 s annealing at the gradient temperatures 60±6 °C
  - 60 s extension at 72 °C
- 10 min final extension at 72 °C.

The success of the PCR was verfied by gel electrophoresis. Suitable PCR reactions were combined and then purified via gel electrophoresis by eluting the DNA out of the agarose gel with the Qiagen QIAprep Spin Miniprep Kit (Qiagen N. V., Venlo, NL).

Table 12. PCR mastermix for 12 reactions of 50 µL.

Volume	Compound	Distributer
497 µL	Milli-Q water	Merck Millipore – Merck KGaA
65 µL	Thermo Scientific™ DreamTaq-buffer	Thermo Fischer Scientific Inc.
32.5 µL	DMSO (dimethyl sulfoxide)	Carl Roth GmbH & Co. KG
13 µL	dNTPs (100 mM dATP, dCTP, dGTP and dTTP each)	Thermo Fischer Scientific Inc.
13 µL	Template DNA	
13 µL	Forward primer (CosmidchkFW)	Eurofins Scientific SE
13 µL	Reversed primer (CosmidchkRev)	Eurofins Scientific SE
3.5 µL	Thermo Scientific™ DreamTaq polymerase	Thermo Fischer Scientific Inc.

3.1.4.5 Gene transfer through transformation

Chemical Transformation was used for *E. coli* ET12567 pUB307. Electroporation was used to transform *E. coli* Gb2005 and *E. coli* GB05 redCC. Competent cells were slowly defrosted and 2.5 µL DNA were mixed to the cell suspension. For chemical transformation the cells were incubated for 60 min on ice, before the cells were heat shocked at 42 °C. For electroporation the DNA was added, mixed with the cells and the cells were pulsed with 1.8 kV in the electroporator. After heat shock or electroporation respectively, the cells were resuspended in 1 mL SOC medium and then incubated in a thermoshaker with 850 rpm for one hour at 37 °C. The cells were plated to LB agar with the appropriate antibiotic and incubated at 37 °C overnight. The next day, single colonies were picked, plated and analyzed for the correct cosmids as shown above.

3.1.4.6 Cosmid manipulation through RedET recombination

For the analysis of the biosynthetic pathway of oxanthromicin, single genes of the BGC were deleted by RedET recombination [141-143]. The homologous recombination that builds the basis for this recombination allows a specific deletion, insertion or substitution of DNA sequences at the desired positions without the need of restriction sites [142]. RedET recombination was performed with the strain *E. coli* GB05 redCC. This is a modified *E. coli* GB2005 strain with the insertion of P_{BAD}-*gbaA* at *ybcC* locus [129]. In the oxanthromicin project the genes were substituted with a hygromycin resistance gene [135, 144] to delete them. Hygromycin B is an antibiotic that inhibits protein biosynthesis [145].

The hygromycin resistance cassette was prepared by a PCR with the pACS-hyg-plasmid [135] as the template and specifically designed primers with homolog regions for both the specific gene to be deleted as well as the hygromycin resistance gene. The PCR was performed as described in chapter 3.1.4.4.

For RedET recombination, the cosmid that harbors the targeted gene for deletion was transformed into *E. coli* GB05 redCC. The cells were incubated at 37 °C on a LB-plate with antibiotics (depending on the cosmids backbone) over night and a single colony was then picked and incubated in an overnight culture of 15 mL LB with 3.75 µL antibiotic at 37 °C and 180 rpm. 300 µL of the overnight culture were added to 14 mL LB. The fresh culture was incubated at 37 °C at 180 rpm for 2 h to reach an OD_{600} of about 0.4-0.5. To induce the culture 400 µL 10% L-rhamnose solution (Carl Roth GmbH & Co. KG) were added. The culture was incubated for another 45 min at 37 °C at 180 rpm to reach an OD_{600} of about 0.7-0.9. 3 mL of this culture were centrifuged, washed twice with sterile MQ-water and resuspended in 100 µL sterile MQ-water. 2 µL eluted PCR-product with the hygromycin resistance cassette (with homolog sequences to the target scene) were added to the resuspended cells and mixed. The mixture was pulsed with 1.8 kV in the electroporator. Subsequently, the cells were resuspended in 1 mL SOC medium. The culture was incubated in a thermo shaker at 37 °C with 850 rpm for an hour and cultivated on an LB-plate with hygromycin overnight. Four single colonies were picked and plated on a new plate overnight. The strains were tested for the desired cosmids with restriction mapping and sequencing after cosmid isolation (chapter 3.1.4.4).

In the desired cosmids, the hygromycin cassette was deleted prior to conjugation in heterologous host strains. For this purpose, the primers used harbored restriction sites for the enzymes *Mss*I and *Bst*1107I. Neither of these restrictions sitesare present within the cosmids. The first step in deleting the hygromycin cassette was an overnight reaction of a 100 µL scale digestion. For the big scale digestion reaction 30 µL cosmid-DNA, 10 µL Thermo Scientific™ 10x buffer blue, 2 µL RNase, 4 µL Thermo Scientific™ *Mss*I-restriction enzyme and 54 µL MQ-water were mixed and incubated at 37 °C over night. The DNA was precipitated by adding 25 µL of 3 M NaAc pH 5.5 (sodium acetate, Carl Roth GmbH & Co. KG), 25 µL 5 M NaCl (sodium chloride, Grüssing GmbH) and 500 µL isopropanol. The solution was mixed, incubated at -80 °C for 30 min and centrifuged (30 min, 0 °C, 21300 rcf). The DNA was washed with cold MQ-water twice (including 30 min incubation at -80 °C and centrifugation at 0 °C and 21300 rcf), dried and redisolved in 86 µL MQ-water. 10 µL Thermo Scientific™ 10x buffer orange and 4 µL Thermo Scientific™ *Bst*1107I-restriction enzyme were added to the solution with the cosmid that had been cut once thus far. The solution was mixed carefully, incubated at 37 °C overnight and precipitated as described above. The dried DNA was resolved in 24 µL MQ-water. The cosmid was cyclized without the hygromycin cassette through ligation with 3 µL Thermo Scientific™ T4-ligation buffer and 3 µL Thermo Scientific™ T4-ligase. Ligation was performed at 18 °C over night without shaking. The ligation product was transformed in electrocompetent *E. coli* GB2005. The resulting cosmid was isolated from the strain, analyzed with restriction mapping and sequencing to choose the colonies with the desired sequence.

In the cyclohuinilsopeptin project the integrase gene of the BACs backbone was substituted by an ampicillin resistance gene through RedET recombination. The ampicillin resistance gene was multiplied from the linearized plasmid pUC19 through PCR with the primers IntAmpF and IntAmpR [136]. The multiplied gene was purified and used as the target for RedET recombination in the BAC 2D19 KO4 to produce the BAC 2D19 KO4 Int/Amp. The received BACs were screened for the desired sequence.

3.1.4.7 Intergenomic gene transfer through Conjugation

As described in chapter 1.1, heterologous expression is a key mechanism to discovery and analysis natural products. To prepare for conjugation, the host strain was cultivated on an agar plate until it produced spores (approximately one week). Three days prior to the planned conjugation the cosmid/BAC was transformed into *E. coli* ET12567 pUB307 on an LB agar plate with kanamycin and the antibiotic that was present on the cosmid/BAC with a resistance cassette. The agar plate was incubated overnight; four single colonies were picked and cultivated overnight on a new LB agar plate. Three full plates of *E. coli* ET12567 pUB307 harbouring the cosmid were prepared from the patches grown on those new LB agar plates.

For the conjugation, the host strain was resuspended in 10 mL sterile water, distributed to seven 1.5 µL reaction tubes, which were incubated in a 50 °C water bath for 10 min. The solutions were centrifuged at 300 x g for 3 min, the supernatant was discarded and the cell pellet was resuspended in 100 µL water. The *E. coli* cells of each plate were resuspended in 4 mL sterile water. The solution was centrifuged at 21300 rcf for 1 min, the supernatant was discarded and the cell pellet was resuspended in 100 µL water. Six of the seven host solutions each were mixed with one of the *E. coli* solutions and plated on separate freshly prepared MS plates. The seventh solution was plated on the seventh MS plate as a control. The plates were incubated at 28 °C for 16 h. The MS plates were overlaid with 1 mL of an antibiotic mixture (100 µL of the antibiotic with resistance on the cosmid backbone and 100 µL nalidixic acid in 8 mL sterile water). The plates were incubated at 28 °C for a week. Grown cells (exconjugants) were picked on freshly prepared MS plates with the respective antibiotics and incubated at 28 °C for one week. The new strains were tested for production. For that purpose, the exconjugants were cultivated in production medium DNPM at 28 °C and 180 rpm. After seven days the cultures were harvested, extracted and the extract was analyzed as described in chapter 3.2.

3.1.4.8 Complementation of the knockout strains with the previous deleted genes

To exclude false results through polar effects after inactivation of single genes, complementation of these genes in the knockout strains was performed [146]. For complementation, the target gene was incorporated into the plasmid vector pRT801_cat_ampery [140]. For this purpose, the plasmid was linearized through digestion with *Eco*RV as well as *Sac*I. If there was a *Sac*I restriction site present in the target gene, *Nde*I was used instead of *Sac*I for plasmid digestion of pRT801_cat_ampery. Each gene was multiplied by PCR with primers that added restriction sites for *Eco*RV and *Sac*I (for genes *oxaC*, *oxaD*, *oxaF*, *oxaG*, *oxaH*, *oxaI* and *oxaK*) or *Nde*I (for genes *oxaJ*, *oxaL* and *oxaM*) to the DNA fragments. The PCR products were digested with the corresponding restriction enzymes. The digested plasmid pRT801_cat_ampery and the digested genes were ligated over night and the resulting plasmid was transformed into GB2005 and isolated. During the experiments the generation of the plasmids pRT 1D11 KompG, pRT 1D11 KompJ, pRT 1D11 KompL and pRT 1D11 KompM was not successful.

The successfully modified pRT801-plasmids were transferred into their corresponding *S. albus* 1D11-Knockout strain through conjugation (shown in chapter 3.1.4.7). The resulting strains were cultivated and the extracts were analyzed for oxanthromicin production (see chapters 3.1.2.1 and 3.2).

3.2 Compound isolation and analysis

3.2.1 Compound isolation and purification

3.2.1.1 Extraction of bacteria cultures

The isolation and purification of the compounds discussed in this work, was performed after cultivation with production medium DNPM of the respective strain.

To analyze the exconjugants strains 50 mL cell culture was centrifuged to separate the biomass from the supernatant. The biomass was extracted with 20 mL of a 1:1 mixture of methanol and acetone for 30 min. 20 mL of the supernatant were extracted with 20 mL ethyl acetate and butanol respectively for 30 min. 10 mL of the organic phase were dried with a Cole-Parmer Techne® sample concentrator (Cole-Palmer Instrument Company, LLC, Vernon Hills, Illinois, USA) under an N_2-stream at 40 °C. The dried extract was resolved in 1 mL methanol and measured with HPLC-MS (chapter 3.2.2.1).

For the isolation and purification of the compounds the 10 L liquid culture was centrifuged. The supernatant was extracted with an equal amount of butanol or ethyl acetate for 30 min. The organic phase was separated and evaporated using an IKA RV-8 rotary evaporator (IKA, Staufen, Germany) at 40 °C.

3.2.1.2 Purification methods

The crude extract was dissolved in methanol and fractionated by flash chromatography (Isolera™ One, Biotage, Uppsala, Sweden) with a Biotage® Sfär Bio C4 D 50 g column (Biotage, Uppsala, Sweden). Per run 2.5 g of crude extract were attached to 25 g Celite®545 (Carl Roth GmbH & Co. KG) and prepared as a precolumn. For the purification run, hexane [A], chloroform [B], ethylacetate [C] and methanol [D] were used as eluents. The flowrate over the whole run was 100 mL/min. The run started with equilibration of the system with 3 column volumes (CVs) 100% A, followed with one additional CV 100% A. For 10 CVs a linear gradient 100% A to 100% B was applied, followed by one CV 100% B. For 15 CVs a linear gradient to 100% C was applied with one CV 100% C. For another 15 CVs a linear gradient to 100% D was applied. The run ended with 3 CVs 100% D. Fractions were analyzed with HPLC-MS and fractions containing the desired compounds were pooled.

For the samples with the desired compounds, size exclusion chromatography with a stationary phase of Sephadex® LH20 (Sigma Aldrich, Germany) in a 90 cm column was performed with methanol as the mobile phase. Fractions were analyzed with HPLC-MS and fractions containing the desired compounds were pooled.

Further purification was performed on a Waters AutoPurification™ system with a single quadrupole mass detector (Waters, Milford, MA, USA). A Nucleodur C18 HTEC, 250x21 mm, 5 µm column (Macherey-Nagel, Düren, Germany) was used as the stationary phase with MQ-H_2O + 0.1% FA [A] and acetonitrile + 0.1% FA [B] as the mobile phase with a linear gradient from 5% to 95% B in 35 min and a flowrate of 20 mL/min was applied. The derivatives containing fractions were pooled.

For the final purification step a reversed-phase HPLC (1260 Infinity II LC System, Agilent, Santa Clara, CA, USA) with a Nucleodur C18 HTEC, 250x10 mm, 5 µm column (Macherey-Nagel, Düren, Germany) as stationary phase was used. As mobile phase a linear gradient of 95% to 5% MQ-H_2O + 0.1% FA [A] with acetonitrile + 0.1% FA [B] was used with a flowrate of 4 mL/min for 20 min. The fractions containing pure compound were pooled and dried.

3.2.2 Methods used for compound analysis

3.2.2.1 HPLC analysis

In the the oxanthromicin and desmethylmensacarcin B projects analyses of the cultures extracts were performed with a HPLC-MS (Dionex Ultimate 3000 UHPLC system) with Acquity UPLC BEH C18, 100x2.1 mm, 1.7 µm dp column (Western Corporation, Milford, MA, USA) and mobile phase ddH_2O + 0.1% FA [A]/acetonitrile + 0.1% FA [B], 5-95% [B] over 20 min, at a flow rate of 0.6 mL/min, coupled to amazon SL speed mass spectrometer (Bruker, Billerica, MA, USA) with ESI source and mass range m/z 200-2000. Data were analyzed using the Compass Data Analysis v. 4.2 (Bruker, Billerica, MA, USA).

In the cyclohuinilsopeptin A project the HPLC analysis was performed with an Acquity UPLC BEH C18, 30x2.1 mm, 1.7 µm dp column (Western Corporation, Milford, MA, USA) was used with a mobile phase ddH2O + 0.1% FA [A]/acetonitrile + 0.1% FA [B], 5-95% [B] over 6.5 min, at a flow rate of 0.6 mL/min. Data were analyzed using the Compass Data Analysis v. 4.2 (Bruker, Billerica, MA, USA).

3.2.2.2 NMR spectroscopy

The NMR spectra were acquired in deuterated dimethyl sulfoxide (DMSO-d_6) and $MeOD_4$ at 298 K on a Bruker Avance III 700 or 500 MHz spectrometer, both were equipped with a 5 mm TXI cryoprobe. NMR shifts were relative to the residual solvent signal DMSO-d_6 at δ 2.50 ^1H and $MeOD_4$ at δ 3.31 ^1H, or to the solvent itself at δ 39.5 (DMSO-d_6) and δ 49.0 ($MeOD_4$) for ^{13}C measurements. NMR data were analyzed using Topspin, version 3.5 pl7 (Bruker, United States) and Spectrus Processor 2018.2.3 (ACD/Labs, Toronto, Canada). NMR measurements and structure elucidation were performed by Dr. Constanze Paulus and Dr. Marc Stierhof.

3.2.2.3 Optical rotation

The optical rotation of oxanthromicin and its derivatives were measured by Dr. Marc Stierhof with a JASCO P-2000 digital polarimeter (28600 Mary's Ct, Easton, MD, USA) at 20 °C and with methanol as a solvent.

3.2.2.4 Antimicrobial susceptibility test and cytotoxicity assay

The minimal inhibitory concentration was determined in a 96-well plate. A serial dilution of oxanthromicin (0.5 to 64 μg/mL) was placed into the wells and a final bacteria solution of 10^4 CFU/mL from single colonies in Müller-Hinton broth was added. The growth inhibition was examined after an overnight incubation of 17 h at 37 °C. 5 μL of thiazolyl blue tetrazolium bromide (MTT, 10 mg/mL) solution were added to each well. The plate was incubated at 30 °C for an additional hour. The minimal inhibitory concentration was determined visually by the oxanthromicin concentration in the well, in which no color change from yellow to dark blue occurred.

The following bacterial strains were tested: *Bacillus subtilis* DSM 10, *Staphylococcus aureus* strain Newman, *Mycobacterium smegmatis* mc2155, *E. coli* BW25113 (wt), *E. coli* JW0451-2 (ΔacrB), *Pseudomonas aeruginosa* PA14, *Acinetobacter baumannii* DSM 30008, *Citrobacter freundii* DSM 30039, *Candita albicans* DSM 1665, *Cryptococcus neoformans* DSM 11959, *Pichia anomala* DSM 6766, and *Mucor hiemalis* DSM 2656.

The biological activity of oxanthromicin was tested by Alexandra Amann at the HELMHOLTZ Institut für Pharmazeutische Forschung Saarbrücken (HIPS).

4 Results and Discussion

4.1 Heterologous expression of the cyclohuinilsopeptin A biosynthesis cluster in new hosts strains

The strain *Kutzneria albida* DSM 43870 is a rare Actinomycete of the *Pseudonocardiaceae* family [130]. In 1968 the strain was discovered and isolated from soil samples in the Gunma Prefecture of Japan [147]. During the search for new natural product, work colleague Dr. Hui Shuai discovered the non-ribosomally synthesized cyclopeptide cyclohuinilsopeptin A through heterologous expression of a BAC from *K. albida* DSM 43870 (Figure 25 and Figure 26) [130, 140]. Cyclohuinilsopeptin A was analyzed and insights into most of its biosynthesis were presented [140]. The peptide consists of the following seven subunits: β-phenylalanine (light green), 3-guanidino-alanine (blue), 3,4-cyclopropyl-proline (red), 2-(2,2,3-trimethyl-cyclopropyl)-glycine (orange), lysine (black), 2-methylmalonic acid (purple) and glutamine (dark green) (Figure 25) [140, 148].

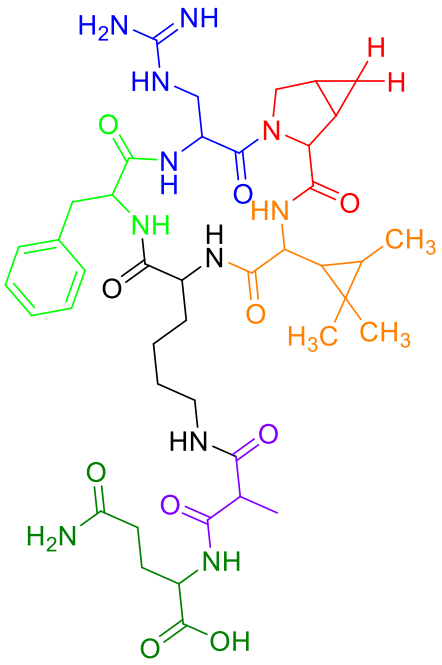

Figure 25. Chemical structure of cyclohuinilsopeptin A (34). The peptide consists of the following seven subunits: β-phenylalanine, 3-guanidino-alanine, 3,4-cyclopropyl-prolin, 2-(2,2,3-trimethyl-cyclopropyl)-glycine, lysine, 2-methylmalonic acid and glutamine.

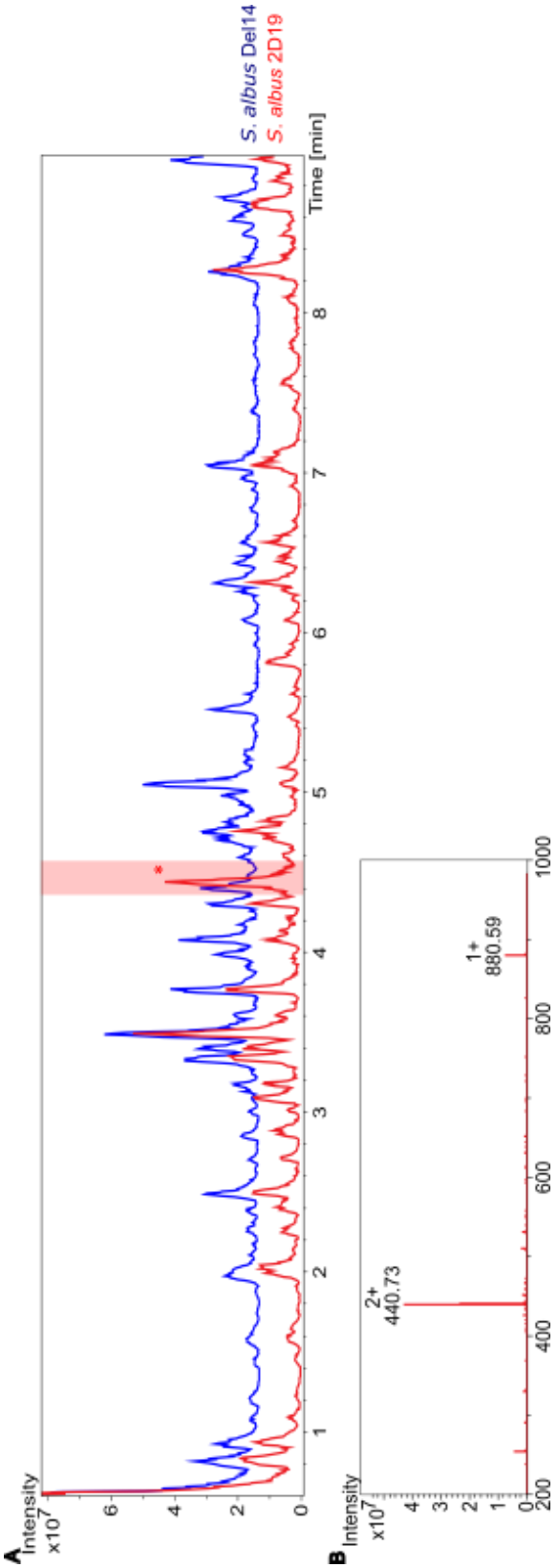

Figure 26. LC-MS chromatograms of butanol extract from *S. albus* Del14 (blue) and *S. albus* 2D19 (red) after cultivation for 7 days at 28°C and 180 rpm in 100 mL DNPM. (A) Base peak chromatograms of *S. albus* Del14 and *S. albus* 2D19. The cyclohuinilsopeptin A (34) peak is indicated by one asterisk (*). (B) Mass spectrum associated to t_R=4.4 min (the cyclohuinilsopeptin A peak (*)) from *S. albus* 2D19 LC-MS chromatogram.

4.1.1 Knockout experiments with the wild type strain *K. albida* DSM 43870

After cyclohuinilsopeptin A was discovered via heterologous expression in *S. albus* Del14, the wild type strain *K. albida* was examined for the compound [140]. In the HPLC-MS analysis of the butanol extract of *K. albida*, cyclohuinilsopeptin A was not detected [140].

For the discovery of cyclohuinilsopeptin A in the wild type strain, the NRPS gene responsible for cyclohuinilsopeptin biosynthesis was set to be deleted in the *K. albida* DSM4370. In order to perform the wildtype knockout, homologous recombination of the biosynthetic gene cluster in *K. albida* was performed. Therefore, the BAC 2D19 KO4, with the deletion of the NRPS gene KALB_5512 [140], was prepared for homologous recombination. Therefore, the integrase gene at the BACs backbone was substituted by an ampicillin resistance gene through RedET recombination to produce the BAC 2D19 Int/Amp. This BAC was conjugated in *K. albida* to initiate the homologous recombination. Despite multiple conjugations no exconjugants were obtained, which led to the assumption that the conjugation with the chosen conditions was not possible in *K. albida*. To confirm this hypothesis, the integrative plasmid pKC1139 was selected as a control for conjugation experiments. Again, no exconjugants were obtained. This result supported the hypothesis that *K. albida* DSM 43870 was not genetically accessible with the used conjugation method. Liquid conjugation was tested as well, without the production of exconjugants.

Kontou *et. al* were able to transfer a BAC13A with a gene knockout back into *Kutzneria* sp. CA-103260 through triparental conjugation with *E. coli* ET12567 and *E. coli* DH10β without including a heat shock [124, 149]. In our experiments biparental conjugation with heat shock was performed. The successful conjugation in *Kutzneria* sp. CA-103260 indicates that conjugation in *K. albida* DSM43870 could also be successful under different conditions, as demonstrated by Kontou *et. al*. This could be tested in further experiments.

4.1.2 Heterologous expression in alternative host strains

Apart from the homologous recombination, heterologous expression of the BAC 2D19 was performed with ten Actinomycetes heterologous host strains (LV strain collection, Table 3, Chapter 3.1.2.2). To rule out the possibility of *S. albus* Del14 modifying the original compound with its own enzymes as a host strain, the BAC 2D19 was conjugated in each of the ten strains. Each conjugation was successful and exconjugants were obtained. In order to find compounds produced by the BAC 2D19, the exconjugants and wild type strains were cultivated as references, extracted with butanol and the extracts analyzed and compared with respective wild type strains. As a reference, the BAC 2D19 was also heterologously expressed in *S. albus* Del14 (Figure 26). Cyclohuinilsopeptin A was detected in the LC-MS chromatogram of the strain *S. albus* Del14 2D19 at a retention time t_R=4.4 minutes with a protonated mass of 880.59 Da (Figure 26).

Analysis of the LC-MS chromatograms of the butanol extracts of the 2D19 derivatives of the strains LV1-4, LV1-18.2, LV1-144, LV1-166, LV1-208, LV1-209 notched, LV1-213 and LV1-625 showed no new compounds compared to the host wild type, (Supplementary Information (SI.1): Figure 62 to Figure 69). In these strains the cyclohuinilsopeptin cluster was not expressed.

Heterologous expression of BAC 2D19 in LV1-22 was successful and a new peak with a retention time of t_R=4.4 min and a corresponding mass of 879.47 Da was detected in the LC-MS chromatogram of the butanol extract of LV1-22 2D19 (Figure 27). Both, the retention time and corresponding mass indicated the production of cyclohuinilsopeptin by LV1-22 2D19. The discovery of cyclohuinilsopeptin A in LV1-22 2D19 led to the conclusion that cyclohuinilsopeptin A is the product of the 2D19 BAC of *K. albida*.

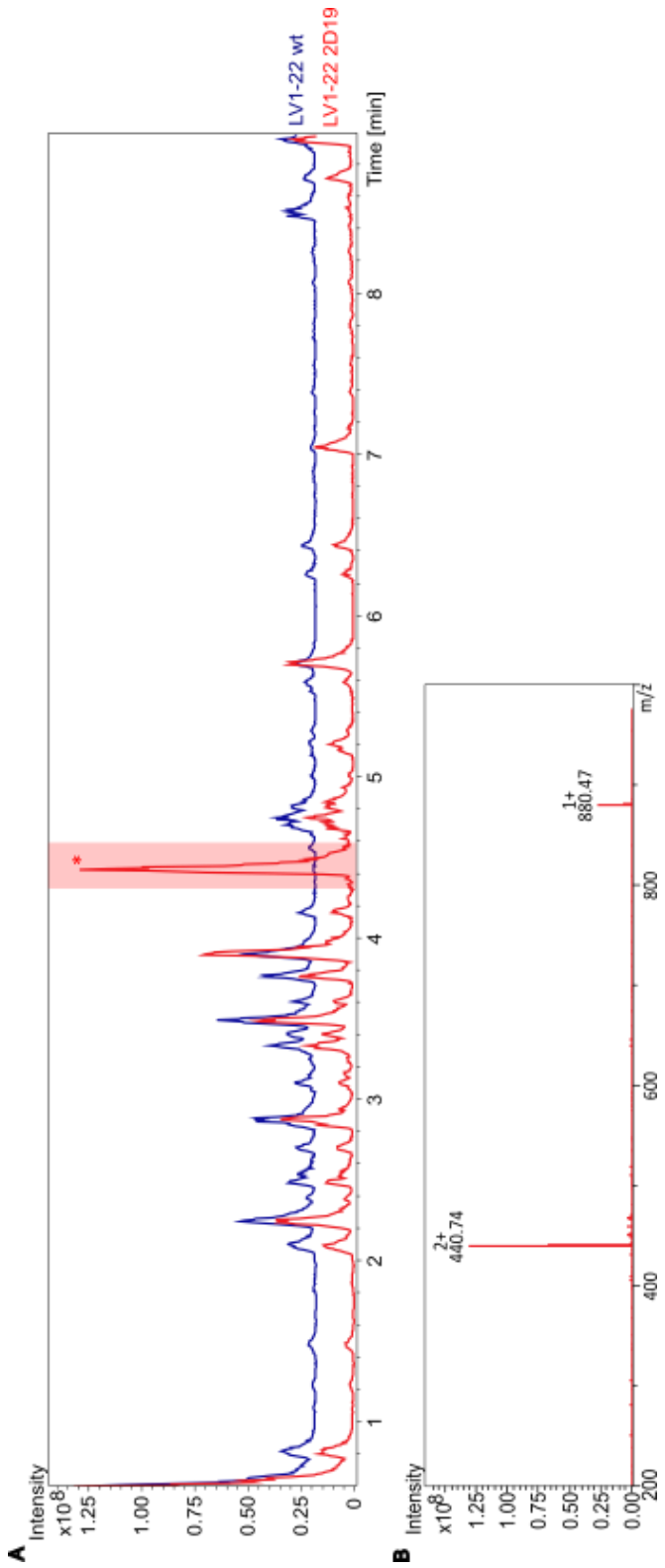

Figure 27. LC-MS chromatograms of butanol extract from LV1-22 (blue) and LV1-22 2D19 (red) after cultivation for 7 days at 28°C and 180 rpm in 100 mL DNPM. (A) Base peak chromatograms of LV1-22 and LV1-22 2D19. The cyclohuinilsopeptin A (1) peak is indicated by one asterisk (*). (B) Mass spectrum associated to t_R=4.4 min (the cyclohuinilsopeptin A peak (*)) from LV1-22 2D19 LC-MS chromatogram.

The butanol extract of the strain LV1-209 smooth showed four new peaks at t_R=3.6 min (*/(35)), t_R=5.5 min ((**/(36)), t_R=6.2 min (***/(37)) and t_R=6.8 min (****/(38)) (Figure 28) compared to the wildtype strain (Figure 28). The compounds showed masses of 275.2 Da (35), 1288.63 Da (36), 1270.64 Da (37) and 1191.64 Da (38) (Figure 28). The mass difference of 18 Da between the compounds (36) and (37) suggested a water loss of (36) to produce (37). As a control 2D19 KO5, the BAC 2D19 with deletion of the gene KALB_5514 encoding for a radical SAM dependent enzyme, was heterologously expressed in LV1-209 smooth. In the butanol extract of LV1-209 smooth 2D19 KO5 the four compounds (35) to (38) were detected as well (Figure 29). This result was first discovered by Gregor Ulrich during his master thesis, when conjugating another cluster in LV-209 smooth [150]. The compounds were analyzed by Gregor Ulrich and Patrick Oberhäuser (unpublished data) [150, 151].

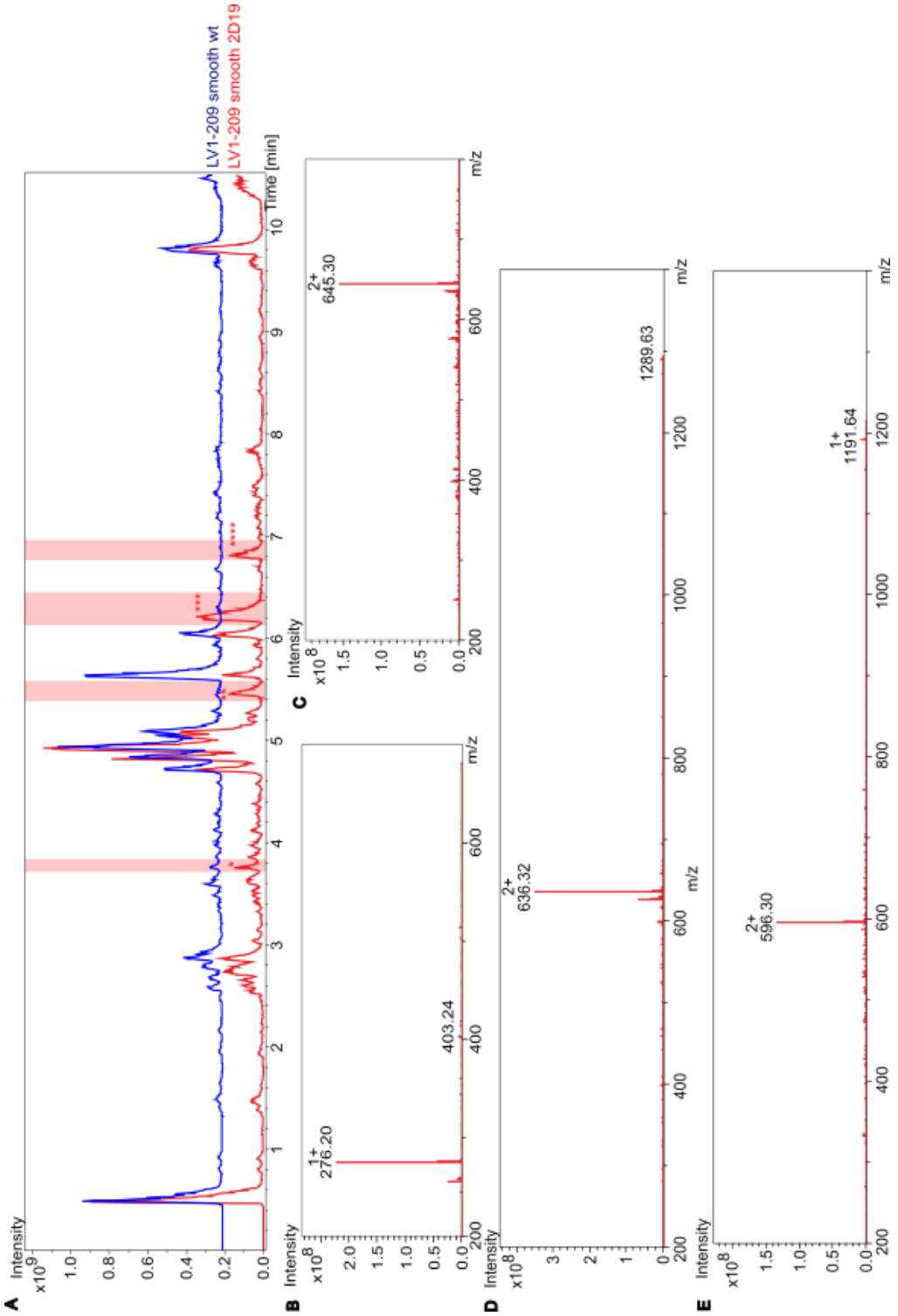

Figure 28. LC-MS chromatograms of butanol extract from LV1-209 smooth (blue) and LV1-209 smooth 2D19 (red) after cultivation for 7 days at 28°C and 180 rpm in 100 mL DNPM. (A) Base peak chromatograms of LV1-209 smooth and LV1-209 smooth 2D19. In red three peaks of new occurring compounds are indicated by asterisks (* (35), ** (36), *** (37), **** (38)). (B) Mass spectrum associated to the peak (*/(35)) at t_R=3.6 min in the LC-MS chromatogram of LV1-209 smooth 2D19. (C) Mass spectrum associated to the peak (**/(36)) at t_R=5.5 min in the LC-MS chromatogram of LV1-209 smooth 2D19. (D) Mass spectrum associated to the peak (***/(37)) at t_R=6.2 min in the LC-MS chromatogram of LV1-209 smooth 2D19. (E) Mass spectrum associated to the peak (****/(38)) at t_R=6.8 min in the LC-MS chromatogram of LV1-209 smooth 2D19.

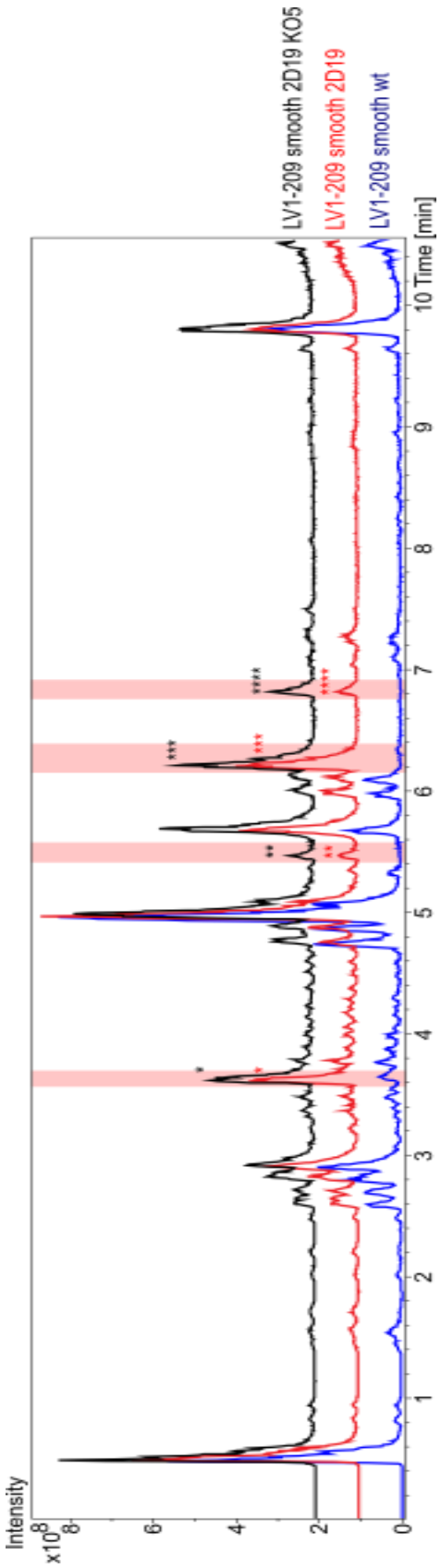

Figure 29. LC-MS chromatograms of butanol extract from LV1-209 smooth (blue), LV1-209 smooth 2D19 (red) and LV1-209 smooth 2D19 KO5 (black) after cultivation for 7 days at 28°C and 180 rpm in 100 mL DNPM.

4.1.3 Concluding remarks on the cyclohuinilsopeptin project

The cyclohuinilsopeptin A project focused on the heterologous expression of the BAC 2D19 from *K. albida* DSM43870 in the LV strains as new hosts for cyclohuinilsopeptin A production and knockout experiments in the wild type strain *K. albida* DSM43870.

Conjugation in *K. albida* DSM43870 was neither successful with the BAC 2D19 KO4 Int/Amp nor with the control plasmid pKC1139. To introduce DNA into *K. albida* DSM43870 transformation experiments as well as triparental conjugation or conjugation without heat shock can be performed in the future [149, 152].

Conjugations of the BAC 2D19 in the LV strains were successful and showed that the strain LV1-22 was able to heterologously express the BAC 2D19 and produce cyclohuinilsopeptin A in the same way as *S. albus* Del14. Both strains produced the same compound, indicating that cyclohuinilsopeptin A is in fact the product of the biosynthetic gene cluster, rather than the product of the interaction of the BAC with the host strain.

Cyclohuinilsopeptin A was not detected in the butanol extracts of *K. albida*. A possible explanation may be that the cyclohuinilsopeptin A biosynthetic gene cluster is a silent BGC and is not expressed under the tested conditions. With a cultivation under stress conditions such as a cultivation in a different medium, e.g. minimal medium or defined medium with different pH values, carbon sources or added metal ions, the cluster could still be activated in the wild type strain [11]. Activation of the cluster in the wild type strain may also be successful through introduction of synthetic promotors preceding key genes [153], as soon as the issue with introduction of DNA into *K. albida* DSM43870 mentioned above is solved.

4.2 Heterologous expression of four T2PKS clusters from *Streptomyces acidiscabies* LU19992 in cluster-free chassis strains

The Gram-positive bacterium *Streptomyces acidiscabies* is a plant-pathogenic responsible for potato scab [154-156]. It emerged in the northeastern United States replacing *Streptomyces scabies* in regions with soil of a lower pH than 5.2 [154]. With over 11 Mb the genome of *S. acidiscabies* is among the larger genomes of Streptomycetes [156].

During the search for new natural products in *Streptomyces acidiscabies* LU19992, work colleague Dr. Constanze Paulus discovered three new scabimycins A-C [131]. Besides the discovery of these new compounds, the anthrone polyketide oxanthromicin was also detected (Figure 30, compound 39) and confirmed with NMR analysis (SI.2: Table 16) [157-159]. Oxanthromicin (39) was discovered in 1984, yet the biosynthesis had not been uncovered until now [157-159].

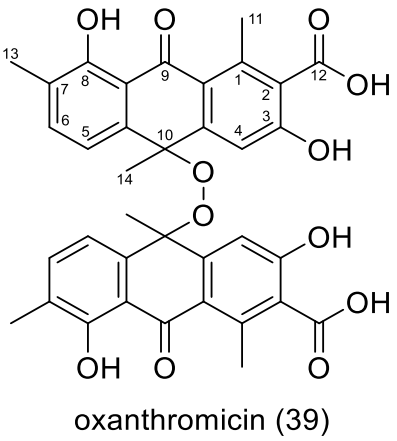

Figure 30. Chemical structure of oxanthromicin (39).

To solve the biosynthesis of oxanthromicin the responsible BCG needed to be detected. Aromatic polyketides, like oxanthromicin are primarily produced by type II polyketide synthases [3, 6]. Using the antiSMASH tool [132], the genome of *S. acidiscabies* LU19992 was screened for T2PKS BGCs. The genome of *S. acidiscabies* LU19992 contains 52 predicted gene clusters involved in secondary metabolism (SI.2:Table 17). Out of the 52 predicted gene clusters the four gene clusters namely 27, 35, 41 and 42 contain genes encodingtype II polyketide synthases (SI.2: Table 17, marked in blue).

The cosmids harboring the PKSII gene clusters were taken from a prepared cosmid library [160]. These cosmids were 9H08 (BGC 27), 2D04 (BGC 35), 1D11 (BGC 41) and 18F05 (BGC 42). They were analyzed using restriction digestion with *Kpn*I and by comparing the predicted fragmentation patterns (Figure 31) as well as the sequences.

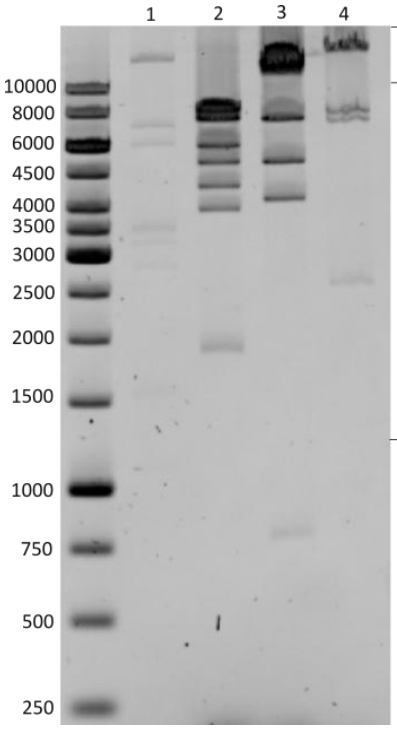

1	2	3	4
1D11	2D04	9H08	18F05
17819	7853	12351	23785
7382	7382	11488	7825
6356	7316	7382	7382
3574	5856	5352	2590
3522	5318	4174	76
3271	4526	790	
2847	3911	76	
1552	1881		
1549	196		
1115	174		
198	137		
147	76		
76			

Figure 31. Restriction mapping after digestion with *Kpn*I of the cosmids 1D11, 2D04, 9H08 and 18F05 containing the T2PKS clusters of *S. acidiscabies*.

The cosmids were heterologously expressed in *S. albus* Del14 and *S. lividans* ΔYA8 as the host strains. The exconjugants were cultivated and their butanol extracts were analyzed for production of oxanthromicin and new compounds. There was no visible production of new compounds in the *S. lividans* strains or the *S. albus* strain containing the 9H08 cosmid (data not shown).

The LC-MS analysis of the butanol extract of *S. albus* 1D11 reveiled a new peak compared to the wild type strain *S. albus* Del14. The peak showed a mass of 654.1729 Da at a retention time of t_R=14 min (Figure 33), which was the same mass and retention time as the peak of oxanthromicin (Figure 30, compound 39) in *S. acidiscabies* LU19995. Furthermore, *S. albus* 1D11 showed another peak at t_R=8.5 min with a corresponding mass of 328.0945 Da (Figure 33). Since this compound exhibited half the mass of oxanthromicin it appeared to be the monomeric derivative *hemi*-oxanthromicin (40) (Figure 32) [158]. This hypothesis was proved after isolation and structure elucidation by NMR spectroscopy of this compound from the strain *S. albus* 1D11 KOC (SI.4: Table 25).

Biosynthesis of oxanthromicin is analyzed and described in chapter 4.4.

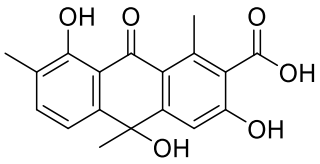

hemi-oxanthromicin (40)

Figure 32. Chemical structure of *hemi*-oxanthromicin (40).

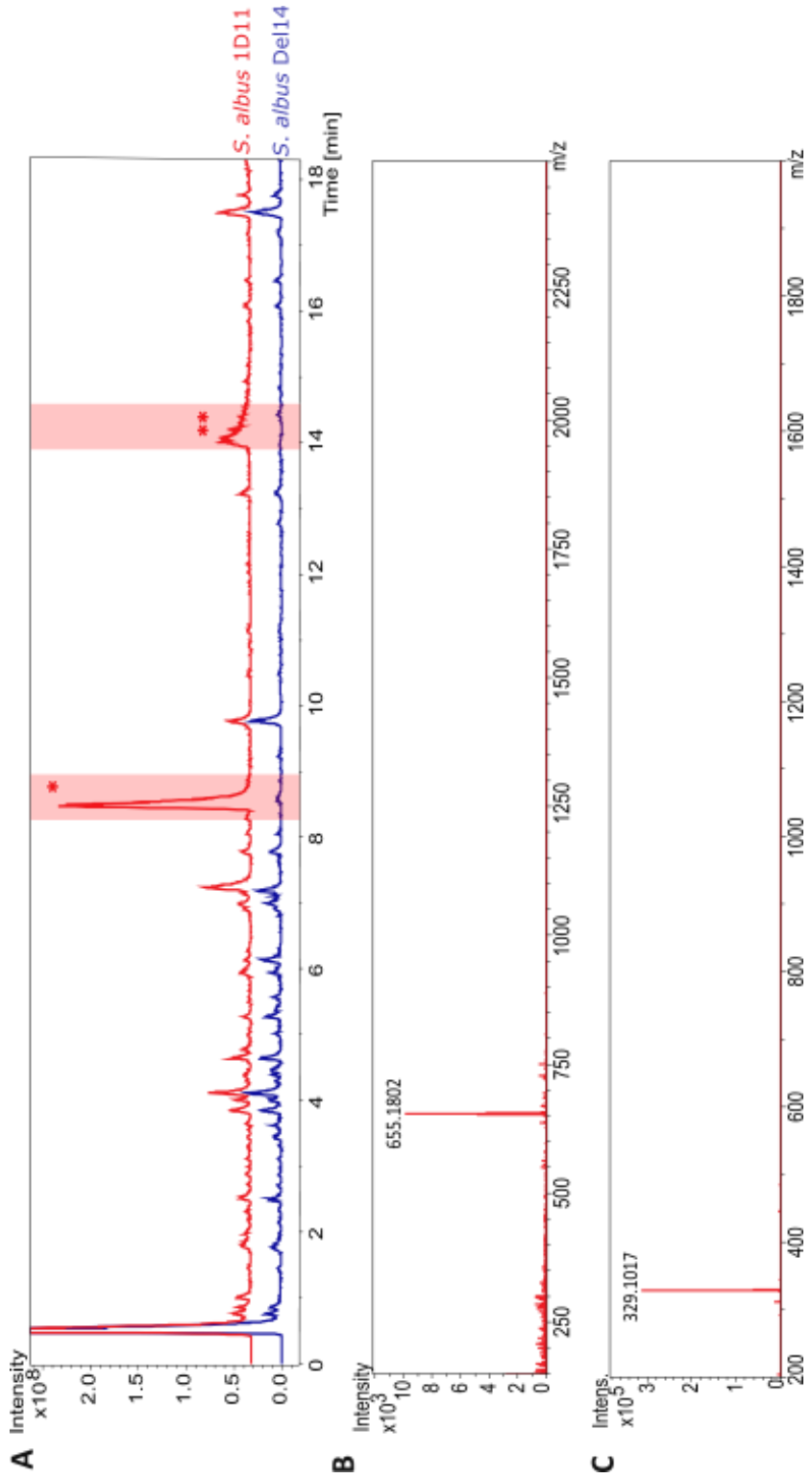

Figure 33. LC-MS chromatograms of butanol extract from *S. albus* 1D11 (red) and *S. albus* Del 14 (blue) after cultivation for 7 days at 28°C and 180 rpm in 100 mL DNPM. (A) Base peak chromatograms of *S. albus* 1D11 and *S. albus* Del14. The oxanthromicin (39) peak is indicated by two asterisks (**) and the *hemi*-oxanthromicin (40) by one asterisk (*). (B) Mass spectrum associated to t_R=14 min (the oxanthromicin peak (**)) from *S. albus* 1D11 LC-MS chromatogram. (C) Mass spectrum associated to t_R=8.5 min (the *hemi*-oxanthromicin peak (*)) from *S. albus* 1D11 LC-MS chromatogram.

A new peak at t_R=5.2 min was discovered in the LC-MS chromatogram of the extract of *S. albus* 2D04. The new peak showed a mass of 767.96 Da (Figure 34). With the expression of 2D04 in *S. albus* Del14 the peak at t_R=9.8 min disappeared (Figure 34). The strain was not further analyzed as the aim of the expression was the discovery of the oxanthromicin cluster. However, the compound may be interesting for further experiments in finding potential new compounds.

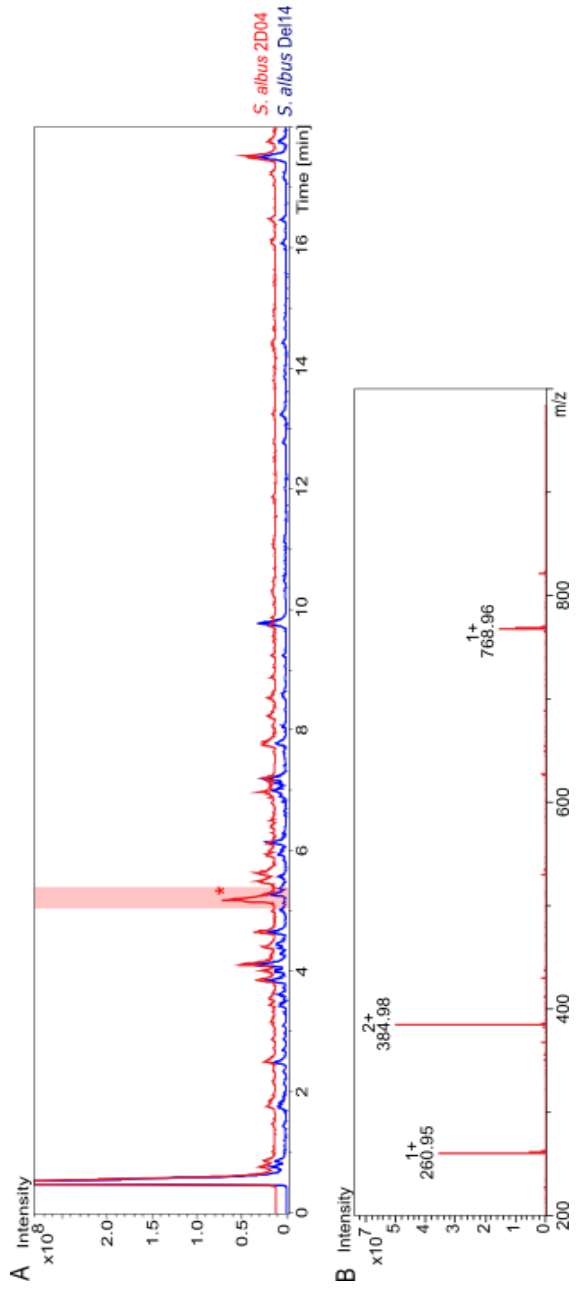

Figure 34. LC-MS chromatograms of butanol extract from *S. albus* 2D04 (red) and *S. albus* Del 14 (blue) after cultivation for 7 days at 28°C and 180 rpm in 100 mL DNPM. (A) Base peak chromatograms of *S. albus* 2D04 (red) and *S. albus* Del14 (blue). The new occurring double peak is indicated by one asterisk (*). (B) Mass spectrum associated to t_R=5.2 min from *S. albus* 2D04 LC-MS chromatogram.

The negative mode HPLC-MS analysis of the extract of the strain *S. albus* 18F05 showed a new double peak at t_R=4.7 min and t_R=4.9 min with corresponding masses of 406.1265 Da and 406.1264 Da respectively (Figure 35). Isolation and analyzation of the compounds encoded in this T2PKS cluster is described in chapter 4.3.

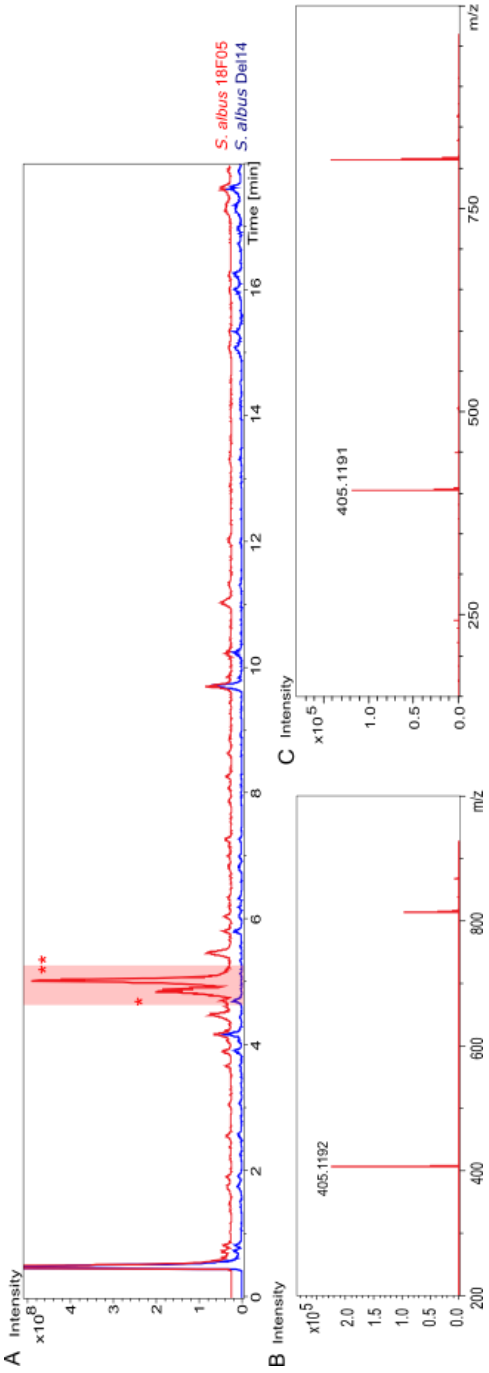

Figure 35. LC-MS chromatograms measured in negative mode of butanol extract from *S. albus* 18F05 (red) and *S. albus* Del 14 (blue) after cultivation for 7 days at 28°C and 180 rpm in 100 mL DNPM. (A) Base peak chromatograms of *S. albus* 18F05 (red) and *S. albus* Del14 (blue). The new occurring peaks are indicated by one and two asterisks (*/**). (B) Mass spectrum associated to t_R=4.7 min (*) from *S. albus* 18F05 LC-MS chromatogram. (C) Mass spectrum associated to t_R=4.9 min (**) from *S. albus* 18F05 LC-MS chromatogram.

4.3 Discovery of a new mensacarcin derivative from *S. acidiscabies* LU19995

The unknown compounds (Figure 35) produced by the strain *S. albus* 18F05 were isolated after a 5 L scale cultivation in DNPM medium. The dried ethyl acetate extract of the culture was purified by size exclusion chromatography and reversed phase chromatography. After purification 0.6 mg (42) and 0.9 mg (44) of the compounds with the masses of 406.1265 Da and 406.1264 Da respectively, were received and their structures were elucidated by NMR spectroscopy (Figure 36, SI.3: Table 18 and SI.3: Table 18). The compound (42) corresponding to the peak at the retention time t_R=4.7 min was identified as desmethylmensacarcin (Figure 36, SI.3: Table 18). The second compound had not been described yet and was named desmethylmensacarcin B (44) (Figure 36, SI.3: Table 19). The difference between desmethylmensacarcin and desmethylmensacarcin B is the swap of the hydroxy group and keto group at C4 and C10 respectively (marked in red, Figure 36).

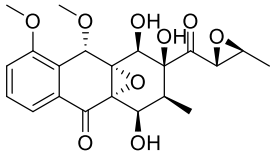

Chemical Formula: $C_{21}H_{24}O_9$
Exact Mass: 420,14
mensacarcin (41)

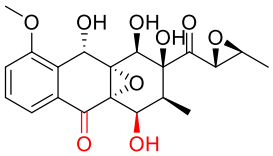

Chemical Formula: $C_{20}H_{22}O_9$
Exact Mass: 406,13
desmethylmensacarcin (42)

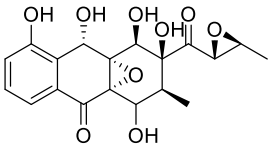

Chemical Formula: $C_{19}H_{20}O_9$
Exact Mass: 392,11
didesmethylmensacarcin (43)

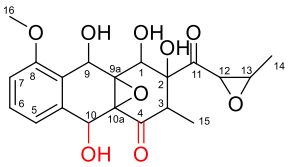

Chemical Formula: $C_{20}H_{22}O_9$
Exact Mass: 406,13
desmethylmensacarcin B (44)

Figure 36. Chemical structures of mensacarcin (41), desmethylmensacarcin (42), didesmethylmensacarcin (43) and the new compound desmethylmensacarcin B (44). The differences between desmethylmensacarcin and desmethylmensacarcin B are depicted in red.

Desmethylmensacarcin (42) is a derivative of mensacarcin (41), which is a hexahydroanthracene polyketide (Figure 36) with an anti-tumor activity [161-164]. Mensacarcin was discovered in the strain *Streptomyces bottropensis* (formerly *Streptomyces* sp. GöC4/4) in 1998 [161-164]. With its high oxygenation, the two epoxy groups and the nine stereo centers, mensacarcin is a pharmaceutically interesting compound [163, 165]. The epoxy group in the side chain is considered the main factor responsible for the anti-tumor activity [163]. Mensacarcin shows activity against 60 cell lines [163-165]. In the years after the discovery the biosynthetic gene cluster was analyzed by Maier *et al*. [163, 165].

In this study the biosynthesis of desmethylmensacarcin B was investigated through comparison with the biosynthesis of mensacarcin and desmethylmensacarcin on the enzyme level. The mensacarcin biosynthetic gene cluster consists of the minimal PKS genes (*msnK1*, *msnK2*, *msnK3*), three cyclase genes (*msnC1*, *msnC2* and *msnC3*), three ketoreductases genes (*msnO1*, *msnO10*, *msnO11*), two oxidoreductase genes (*msnO3*, *msnO9*), one thioesterase gene (*msnH7*), one dehydrogenase gene (*msnH6*), three luciferase-like monooxygenase genes (*msnO2*, *msnO4* and *msnO8*) and three anthrone oxygenase genes (*msnO5*, *msnO6* and *msnO7*) (Figure 37 B) [165].

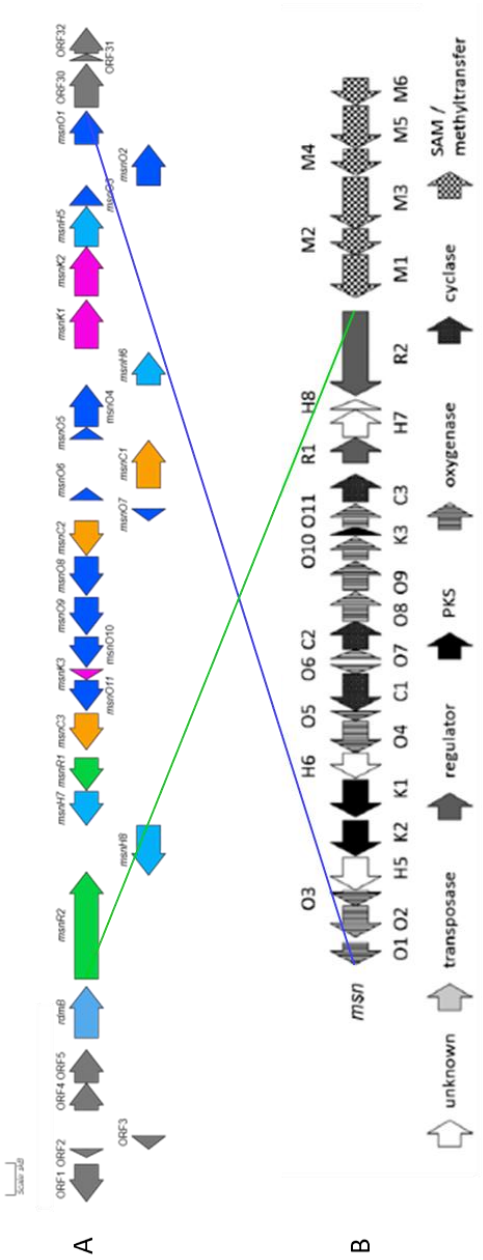

Figure 37. Biosynthetic gene clusters of Desmethylmensacarcin B and Mensacarcin. A: Biosynthetic gene cluster of Desmethylmensacarcin B from *S. acidiscabies* LU19992 cosmid 18F05. Purple: Genes encoding the minimal PKS; Orange: genes encoding cyclases; Green: regulatory genes; Blue: genes encoding for reductases and oxygenases and Light Blue: genes encoding hypothetical proteins and the gene encoding for RdmB as SAM dependent enzyme. B: Biosynthetic gene cluster of Mensacarcin from *Streptomyces bottropensis*. Genes encoding the minimal PKS are colored black, genes encoding cyclases are dark grey and spotted, regulatory genes are colored grey, genes encoding for reductases and oxygenases are striped, genes encoding hypothetical proteins are shown in white and the genes encoding for enzymes involved in methylation and SAM regeneration are shown checkered [165].

The cosmid 18F05 was analyzed using the antiSMASH tool [132] and the Geneious software [134]. The cosmid comprises 31 kB of genomic DNA from *S. acidiscabies* LU19992 with 32 open reading frames (ORF) (Figure 37 A). The enzymes encoded on the cosmid 18F05 were compared on the protein level with the genes of the mensacarcin BGC. Out of the 32 enzymes encoded in the BGC 23 showed high homology to the enzymes present in the mensacarcin biosynthetic pathway (Table 13), while nine enzymes did not show homologies to the mensacarcin pathway. These nine enzymes were annotated as a dioxygenase, a phytase, a regulator, the SAM-dependent 10-hydroxylase RdmB [166] and five putative proteins. The five putative proteins were not annotated with any activity.

Table 13. Proposed functions of enzymes encoded by the genes of the biosynthetic gene cluster of desmethylmensacarcin B and their neighboring genes. Homology of the products of the genes with the products of genes involved into the mensacarcin biosynthesis is shown in the last two columns.

Gene	Proposed function	Homolog in mensacarcin pathway [164]	Identity/Similarity
ORF1	Quercetin dioxygenase		
ORF2	Putative protein		
ORF3	Putative protein		
ORF4	Phytase		
ORF5	Regulator		
ORF6	10-hydroxylase RdmB		
ORF7	Regulator	MsnR2	52%/65%
ORF8	Macrolide efflux protein	MsnH8	70%/80%
ORF9	Hydrolase	MsnH7	72%/79%
ORF10	Regulator	MsnR1	72%/84%
ORF11	Cyclase	MsnC3	82%/88%
ORF12	Ketoacyl reductase	MsnO11	89%/93%
ORF13	Acyl-carrier protein	MsnK3	83%/90%
ORF14	Reductase	MsnO10	80%/88%
ORF15	Reductase	MsnO9	86%/94%
ORF16	Monooxygenase	MsnO8	90%/93%
ORF17	Cyclase	MsnC2	82%/90%
ORF18	Monooxygenase	MsnO7	87%/92%
ORF19	Monooxygenase	MsnO6	74%/85%
ORF20	Hydroxylase/cyclase	MsnC1	64%/76%
ORF21	Monooxygenase	MsnO5	81%/92%
ORF22	Monooxygenase	MsnO4	85%/92%
ORF23	Reductase	MsnH6	76%/83%
ORF24	Alpha ketoacylsynthase	MsnK1	95%/97%
ORF25	Beta ketoacylsynthase	MsnK2	90%/93%
ORF26	Phosphotransferase	MsnH5	76%/80%
ORF27	Monooxygenase	MsnO3	76%/86%
ORF28	Dehydrogenase	MsnO2	89%/95%
ORF29	Reductase	MsnO1	88%/94%
ORF30	Putative protein		
ORF31	Putative protein		
ORF32	Putative protein		

The homologies between the enzymes involved in mensacarcin and desmethylmensacarcin B biosynthesis were all above 76% [164]. The regulator encoded by ORF7 is an exception to this as it only showed a 65% similarity to MsnR2 (Table 13) [164]. The enzyme encoded by ORF8 annotated as a macrolide efflux factor (Table 13). The homology of the product of ORF8 and MsnH8 was 80% [162]. With 431 amino acids, however, the product of ORF8 is significantly larger than MsnH8 that consists of 111 amino acids [162]. Probst *et al*. discovered that during the biosynthesis of didesmethylmensacarcin MsnH8 was not transcribed [162], leading to the assumption that MsnH8 is not a functional enzyme based on its small size [162]. ORF8 may act as an active transporter in the desmethylmensacarcin B biosynthesis of *S. acidiscabies* LU19992.

Through the comparison of the enzymes present in desmethylmensacarcin B biosynthesis with the one known from mensacarcin biosynthesis we were able to propose the biosynthesis of desmensacarcin B from *S. acidiscabies* LU19992. With homologies of 97%, 93% and 90% to their respective counterparts in mensacarcin biosynthesis (Table 13), the minimal PKS in the desmethylmensacarcin B cluster is encoded by ORF24 (counterpart to MsnK1), ORF25 (MsnK2) and ORF13 (MsnK3) [162, 165]. The minimal PKS elongates the malonyl-CoA starter unit with nine malonyl units (Figure 38 I) [162, 164, 165]. The minimal PKS seems to be supported by the product of ORF15, which controls the polyketide chain length [165]. In the mensacarcin biosynthesis MsnO9, which is responsible for chain length control in mensacarcin biosynthesis, shows a 95% homology to the product of ORF15 [165]. Subsequently, the C9 position proposedly is reduced by the product of ORF12 (Figure 38 II), which has a 93% similarity to MsnO11 (Table 13). Cyclization of the poly-keto-chain presumably is performed by the products of ORF20, ORF17 and ORF11 (Figure 38 II). The cyclases show a high similarity of 76%, 90% and 88% to the cyclases MsnC1, MsnC2 and MsnC3 in mensacarcin biosynthesis (Table 13) [162, 164, 165]. The product of ORF9 shows a homology of 79% to the thioesterase MsnH7 (Table 13) [164]. The hydrolase encoded by ORF9 is presumably responsible for the release of the polyketide core from ORF13 the ACP (Figure 38 III).

The next step in the mensacarcin biosynthesis is the incorporation of the keto group at C10 [164, 165]. In comparison to desmethylmensacarcin in desmethylmensacarcin B the keto

group and hydroxyl group at C4 and C10 respectively are switched (Figure 36). The products of ORF21 and ORF19 show high homologies to the anthrone oxygenases MsnO5 and MsnO6, which, together, are responsible for C10 oxidation in mensacarcin biosynthesis of 92% and 85%, respectively (Table 13) [164, 165]. It is likely that the small differences in the enzymes slightly changed the preferred target for the oxidation from C10 to C4. Therefore, it is proposed that ORF21 and ORF19 are responsible for C4 oxidation and creation of the C4 keto group of compound 54 (Figure 38 IV). Compound 54 is an intermediate in both desmethylmensacarcin B as well as desmethylmensacarcin biosynthesis. Since both compounds desmethylmensacarcin and desmethylmensacarcin B were detected in *S. albus* 18F05, it is plausible that ORF21 and ORF19 do not show a strong selectivity to a specific compound.

Similar to reactions in the mensacarcin biosynthesis, the next reactions generate the epoxy moiety between C12 and C13. These reactions are presumably performed by the products of ORF28 and ORF16 (Figure 38 V-VI). The dehydrogenase encoded by ORF28 shows a homology of 95% to MsnO2 and the monooxygenase encoded by ORF16 shows a 93% homology to MsnO8 (Table 13) [163-165]. Meier *et al*. proposed that MsnO4 has multiple functions in the mensacarcin biosynthesis [165]. In their experiments they found evidence that MsnO4 introduces two hydroxyl groups and the epoxy group to the third ring of mensacarcin [165]. The product of ORF22 shows a 92% homology to MsnO4 (Table 13). The enzyme MsnO3 supports the activities of MsnO2, MsnO4 and MsnO8 [165]. The product of ORF27 shows an 86% homology to the flavin reductase MsnO3. We propose that the product of ORF27 supports the enzymes encoded by ORF28, ORF22 and ORF16, like MsnO3 does with MsnO2, MsnO4 and MsnO8 by providing the reduced flavin mononucleotide [165]. Through the incorporation of the keto group at C4 in the third ring of desmethylmensacarcin B, the C4 position is blocked and the C10 in the second ring needs to be hydroxylated in parallel to C2 hydroxylation and the epoxidation between the second and third ring (Figure 38 VII).

There are no genes encoding for methyltransferases found within the cosmid 18F05 (Table 13). The enzyme encoded by ORF6 is annotated as an RdmB-like 10-hydroxylase. The product of ORF6 shows a 54% homology to RdmB [166]. RdmB is a SAM-dependent protein,

whose activity changed from a methyltransferase activity to the hydroxylase activity [121]. The homology of 54% may imply that ORF6 encodes for a SAM-dependent protein that still acts as a methyltransferase. Since there are no methyltransferases encoded in the genes of the desmethylmensacarcin B biosynthetic gene cluster, it is likely that the product of ORF6 still has the methyltransferase activity and is responsible for C8-O methylation (Figure 38 VIII). In mensacarcin biosynthesis methylation of both C8-O and C9-O is performed by MsnM6 [164]. In the butanol extract of *S. albus* 18H05 no mensacarcin was detected. This indicates that ORF6 is selective for the C8-O methylation.

The products of ORF7 and ORF10 show homologies of 65% and 85% to MsnR2 and MsnR1, respectively. MsnR1 acts as the activator for the mensacarcin biosynthesis [165]. The regulatory activity of MsnR2 is not discovered yet [162, 165], hence there was no proposed function assigned to ORF7. Based on their homology, it is proposed that ORF10 similar to MsnR1 functions as an activator for the desmethylmensacarcin B biosynthesis [165].

The product of ORF23 shows an 83% homology to MsnH6, which represses the biosynthesis of mensacarcin [165]. Presumably, when activated ORF23 represses the biosynthesis of desmethylmensacarcin B, similarly to MsnH6 does in mensacarcin biosynthesis. The enzyme encoded by ORF14 is annotated as a reductase, which shows an 88% homology to MsnO10 [165]. MsnO10 in the mensacarcin biosynthesis has a stabilizing effect on the polyketide side chain during synthesis [165]. The product of ORF18 shows a 92% homology to MsnO7, a monooxygenase that has shown an impact on mensacarcin production with a not described function [165].

Based on the high homologies of the discovered cluster on cosmid 18H05 to the previously described mensacarcin cluster, a biosynthetic pathway for desmethylmensacarcin B production is postulated (Figure 38).

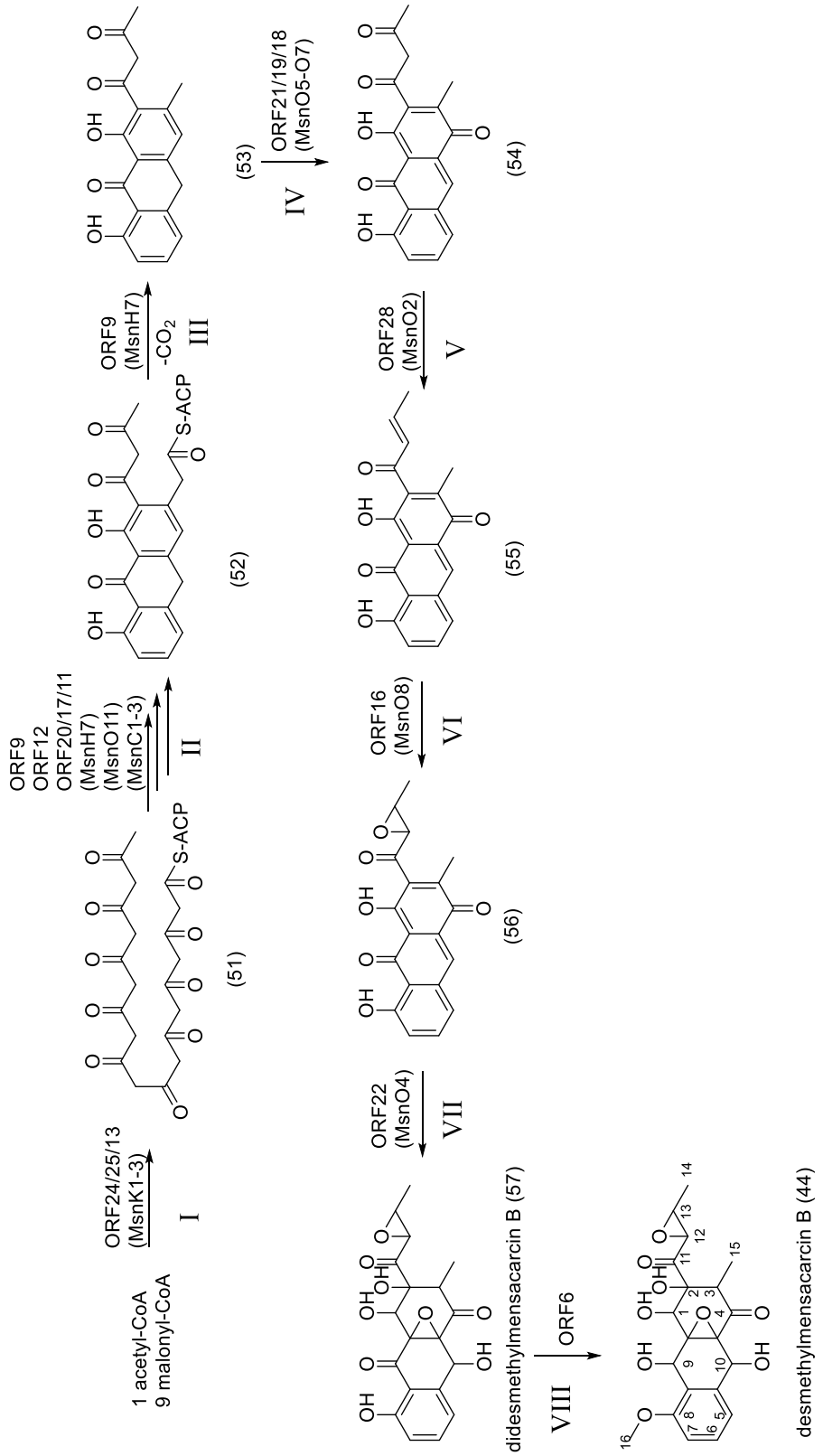

Figure 38. Proposed pathway for desmethylmensacarcin B biosynthesis.

4.4 Insights into the biosynthetic pathway of oxanthromicin

Oxanthromicin (39) is a yellow amorphous compound that was discovered by Patel *et al*. in *Actinomadura sp*. SCC 1646 in 1984 [157-159]. It shows activity against fungi from the division of Ascomycota as well as against *Staphylococcus aureus* and *Bacillus subtilis* (Table 14) [157, 167]. Salim *et al*. showed that oxanthromicin (39) also inhibits the K-Ras membrane localization and thus blocks the oncogenic activity of K-Ras [168].

Table 14. Bioactivity of oxanthromicin, MIC (minimal inhibition concentration) shown in literature ([157]/[167]) and measured in this study (*) (Measurements performed by HIPS).

Organism	Bioactivity – MIC	Organism	Bioactivity – MIC
Candida albicans	32 µg/ml *; moderate activity [157]	*Staphylococcus aureus*	32 µg/ml * moderate activity [157]
Colletotrichum capsici	6.25 µg/ml [167]	*Bacillus subtilis*	32 µg/ml *
Colletotrichium gloeosporioides	6.25 µg/ml [167]	*Pichia anomola*	32 µg/ml *;
		dermatophytes	Good activity [157]

Additionally to oxanthromicins (39) bioactivity, its chemical structure is interesting as well. Oxanthromicin is a dimeric anthrone compound (Figure 39), in which the two monomeric units are connected over a peroxide bridge [158]. Thus far this feature is unique in bacteria [158, 169]. The 2015 discovered neolignan bishonokiol A (58) (Figure 39) isolated from seeds of *Magnolia grandiflora* L. shares this dimerization feature with oxanthromicin (39) [169].

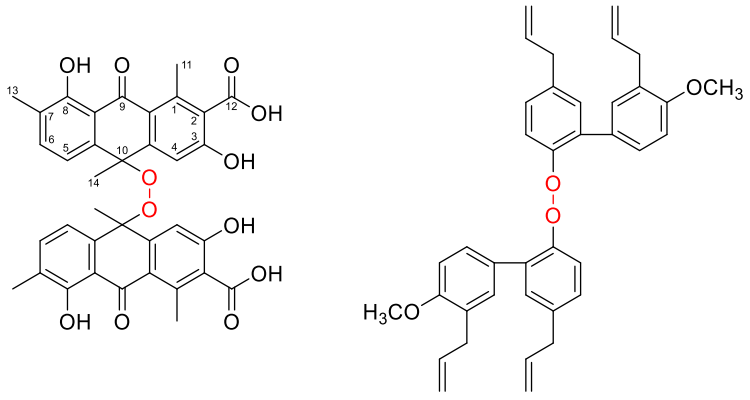

Figure 39. Chemical structures of oxanthromicin (39) and bishonokiol A (58), the peroxide bridge is marked in red.

The biosynthesis of oxanthromicin (39) was investigated in 1985 by Puar *et al*. [159]. In their experiments, *Actinomadura sp*. was fed with L-[methyl-^{13}C]methionine, Na-[1-^{13}C]acetate and Na-[2-^{13}C]acetate to analyze the incorporation of labeled carbon atoms during biosynthesis [159]. They discovered that oxanthromicin is produced by a type II polyketide synthase [159]. It was shown that the methyl groups at C7 and C10 result from methylation with methionine as methyl donor (Figure 40 green) and the C11 methyl group is part of the PKS core (Figure 40 blue) [159].

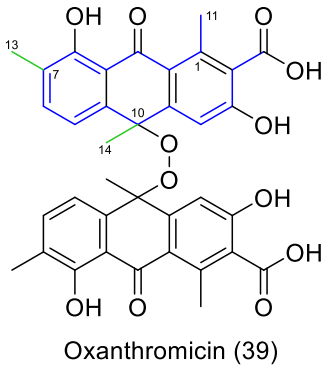

Figure 40. Methylation pattern of oxanthromicin regarding to Puar *et al*. 1985 [159]. Carbon atoms from PKS backbone colored blue, carbon atoms introduced through methylation with SAM colored green.

In this work we further investigated the biosynthesis of oxanthromicin using the biosynthetic gene cluster found in *S. acidiscabies* LU19995. From a constructed cosmid library the oxanthromicin BGC was located on one cosmid (chapter 4.2) [160]. Expression of the cosmid 1D11 in S. albus Del14 led to oxanthromicin production (chapter 4.2, Figure 33). Therefore, gene deletion experiments and heterologous expression in *S. albus* Del14 were performed. The cosmid 1D11 covers 39 kb of genomic DNA of *S. acidiscabies* LU19992. Overall there are 21 open reading frames (ORF) within the cosmid 1D11 (Figure 41 and Table 15). For identification of the oxanthromicin (39) biosynthesis the genes were analyzed with AntiSMASH [132] and NCBI blast [133] and gene deletion experiments were performed. The results of sequence analysis and gene deletion experiments were compared to the actinorhodin (Figure 15) biosynthesis as it is one of the best studied type II polyketides [170-172]. Actinorhodin was one of the first aromatic polyketides analyzed on a genetic level and to date remains one of the model compounds [58, 170-172].

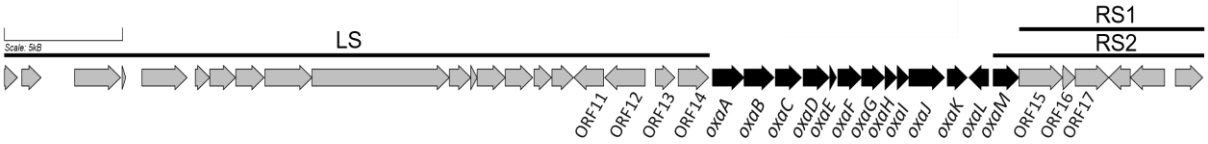

Figure 41. Biosynthetic gene cluster of oxanthromicin and neighboring genes from chromosomal DNA of *S. acidiscabies*.

Table 15. Proposed functions of enzymes encoded by the genes of the biosynthetic gene cluster of oxanthromicin and their neighboring genes. Homology of the products of the genes with the products of genes involved into the actinorhodin biosynthesis is shown in the last two columns [170-172].

Gene	Proposed function	Homolog in actinorhodin pathway	Identity/Similarity
ORF1	Oxygenase		
ORF2	NAD(P)H Dehydrogenase		
ORF3	Ligase		
ORF4	Ketoacylsynthase PKSI		
ORF5	Dehydrogenase		
ORF6	Ligase		
ORF7	Acryloyl-CoA reductase		
ORF8	Methoxymalonate biosynthesis protein		
ORF9	Haloalkan dehalogenase		
ORF10	Beta-lactamase		
ORF11	Aminotransferase		
ORF12	Putative protein		
ORF13	Membrane-protein		
ORF14	Histidine-kinase		
oxaA	Alpha ketoacylsynthase	*act*IORF1	70%/82%
oxaB	Beta ketoacylsynthase	*act*IORF2	60%/72%
oxaC	Methyltransferase		
oxaD	Methyltransferase		
oxaE	Acyl-carrier protein	*act*IORF3	48%/66%
oxaF	Cyclase	*act*VII	42%/52%
oxaG	Cyclase	*act*IV	56%/66%
oxaH	Hypothetical protein		
oxaI	Dioxygenase		
oxaJ	Oxidase		
oxaK	Regulatory protein	*act*IIORF4	41%/56%
oxaL	Ketoacyl reductase	*act*III	64%/76%
oxaM	Methyltransferase		
ORF15	Acetyl-CoA carboxlase carboxyltransferase		
ORF16	Carboxyl carrier protein		
ORF17	Carboxyl carrier protein		
ORF18	Integral membrane protein		

4.4.1 Discovery of the biosynthetic gene cluster of oxanthromicin and determination of the minimal oxanthromicin gene cluster

To determine the minimal oxanthromicin gene cluster the genes of the BGC were compared with the genes in the actinorhodin BGC (Table 15). Furthermore, the proposed gene functions of the genes next to actinorhodin homolog genes were analyzed.

The product of the genes encoding for KSα (OxaA), CLF (OxaB) and ACP (OxaE) were detected after comparison with homolog enzymes in actinorhodin biosynthesis. The cyclases (OxaF and OxaG) as well as the ketoacyl reductase (OxaL) and the regulatory protein (OxaK) showed homology to the enzymes involved in actinorhodin biosynthesis as well. According to the results of Puar *et al*., two additional methyltransferases are most likely involved in the oxanthromicin biosynthesis [159]. The cosmid 1D11 contains three genes encoding for putative methyltransferases (OxaC, OxaD and OxaM). All three methyltransferase genes were analyzed via knockout experiments, the new compounds were isolated from the butanol extracts and their structures were elucidated using NMR spectroscopy. The genes *oxaH*, *oxaI* and *oxaJ* encode for a putative protein, a dioxygenase and an oxidase, respectively (Table 15). Neither of these two shows a homology to proteins active in actinorhodin biosynthesis.

The genes upstream of *oxaA* encode for a histidine-kinase (ORF14), a membrane protein (ORF13), a putative protein (ORF12) and an aminotransferase (ORF11) (Table 15). A function within the oxanthromicin biosynthesis was neither assigned to any of the proteins encoded by these four genes nor the other ten enzymes encoded by the genes upstream of ORF11 (Table 15). Thus it was assumed that *oxaA* is the 5′ boundary of the oxanthromicin biosynthetic gene cluster. For analysis of the 5′ boundary of the BGC the 20 kb DNA fragment containing the genes ORF1 to ORF14 was deleted using RedET recombination. This led to the cosmid 1D11 LS (Figure 41, restriction mapping SI.4: Figure 70). The cosmid was introduced to *S. albus* Del14. The resulting strain *S. albus* 1D11 LS was cultivated for analysis. The butanol extract of the culture broth was analyzed using HPLC-MS. Compared to *S. albus* 1D11 the oxanthromicin production was not influenced (Figure 42). These results indicated that the genes upstream of *oxaA* are not essential for oxanthromicin production and *oxaA* is the 5′ end of the oxanthromicin biosynthetic gene cluster.

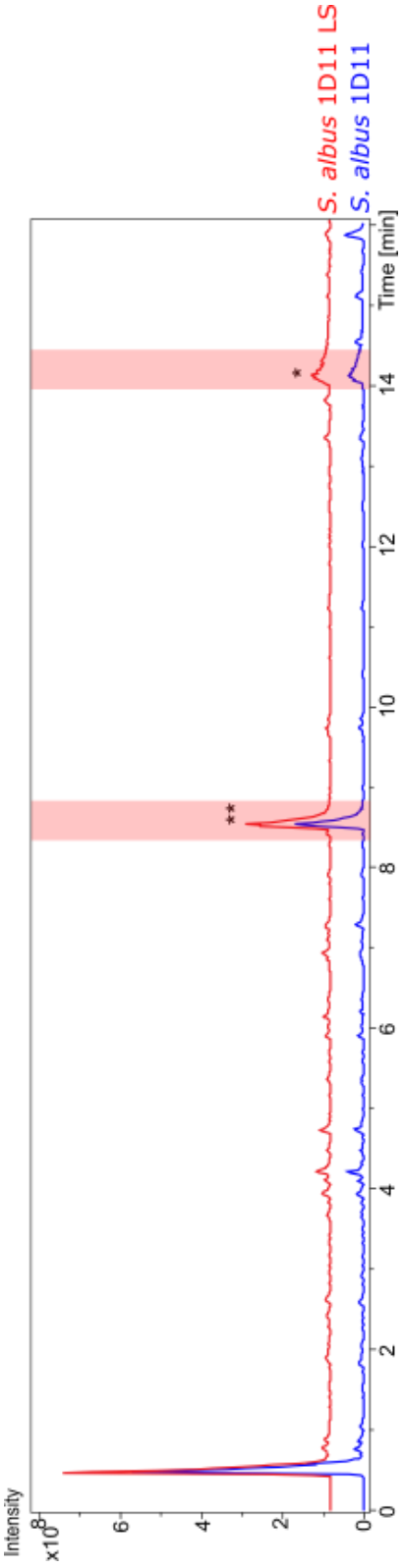

Figure 42. LC-MS chromatograms of butanol extract from *S. albus* 1D11 (blue) and *S. albus* 1D11_LS (red) after cultivation for 7 days at 28°C and 180 rpm in 100 mL DNPM. The oxanthromicin (39) peak is indicated by an asterisk (*). The *hemi*-oxanthromicin (40) peak is indicated by two asterisks (**). Both oxanthromicin (39) and *hemi*-oxanthromicin (40) were detected in the butanol extract from *S. albus* 1D11 and *S. albus* 1D11_LS.

Based on sequence analysis, the determination of the 3′ boundary of the oxanthromicin BGC was more complex than the determination of the 5′boundary. The last gene that shows homology to the actinorhodin biosynthesis is *oxaL*. But with *oxaM* there is a third methyltransferase encoding gene detectable on the cosmid. As depicted by Puar *et al*., only two methyltransferases are needed for oxanthromicin biosynthesis [159]. The genes ORF15 to ORF17 encode for an acetyl-CoA carboxylase carboxyltransferase and two carboxyl carrier proteins (Table 15). These enzymes participate in the synthesis of malonyl-CoA [48]. The synthesis of malonyl-CoA is not usually part of the T2PKS BGC [38]. Hence, the boundary of the gene cluster can be *oxaL* or *oxaM*. Therefore, two different knockout experiments were performed. In cosmid 1D11 RS1 5.8 kb genomic DNA were deleted downstream of *oxaM*, while 6.8 kb genomic DNA were deleted downstream of *oxaL* in 1D11 RS2 (Figure 41, restriction mapping SI.4: Figure 70). Both cosmids were transferred to *S. albus* Del14 through heterologous expression. The resulting strains were cultivated and their butanol extracts tested for oxanthromicin production. The knockout strain containing the cosmid 1D11 RS1 showed oxanthromicin production (Figure 43), while oxanthromicin production was abolished in *S. albus* 1D11 RS2 (Figure 43). Here, four new peaks were detected in the HPLC chromatogram of *S. albus* 1D11 RS2 instead of oxanthromicin. Two of which showed a corresponding mass of 595.1590 Da (59) each, while the other two peaks both showed a corresponding mass of 551.2590 Da (60). The production of these compounds instead of oxanthromicin showed that OxaM is essential for oxanthromicin production. However, the corresponding masses of the compounds do not indicate methyltransferase activity. To understand the activity of OxaM, *oxaM* was analyzed in a separate knockout experiment as described in chapter 4.4.2.3.

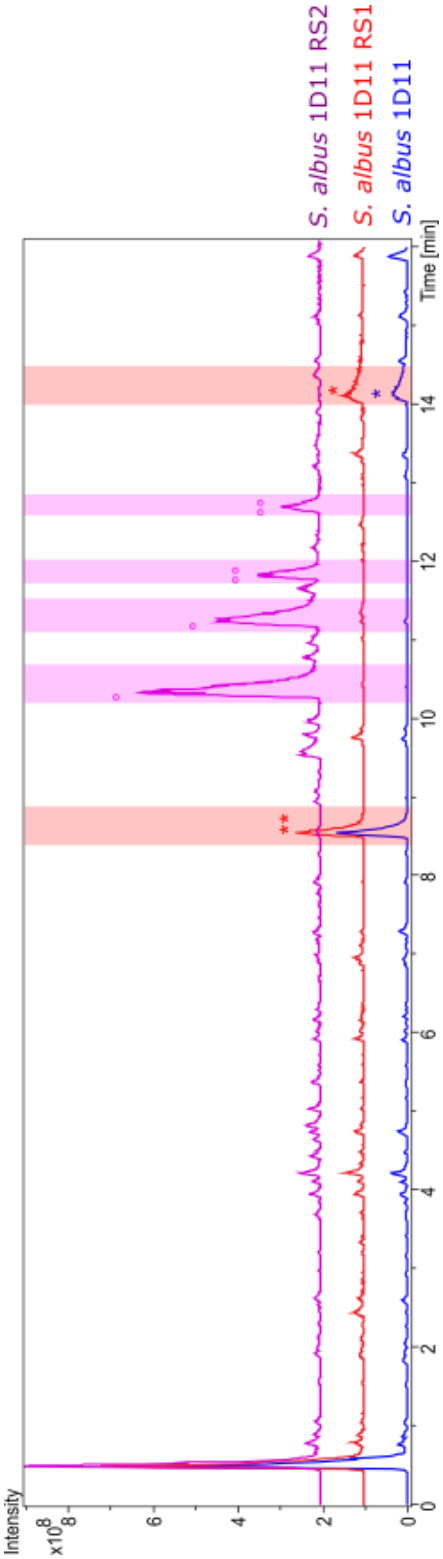

Figure 43. LC-MS chromatograms of butanol extract from *S. albus* 1D11 (blue), *S. albus* 1D11_RS1 (red) and *S. albus* 1D11_RS2 (purple) after cultivation for 7 days at 28°C and 180 rpm in 100 mL DNPM. The oxanthromicin (39) peak is indicated by an asterisk (*). The *hemi*-oxanthromicin (40) peak is indicated by two asterisks (**). Both oxanthromicin (39) and *hemi*-oxanthromicin (40) were detected in the butanol extract from *S. albus* 1D11 and *S. albus* 1D11_RS1, but not in the butanol extract of *S. albus* 1D11_RS2. In the butanol extract of *S. albus* 1D11_RS2 four new peaks were discovered, indicated by ° and °°.

The knockout experiments showed that gene deletions upstream of *oxaA* and downstream of *oxaM* did not influence the oxanthromicin (39) biosynthesis in the heterologous host *S. albus* Del14. The cosmid 1D11 KO0 with the minimal cluster *oxaA* to *oxaM* was generated by deletion of the genes ORF1 to ORF14 in the cosmid 1D11 RS1 (restriction mapping SI.4: Figure 70). The strain *S. albus* 1D11 KO0 containing the minimal cluster showed oxanthromicin production (SI.4: Figure 71). The cosmid 1D11 KO0 was used to perform single gene deletions for the knockout experiments. *S. albus* 1D11 KO0 was used as the reference strain in the single gene deletions described in chapter 4.4.2.

4.4.2 Biosynthesis of oxanthromicin

The biosynthetic gene cluster of oxanthromicin contains 13 open reading frames with 12.3 kb of genomic DNA of *S. acidiscabies* LU19992. All thirteen genes were analyzed in order to unveil their function within the biosynthesis. Combined with the sequence analysis, knockout experiments with ten of the thirteen genes were performed in order to elucidate the biosynthesis of oxanthromicin. Of the thirteen genes present in the oxanthromicin BGC seven showed homology on the protein level to the genes of the actinorhodin biosynthetic gene cluster, the model compound for type II polyketides (Table 15) [170-172].

Key part in solving the biosynthesis of oxanthromicin was the analysis of the methyltransferases. Though there are three genes encoding putative methyltransferases in the oxanthromicin biosynthetic gene cluster, only two of them (C7 and C10, Figure 39) originate from a methyl group transfer from *S*-adenosyl-methionine [159]. The C11 methyl group is produced during the synthesis of the polyketide core [159]. The analyses of the genes encoding the putative methyltransferases are described in chapter 4.4.2.3.

4.4.2.1 Minimal PKS in oxanthromicin biosynthesis

The genes *oxaA*, *oxaB* and *oxaE* encode for a ketosynthase (KS), a chain length factor (CLF) and an acyl carrier protein (ACP), respectively. These three enzymes OxaA, OxaB and OxaC represent the minimal PKS, which is responsible for production of the polyketo chain. The enzymes of the minimal PKS were compared to their homologues ActIORF1-3 in the actinorhodin biosynthetic pathway [171]. The ketosynthase OxaA shows a homology of 82% to the ketosynthase ActIORF1 [171]. OxaB shows a 72% homology to ActIORF2, the CLF [171]. The ACP OxaE shares a 66% homology to ActIORF3 [171].

In knockout experiments full abolishment of the synthesis is expected. Hence only sequence analysis was performed. The minimal PKS performs the synthesis of a 16C poly-β-keto chain (61). Through Claisen condensation an acetyl-CoA starter unit is elongated with seven malonyl-CoA units (Figure 44).

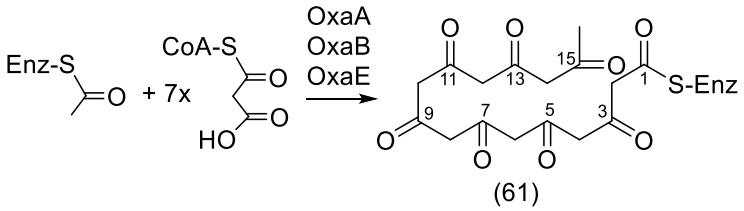

Figure 44. Biosynthesis of oxanthromicin part I: polyketide core.

4.4.2.2 Auxiliary polyketide enzymes in oxanthromicin biosynthesis

The three genes *oxaL*, *oxaF* and *oxaG* encode for a ketoacyl reductase, and two cyclases, respectively. These enzymes are presumably involved in the oxanthromicin (39) biosynthesis as auxiliary polyketide enzymes. All three genes were deleted separately on the cosmid 1D11. For the analysis the produced cosmids were heterologous expressed in *S. albus* Del14 and subsequently cultivated. The butanol extracts of the cultures were analyzed for the production of oxanthromicin (39), its derivatives and shunt products.

OxaL encodes for the putative ketoacyl reductase OxaL. This enzyme shows a 76% homology to ActIII, the ketoreductase in actinorhodin biosynthesis [170, 171]. OxaL is proposed to reduce the C9 carbonyl group of compound 61 to a hydroxy group in compound 62, which leads to a conformational change of the poly-keto chain (Figure 45) [6]. This conformational change supports the cyclization through the U-shape orientation [6].

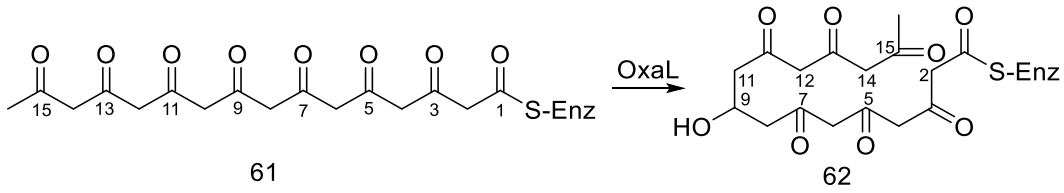

Figure 45. Ketoreduction reaction performed by OxaL during biosynthesis of oxanthromicin.

The gene *oxaL* was deleted in cosmid 1D11 KO0, resulting in the cosmid 1D11 KOL+Hyg(SI.4: Figure 72). The hygromicin resistance was removed and the resulting comsid 1D11 KOL was heterologously expressed in *S. albus* Del14. The new strain *S. albus* 1D11 KOL was cultivated and extracted with butanol for analysis. The knockout of gene *oxaL* abolished the oxanthromicin (39) production. No intermediates or shunt products were detected in the LC-MS chromatogram of the butanol extract of the knockout strain (SI.4: Figure 73). The complementation plasmid pRT801 1D11 KompL could not succesfully be produced, because ligation did not work in the plasmids with the *Nde*I restriction site. Hence no complementation experiment was performed.

OxaF is a putative cyclase/aromatase which shows a 52% homology to ActVII [173]. ActVII acts as the first ring cyclase and aromatase in the actinorhodin biosynthesis [173]. The enzyme OxaF likewise is assumed to perform cyclization followed by aromatization of the first ring in oxanthromicin biosynthesis as well (Figure 46).

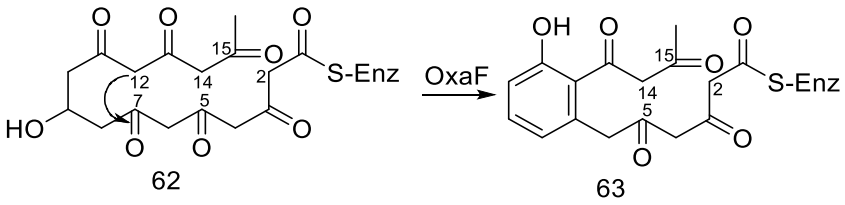

Figure 46. First ring cyclization performed by OxaL during biosynthesis of oxanthromicin.

Using RedET recombination, the gene *oxaF* was deleted in the cosmid 1D11 and the inserted hygromicin resistence gene was deleted in the resulting cosmid 1D11 KOF (SI.4: Figure 74). The constructed cosmid with oxaF deletion was transferred to *S. albus* Del14 by conjugation to create the knockout strain *S. albus* 1D11 KOF. This knockout strain was cultivated and its butanol extract analyzed for oxanthromcin production. No production of oxanthromicin (39), its derivatives or shunt products were observed in the butanol extract (SI.4: Figure 75). Complementation of *oxaF* restored the oxanthromicin production.

The second ring closure in actinorhodin biosynthesis is performed by ActIV [58]. *OxaG* encodes for a putative cyclase that shows 66% homology to ActIV. It is assumed that OxaG is responsible for the second ring closure in oxanthromicin biosynthesis. In actinorhodin the third ring is an oxygen heterocycle [174]. Third ring closure in actinorhodin biosynthesis occurs spontaneously after C3 ketoreduction [174]. In contrast to actinorhodin, the third ring of oxanthromicin is not a heterocycle. In the trioxacarcin biosynthesis the third ring closure is performed by TxnC3, a specific 2-3-cyclase [68]. OxaG also shows a 64% homology to TxnC3. It is proposed that OxaG performs the second and third ring closures in oxanthromicin biosynthesis similar to TxnC3 in trioxacarcin biosynthesis (Figure 47).

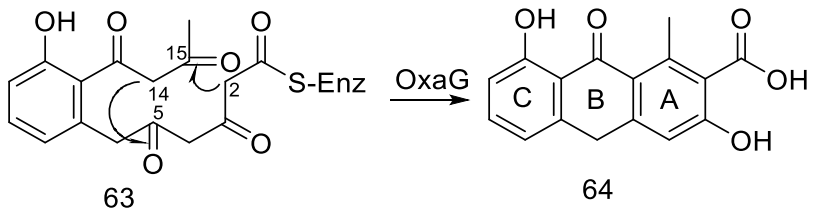

Figure 47. Second and third ring cyclization performed by OxaG during biosynthesis of oxanthromicin.

The gene *oxaG* was deleted in the cosmid 1D11 using RedET recombination (SI.4: Figure 74). The butanol of the knockout strain *S. albus* 1D11 KOG extract was analyzed for production of oxanthromicin, its derivatives and shunt products. Compared to the control strain *S. albus* Del14, two new peaks were observed in *S. albus* 1D11 KOG (SI.4: Figure 76). The two new peaks showed masses of 719.19965 Da and 579.1664 Da respectively (SI.4: Figure 76). Isolation of neither compound was possible; hence their structures were not solved. These new peaks could represent shunt products of spontaneous cyclization.

After the extraction of the knockout strains *S. albus* 1D11 KOL, *S. albus* 1D11 KOF and *S. albus* 1D11 KOG no production of oxanthromicin (39) was observed. In the butanol extract of *S. albus* 1D11 KOG two new compounds were detected that may represent shunt products of spontaneous cyclization. No compounds could be isolated from the three knockout strains. Based on the sequence analysis along with a comparison to auxiliary polyketide enzymes of other polyketide biosynthetic pathways we proposed the functions of OxaL, OxaF and OxaG. We propose OxaL to be a C9 ketoreductase and both OxaF and OxaG to be cyclases.

OxaL reduces the C9-keto group to a hydroxy group, which triggers a conformational change which in turn benefits the cyclization (Figure 48 A) [6]. We suggest that OxaF is a first ring cyclase and OxaG acts as a second and third ring cyclase (Figure 48 B). OxaF catalyzes the first ring cyclization between C7 and C12, followed by aromatization of the first ring [67, 175]. The second ring cyclization between C5 and C14 is catalyzed by OxaG. Similar to TxnC3 in the trioxarcarcin biosynthesis the third ring cyclization is most likely also catalyzed by OxaG [68]. In actinorhodin biosynthesis, the second ring cyclase ActIV is a bifunctional enzyme, which is responsible for the release of the polyketide chain. Therefore, no dedicated thioesterase is recquired (Figure 48) [55, 58]. It is proposed that like ActIV, OxaG is also

responsible for polyketide chain release. Together the three enzymes OxaL, OxaF and OxaG transform the 16C poly-β-keto chain (61) into 3,8-dihydroxy-1-methyl-9-oxo-9,10-dihydroanthracene-2-carboxylic acid (64) (Figure 48).

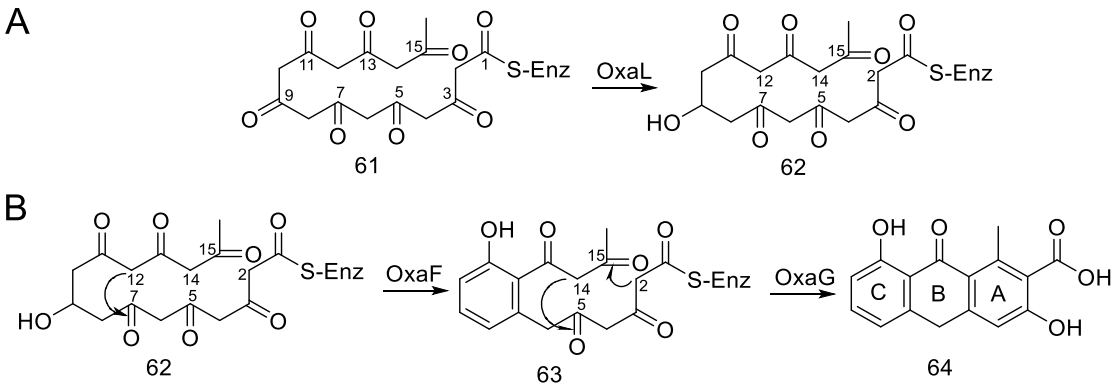

Figure 48. Biosynthesis of oxanthromicin part II: auxiliary polyketide enzymes. A: Ketoreduction reaction performed by OxaL. B: Cyclization and aromatization reactions performed by OxaF and OxaG.

4.4.2.3 Polyketide tailoring in oxanthromicin biosynthesis

The three-ring precursor molecule (64) is modified by the tailoring enzymes OxaC, OxaD, OxaI, OxaJ and OxaM. Compared to the three-ringed precursor molecule (64), oxanthromicin (39) is methylated at C7 and C10, as well as hydroxylated and dimerized at C10 (Figure 49). Sequence analysis showed that OxaI is annotated as a dioxygenase and OxaJ as an oxidase. The enzymes OxaC, OxaD and OxaM are annotated as SAM dependent methyltransferases. In oxanthromicin (39) biosynthesis, only the methyl groups at C7 and C10 originate from the activity of methyltransferases [159]. Therefore, it is possible that one of the methyltransferases fulfills another function. Comparison of the three putative methyltransferases showed that OxaC and OxaD have a 74% homology, while OxaM only shows a homology of 47% to OxaC and a homology of 50% to OxaD. This indicates that OxaC and OxaD are more similar to each other than to OxaM, hence may have similar activities or targets.

The genes *oxaC*, *oxaD*, *oxaI*, *oxaJ* and *oxaM* were deleted separately in the cosmid 1D11 KO0 using RedET recombination in order to generate the cosmids 1D11 KOC, 1D11 KOD, 1D11 KOI, 1D11 KOJ and 1D11 KOM. Each of these cosmids was heterologously expressed in *S. albus* Del14 and the resulting strains were cultivated, extracted and their butanol extracts analyzed for production of oxanthromicin (39) or any derivatives.

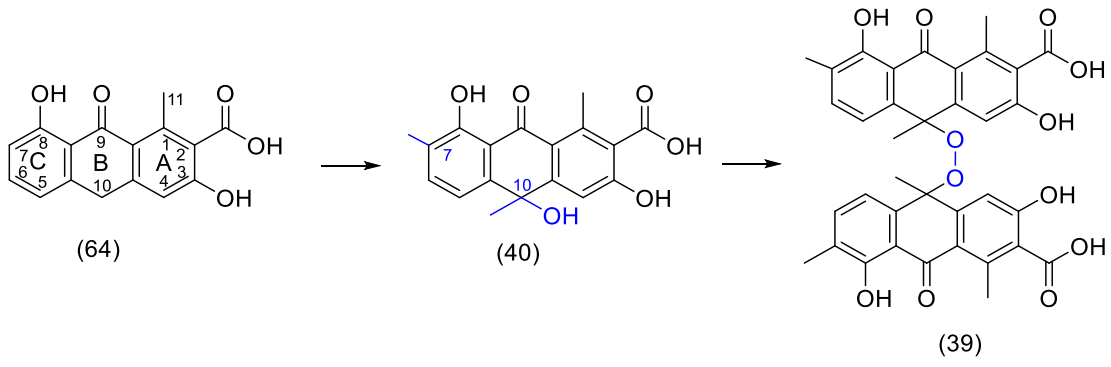

Figure 49. Biosynthesis of oxanthromicin part III: tailoring enzymes.

According to chemical experiments by Salim *et al*., at first the hydroxylation of C10 takes place [168]. It is proposed that hydroxylation is performed by the oxygenase OxaI (Figure 50, reaction I). OxaI is annotated as a dioxygenase that shows a 48% homology to flavoprotein OxyS. The latter is the hydroxylase responsible for hydroxylation of methylated C10 in oxytetracycline biosynthesis [44]. The gene *oxaI* was deleted using RedET recombination (SI.4: Figure 77). The constructed cosmid 1D11 KOI was heterologously expressed in *S. albus* Del14. In the butanol extract of *S. albus* 1D11 KOI neither an oxanthromicin derivative nor a new compound were detected (SI.4: Figure 78). Due to the deactivation of the dioxygenase the biosynthesis of oxanthromicin was terminated. It was proposed that like OxyS in the oxytetracycline biosynthesis, OxaI is also responsible for C10 hydroxylation to produce compound 65 (Figure 50, reaction I) [44]. An intermediate was not detected which indicates that a not hydroxylated intermediate might not be stable or is dismantled. Complementation of *oxaI* restored oxanthromicin production.

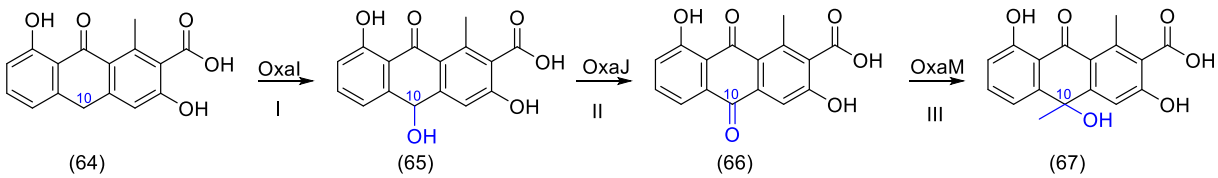

Figure 50. Hydroxylation and methylation of C10 in oxanthromicin biosynthesis.

Following hydroxylation the C10 hydroxyl group is oxidized to a keto group. This oxidation is proposed to be performed by OxaJ (Figure 50, reaction II). OxaJ is annotated as an FAD-binding oxidoreductase with a 59% homology to McrA, which is the radical oxidase involved in mitomycin resistance mechanism [176, 177]. McrA is responsible for the oxidative inactivation of the reduced toxic mitomycin intermediate (68) to mitomycin (69) (Figure 51) [177].

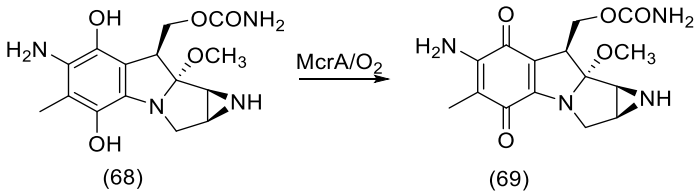

Figure 51. Mitomycin biosynthesis step performed by McrA.

To analyze the function of OxaJ, a knockout of gene *oxaJ* in cosmid 1D11 was prepared using RedET recombination (SI.4: Figure 77). For heterologous expression the constructed cosmid was transferred to *S. albus* Del14 through conjugation. The butanol extract of the culture of *S. albus* 1D11 KOJ contained a new compound (70) with a mass of 618.1491 Da. It also contained *hemi*-oxanthromicin as detected by the LC-MS and depicted in the chromatogram (Figure 52). The new compound was isolated and analyzed with NMR spectroscopy (Table 20). The compound was identified as *spiro*-oxanthromicin A (70) (Figure 53 A) [168]. *Spiro*-oxanthromicin A (70) was first discovered in a *Streptomyces* extract in 2015 by Salim *et al*. as a derivative of oxanthromicin (39) [168]. It was the first detected naturally occurring *spiro* dimerized compound that had been described in 1979 by Becker and Sanchez [168, 178]. Introduction of a spiro moiety positively impacts the drug usability of a compound in regards to potency and selectivity [179].

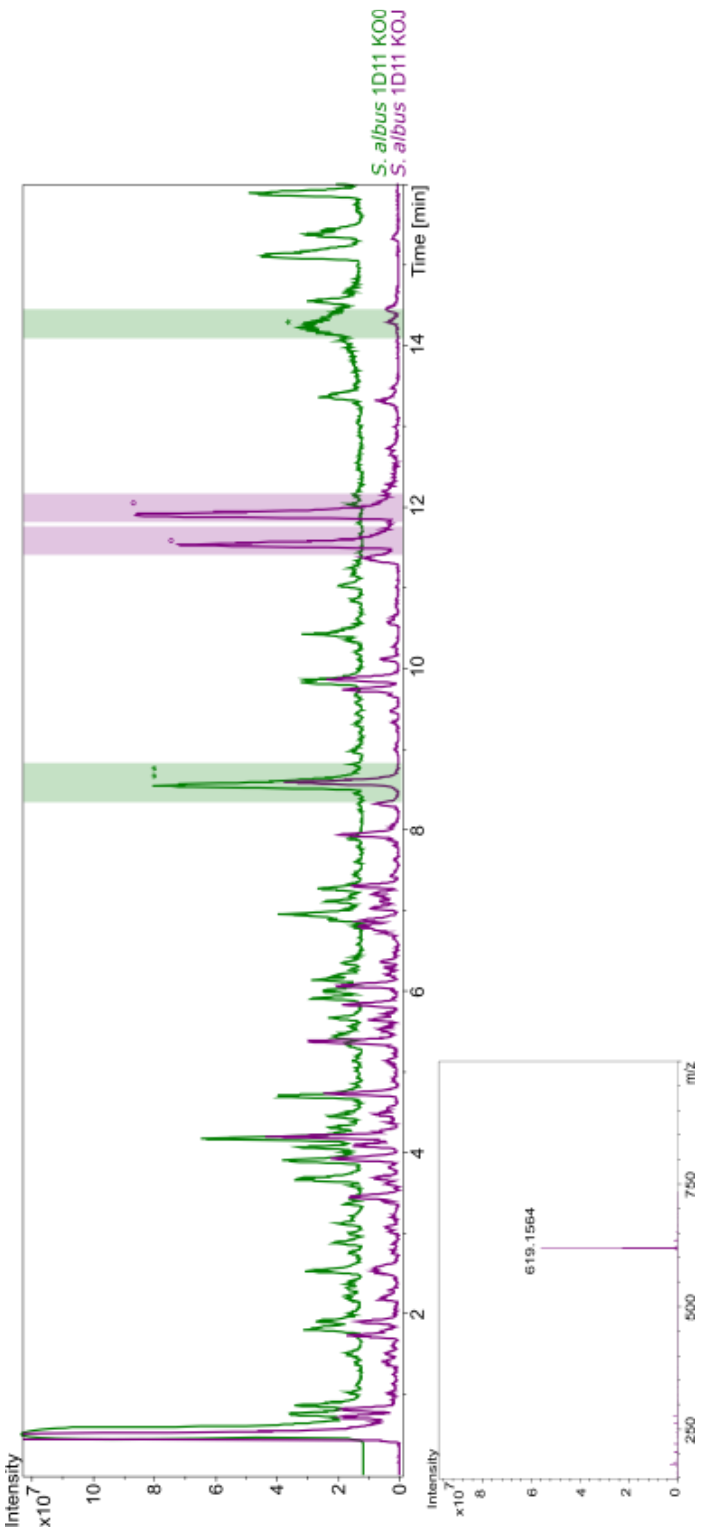

Figure 52. LC-MS chromatograms of butanol extract from *S. albus* 1D11 (green) and *S. albus* 1D11 KOJ (purple) after cultivation for 7 days at 28°C and 180 rpm in 100 mL DNPM. (A) Base peak chromatograms of *S. albus* 1D11 and *S. albus* 1D11 KOJ. In green the oxanthromicin (39) peak is indicated by one asterisk (*) and *hemi*-oxanthromicin (40) by two asterisks (**). In purple the *spiro*-oxanthromicin (70) peak is indicated by one circle (°). (B) Mass spectrum associated to t_R=11.5 min and t_R=12.0 min (*spiro*-oxanthromicin (70)) from *S. albus* 1D11 KOJ LC-MS chromatogram.

Based on the results of Becker and Sanchez, Salim *et al*. proposed a possible reaction mechanism (Figure 53 B) [168, 178]. Spontaneous acid mediated dehydration of *hemi*-oxanthromicin (40) results in the *hemi*-oxanthromicin carbocation (71). This carbocation is dimerized to generate a (±)-*spiro*-oxanthromicin carbocation (72), which is then hydroxylated and dehydroxylated to form *spiro*-oxanthromicin A (70) (Figure 53 B).

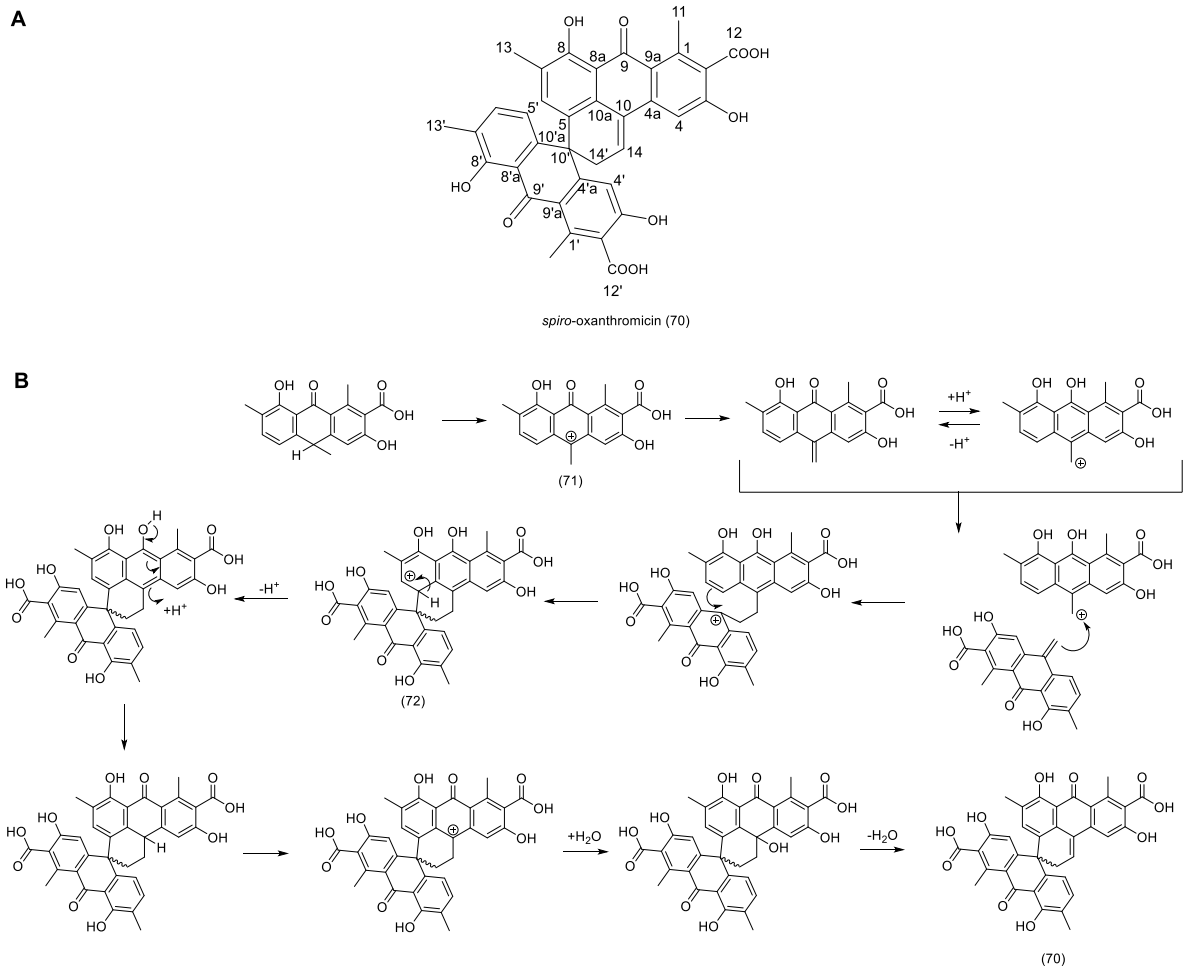

Figure 53. A: Chemical structure of *spiro*-oxanthromicin (70). B: Proposed reaction mechanism for synthesis of *spiro*-oxanthromicin A proposed by Salim *et al*. [168].

Based on the sequence analysis of OxaJ, it is proposed that OxaJ oxidizes the C10 hydroxy group as preparation for methylation (Figure 50). The side product *spiro*-oxanthromicin does not show a function in oxanthromicin biosynthesis.

Next, the C10 position of compound 66 is methylated by OxaM (Figure 50, reaction III). Using RedET recombination the cosmid 1D11 KOM was constructed (SI.4: Figure 79) and heterologously expressed in *S. albus* Del14. In the LC-MS analysis of the butanol extract of *S. albus* KOM four new peaks were identified (Figure 54). Of the four compounds two showed a mass of 594.1514 Da (59) each and the remaining two showed a mass of 550.1623 Da (60) each (Figure 54). The masses of these four compounds did not show any indications to a methyl group loss or to be oxanthromicin derivatives. To analyze them, the four compounds were isolated from a cultivation of *S. albus* 1D11 KOM followed by structure elucidation with NMR analysis. The compounds with the mass of 594.1514 Da (59) showed similar NMR spectra to one another indicating that the compounds were diastereomers (SI.4: Table 21). Thus, both compounds with the mass of 594.1415 Da were treated as the same compound 59 in further discussions. The same was proposed for the compounds with the mass of 550.1623 Da, which were treated as compound 60. Stereo chemistry of the compounds 59 and 60 was not analyzed.

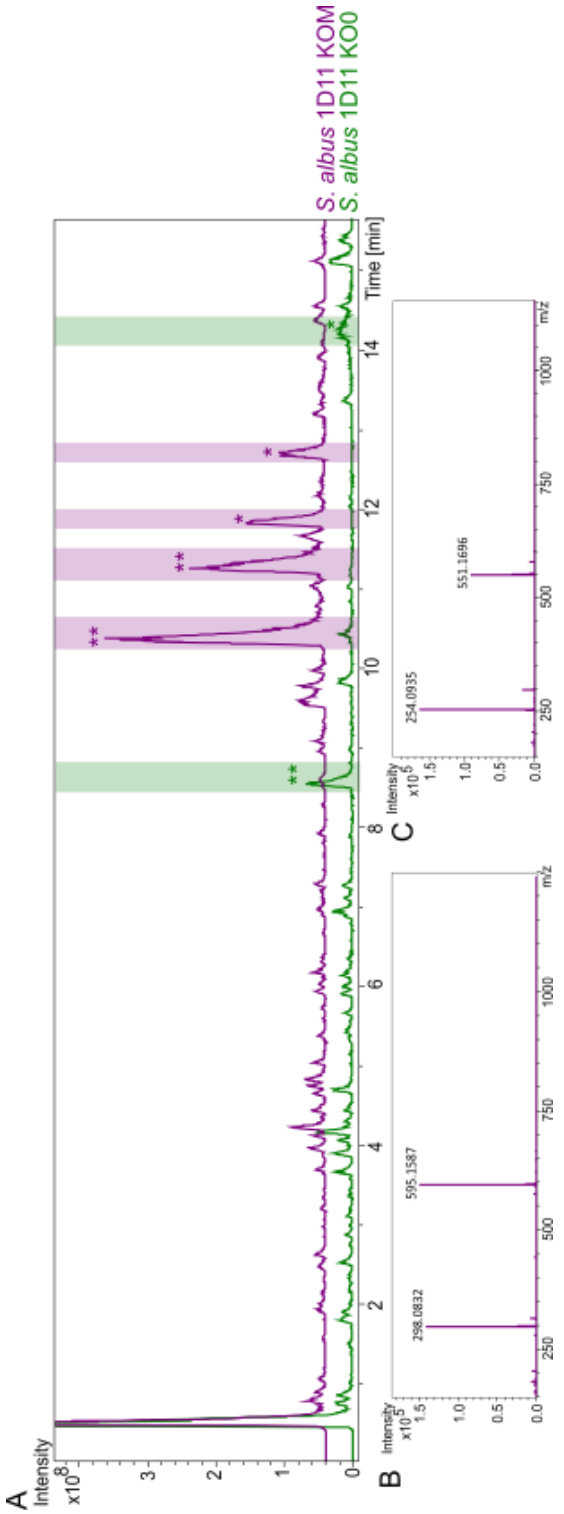

Figure 54. LC-MS chromatograms of butanol extract from *S. albus* 1D11 (green) and *S. albus* 1D11 KOM (purple) after cultivation for 7 days at 28°C and 180 rpm in 100 mL DNPM. (A) Base peak chromatograms of *S. albus* 1D11 and *S. albus* 1D11 KOM. In green the oxanthromicin (39) peak is indicated by one asterisk (*) and *hemi*-oxanthromicin (40) by two asterisks (**). In purple the desperoxyoxanthromicin (59) peak is indicated by two asterisks (**) and decarboxydesperoxyoxanthromicin (60) peak by one asterisk (*). (B) Mass spectrum associated to t_R=10.4 min and t_R=11.3 min (desperoxyoxanthromicin (59)) from *S. albus* 1D11 KOM LC-MS chromatogram. (C) Mass spectrum associated to t_R=11.8 min and t_R=12.7 min (decarboxydesperoxyoxanthromicin (60)) from *S. albus* 1D11 KOM LC-MS chromatogram.

NMR analysis of the compound with the mass of 594.1514 Da showed that these compounds (59) consist of two tricyclic monomer units connected through a C-C-bond at C10 instead of the peroxide bridge in oxanthromicin (39) (Figure 55, SI.4: Table 21). The compounds were named desperoxyoxanthromicin. The compounds with the mass 550.1623 Da have a mass that is 44 Da lower than that of the desperoxyoxanthromicins (Figure 54 B-C). This mass difference indicates the loss of a carboxyl group. NMR analysis of the compounds 60 supported the theory of decarboxylation (SI.4: Table 22). The compounds were named decarboxydesperoxyoxanthromicin (60).

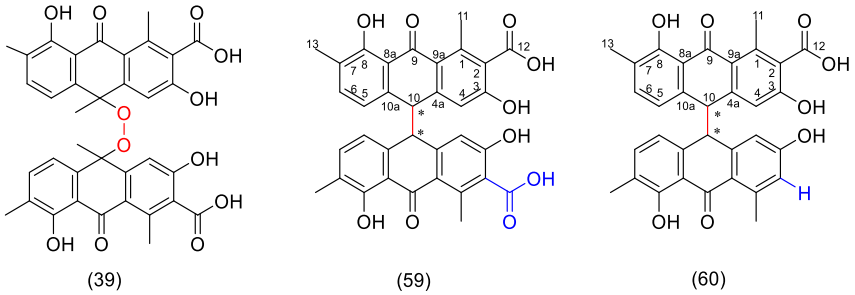

Figure 55. Chemical structures of oxanthromicin (39), desperoxyoxanthromicin (59) and decarboxydesperoxy-oxanthromicin (60). Changes in dimerization between the compounds depicted in red, the difference between desperoxyoxanthromicin and decarboxydesperoxyoxanthromicin in blue.

In desperoxyoxanthromicin (59) the C10 methyl group as well as the C10 hydroxy group and peroxide bridge are absent. OxaM shows a 70% homology to OxyF which is responsible for B-ring methylation in oxytetracycline biosynthesis [44, 180]. Furthermore, OxaM shows a 71% homology to DacM1 and a 62% homology to SsfM4, both of which are C-MTs in the dactylocycline and SF2575 biosynthesis [181, 182]. Together the missing C10 methyl group as well as the high homology of OxaM to the C-MTs indicate that the putative methyltransferase OxaM is responsible for C10 methylation in oxanthromicin biosynthesis. Production of compound 65 (Figure 50, reaction III) was expected.

The compounds produced by the knockout strain *S. albus* 1D11 KOM are dimers without C10 methylation and hydroxylation. The fact that the dimer is not oxidized may indicate that dimerization occurs prior to oxidation. This, however,is not in accordance with results of Salim *et al*. [168]. Considering the results of Salim *et al*., it is expected that the hydroxy groups are removed during dimerization [168]. With the high homology of OxaI to OxyS there is still the possibility that C10 is methylated first [44].

The second studied putative methyltransferase OxaD shows a 53% homology to OxyF and a 42% homology to MtmMII, which functions as the C7 C-MT from mithramycinone biosynthesis [183, 184]. *OxaD* was knocked out and heterologously expressed in *S. albus* Del14 (SI.4: Figure 80). In the LC-MS chromatogram of the butanol extract after cultivation two new peaks were discovered (Figure 56). The new peaks had a mass of 314.0789 Da at t_R=7.0 min (67) and 626.1423 Da at t_R=11.8 min (68), respectively (Figure 56 B-C). The mass difference between the two new compounds indicated that the compound 314.0789 Da (67) was the monomer of the compound 626.1423 Da (68). The mass of the first compound (67) at t_R=7.0 min was 14 Da smaller than *hemi*-oxanthromicin (40). The mass of the second compound (68) at t_R=11.8 min was 28 Da smaller than oxanthromicin (39). The difference in mass compared to oxanthromicin (39) and *hemi*-oxanthromicin (40) strongly pointed to the loss of one or two methyl groups respectively. This indicated that OxaD is indeed a methyltransferase. To verify assumption, both new compounds were isolated and their structures were solved using NMR-spectroscopy (SI.4: Table 23, Table 24). In both new compounds the C7 positions were not methylated (Figure 57 A). Neither of the compounds had been described and thus were named 7,7′-didesmethyloxanthromicin (67) and (±)-*hemi*-7-desmethyloxanthromicin (68). The results of the knockout experiments showed that OxaD is responsible for one of the C7 methylation steps in oxanthromicin (39) biosynthesis (Figure 57 B). Complementation of the gene *oxaD* restored oxanthromicin (39) production.

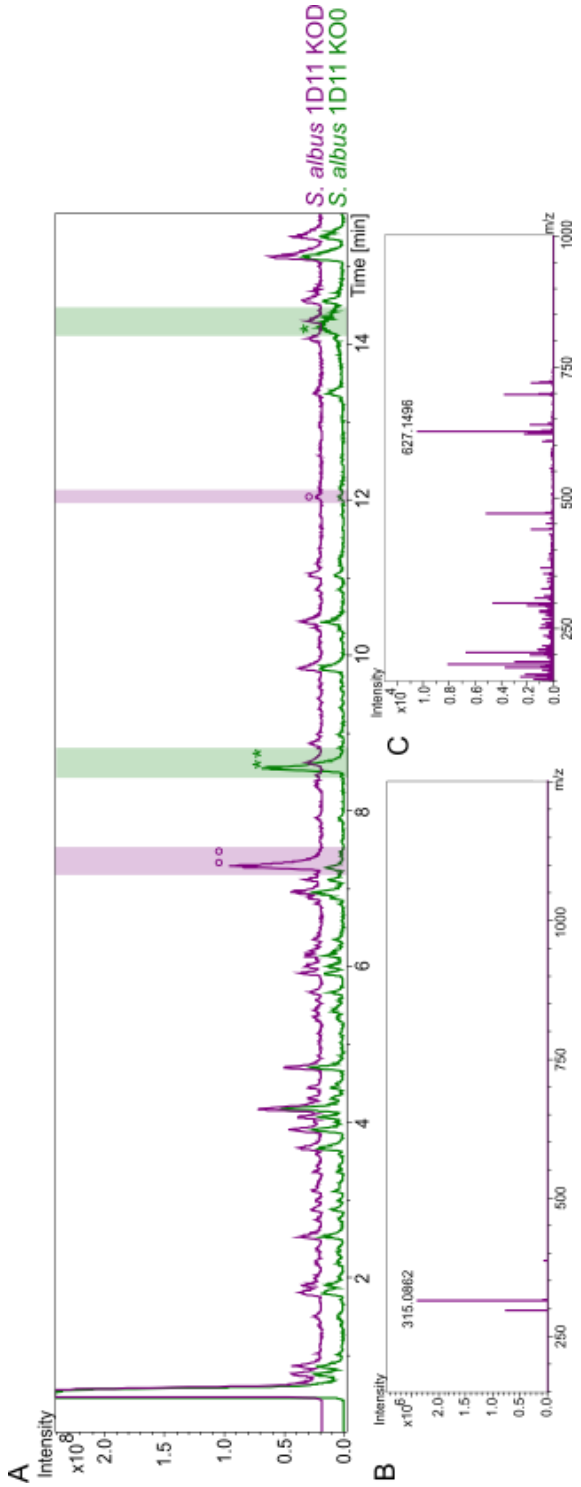

Figure 56. LC-MS chromatograms of butanol extract from *S. albus* 1D11 (green) and *S. albus* 1D11 KOD (purple) after cultivation for 7 days at 28°C and 180 rpm in 100 mL DNPM. (A) Base peak chromatograms of *S. albus* 1D11 and *S. albus* 1D11 KOD. In green the oxanthromicin (39) peak is indicated by one asterisk (*) and *hemi*-oxanthromicin (40) by two asterisks (**). In purple the 7,7-didesmethyloxanthromicin (68) peak is indicated by one circle (°) and *hemi*-7-desmethyloxanthromicin (67) peak by two circles (°°). (B) Mass spectrum associated to t_R=7.0 min (7,7-didesmethyloxanthromicin (68)) from *S. albus* 1D11 KOD LC-MS chromatogram. (C) Mass spectrum associated to t_R=11.8 min (*hemi*-7-desmethyloxanthromicin (67)) from *S. albus* 1D11 KOD LC-MS chromatogram.

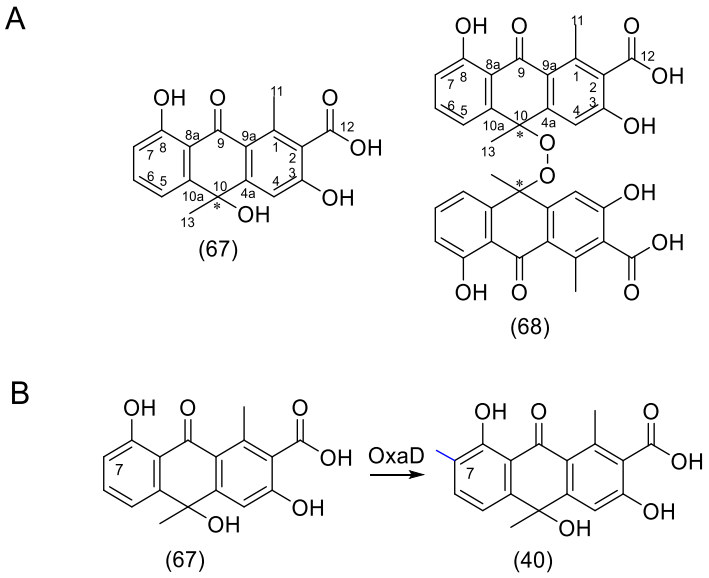

Figure 57. A: Chemical structures of (±)-*hemi*-7-desmethyloxanthromicin (66) and 7,7′-didesmethyloxanthromicin (67). B: Methylation of the C7 position in oxanthromicin biosynthesis.

OxaC is the third putative methyltransferase in the oxanthromicin (39) biosynthetic gene cluster (Table 15). This enzyme shows a homology of 52% to OxyF and a homology of 39% to MtmMII [44, 180, 183, 184]. The gene *oxaC* was deleted in the cosmid 1D11 KO0 using RedET recombination leading to the cosmid 1D11 KOC (SI.4: Figure 81). To analyze the effect of this knockout, the cosmid 1D11 KOC was introduced to *S. albus* Del14 through conjugation. The strain *S. albus* 1D11 KOC was cultivated and the culture broth was extracted with butanol. The extract was analyzed with LC-MS. In the LC-MS chromatogram no oxanthromicin (39) was detected, but a peak putatively corresponding to the monomeric *hemi*-oxanthromicin (40) was detected at t_R=8.5 min (Figure 58, Figure 59). To confirm this assumption, the compound was isolated and its structure was analyzed by NMR spectroscopy [158]. The compound was verified to be *hemi*-oxanthromicin (40) (SI.4: Table 25). The result of this knockout experiment showed that OxaC is not involved in the methyl group transfer. Despite the high similarity of 74% between OxaC and OxaD it appears as though OxaC shows no methyltransferase activity.

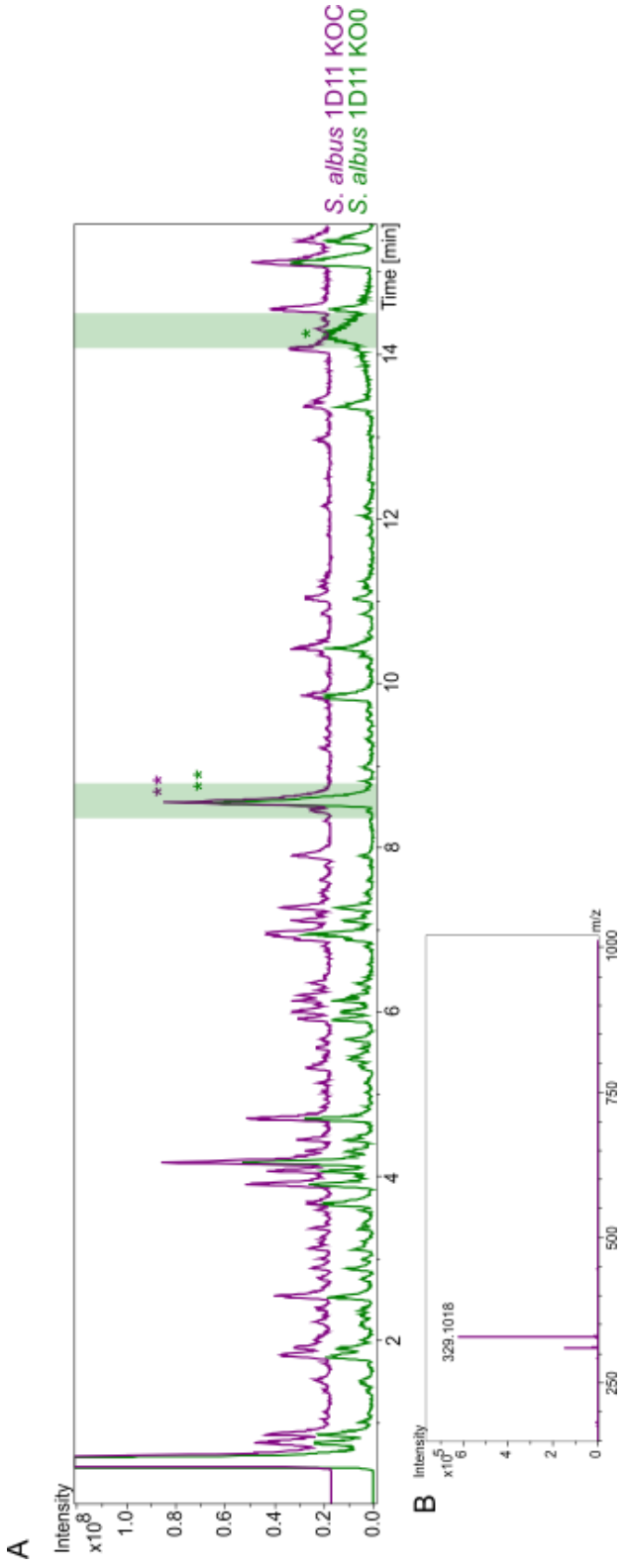

Figure 58. LC-MS chromatograms of butanol extract from *S. albus* 1D11 (green) and *S. albus* 1D11 KOC (purple) after cultivation for 7 days at 28°C and 180 rpm in 100 mL DNPM. (A) Base peak chromatograms of *S. albus* 1D11 and *S. albus* 1D11 KOC. In green the oxanthromicin (39) peak is indicated by one asterisk (*) and *hemi*-oxanthromicin (40) by two asterisks (**). In purple the *hemi*-oxanthromicin (40) peak is indicated by two asterisks (**). (B) Mass spectrum associated to t_R=8.5 min (the *hemi*-oxanthromicin peak (**)) from *S. albus* 1D11 LC-MS chromatogram.

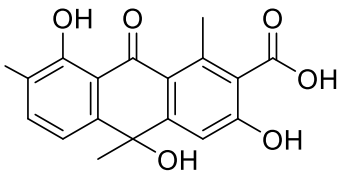

(40)

Figure 59. Chemical structure of *hemi*-oxanthromicin (40).

The exclusive production of *hemi*-oxanthromicin (40) indicates that OxaC is involved in the dimerization during oxanthromicin (39) biosynthesis. As described above (chapter 1.3.3.3) there are SAM dependent enzymes that support other reactions than methylations [121]. OxaC shows a 41% homology to DnrK, a 44% homology to RdmB and a 46% homology to CalMB [122, 166, 185, 186]. DnrK is a bifunctional enzyme that shows a 4-*O*-methyltransferase activity as well as a 10-decarboxylation activity [122, 185]. RdmB and CalMB are SAM-dependent 10-hydroxylases that show a typical methyltransferase structure [166, 186]. We propose that, similar to RdmB and CalMB, OxaC lost its methyltransferase functionality. In oxanthromicin (39) biosynthesis OxaC seems to be responsible for the dimerization of *hemi*-oxanthromicin (40). The dimerization reaction of *hemi*-7-desmethyloxanthromicin (66) to 7,7'-didesmethyloxanthromicin (67) shows that this dimerization is not completely substrate dependent.

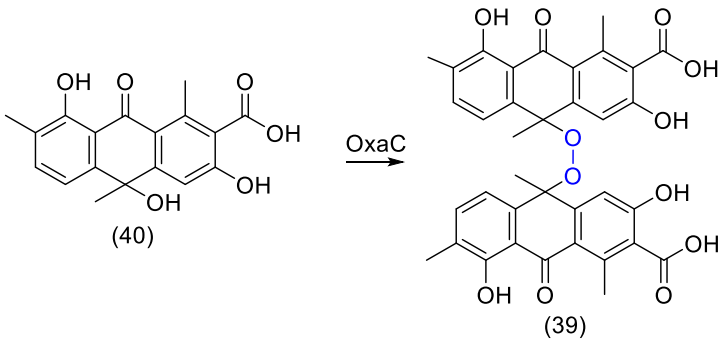

Figure 60. Oxanthromicin biosynthesis part VI: Proposed dimerization reaction.

The two remaining genes within the oxanthromicin BGC are *oxaH* and *oxaK* which are annotated as a hypothetical protein and as a regulator. OxaH is described as a protein with the NTF2-like (nuclear transport factor 2) structure. Enzymes with the NTF2-like structure show a wide variety of functions, e.g. as cyclases, isomerases and receptors, but they can also support conjugation by mediation of plasmid DNA transfer [187-190]. OxaH shows no homologies to enzymes present in actinorhodin biosynthesis or any other known enzymes [133, 170-172]. The gene *oxaH* was deleted in the cosmid 1D11 leading to cosmid 1D11 KOH (SI.4: Figure 82), which was transferred to *S. albus* Del14 through heterologous expression. The knockout strain was cultivated and extracted with butanol. The LC-MS analysis of the butanol extract of *S. albus* KOH showed that oxanthromicin production was abolished, but hemi-oxanthromicin was detected. No new peaks were detected in the chromatogram compared to the *S. albus* 1D11 KO0 control strain (SI.4: Figure 83). Complementation restored oxanthromicin production. The role of OxaH in oxanthromicin (39) biosynthesis was not clarified through knockout experiments. Since the oxanthromicin production was abolished in the knockout experiments, yet *hemi*-oxanthromicin was detected, (SI.4: Figure 83) OxaH might be involved in the dimerization reaction as an activator for OxaC.

OxaK shows a 56% homology to actIIORF4 from the actinorhodin biosynthesis [191] as well as a 64% homology to DnrI from daunorubicin biosynthesis [192]. Both enzymes act as transcriptional activators in their respective biosynthesis routes, and also induce overproduction when introduced into the wild type strains [191, 192]. Neither oxanthromicin (39), its derivatives nor any new peaks were detected (SI.4: Figure 85) in the butanol extract of the knockout strain *S. albus* 1D11 KOK comprising the cosmid 1D11 KOK (SI.4: Figure 84). The abolishment of oxanthromicin (39) biosynthesis along with the comparison of OxaK with DnrI and actIIORF4 led to the assumption that OxaK is an activator in oxanthromicin biosynthesis. Hence, it increases the expression of the genes involved in the biosynthesis [191, 192].

4.4.3 Analysis of the optical rotation of oxanthromicin and its derivatives

Additionally to the results of the knockout experiments the optical rotation of oxanthromicin (39), *hemi*-oxanthromicin (40) and *spiro*-oxanthromicin (70) was measured. The optical rotation for oxanthromicin (39) was measured with $[\alpha]^{20}_{D}$= -89 (c 0.12 MeOH), for *hemi*-oxanthromicin (40) $[\alpha]^{20}_{D}$= -3 (c 5.7 MeOH) and for *spiro*-oxanthromicin (70) $[\alpha]^{20}_{D}$= -83 (c 0. 2 MeOH). Patel *et al*. measured an optical rotation for (-)-oxanthromicin (39) of $[\alpha]^{26}_{D}$= -172.1 (c 0.3 EtOH) [157, 158], and Salim *et al*. in their experiments measured (+)-oxanthromicin (39) of $[\alpha]^{20}_{D}$= +157 (c 0.26 EtOH) [168].

In this work methanol was used as solvent and Patel *et al*. and Salim *et al*. used ethanol as solvent. Since the optical rotation is dependent on the solvent, the difference in the result can be explained by the use of methanol instead of ethanol as solvent. It appears that *S. acidiscabies* produces (-)-oxanthromicin (39) as discovered in 1984 [157]. Salim *et al*. also isolated the racemic (±)-*hemi*-oxanthromicin (40) and (±)-*spiro*-oxanthromicin (70). In the chromatogram of the butanol extract of *S. albus* 1D11 KOJ two compounds were detected (Figure 52). The isolation of only (-)-*spiro*-oxanthromicin (70) was successful, (+)-spiro-oxanthromicin was not isolated. The optical rotation of $[\alpha]^{20}_{D}$= -3 (c 5.7 MeOH) for *hemi*-oxanthromicin (40) indicates, that a racemic compound, with a slight excess of (-)-*hemi*-oxanthromicin, was isolated.

4.4.4 Concluding remarks on oxanthromicin biosynthesis

During this project the oxanthromicin biosynthetic gene cluster of *S. acidiscabies* was detected through heterologous expression of four T2PKS gene clusters in *S. albus* Del14. The biosynthesis of oxanthromicin was analyzed and solved through gene deletion experiments, bioinformatic comparisons of genes of known functions, and by analysis of the production spectrum of knockout strains (Figure 61). The oxanthromicin BGC consists of 13 genes. This was proven by deletion of the up- and downstream regions. The 14 ustream genes and 4 downstream genes of the BGC are not essential for oxanthromicin production. The regions up- and downstream of the BGC were deleted in the original cosmid 1D11 to obtain the minimal BGC for further biosynthesis studies. The enzyme products ORF15 to ORF17 are annotated as an acetyl-CoA carboxylase carboxyltransferase and two carboxyl carrier proteins and participate in malonyl-CoA synthesis. However, malonyl-CoA synthesis is normally not considered part of T2PKS [38, 48]. The synthesis of malonyl-CoA can be performed by the host strain *S. albus* Del14 [16]. Hence, the genes were cross-complemented by genes of the heterologous host. The influence of the malonyl-CoA synthesis performed by the enzymes encoded by ORF15-ORF17 on the biosynthesis of oxanthromicin was not investigated.

With the help of the deletion experiments, purified intermediates and comparison to genes of known function the biosynthesis was proposed as depicted in Figure 61. OxaK acts as the activator for the biosynthesis of oxanthromicin (39). OxaA, OxaB and OxaE are the minimal PKS responsible for synthesis of the 16C-poly-β-keto chain (61) (Figure 61, reaction I). At position C9 this chain is reduced by OxaL, followed by cyclization and aromatization by OxaF and OxaG (reactions II-IV). The resulting intermediate (64) is methylated by OxaM and hydroxylated by OxaI at the C10 position and methylated by OxaD at the C7 position (reactions V and VI). These modifications lead to the synthesis of *hemi*-oxanthromicin (40). *Hemi*-oxanthromicin is dimerized by OxaC to produce oxanthromicin (39) (reaction VII).

During the knockout experiments we discovered and characterized four new oxanthromicin derivatives. *Hemi*-7-desmethyloxanthromicin (66) and 7,7′-didesmethyl-oxanthromicin (67) are intermediates of the oxanthromicin (39) biosynthesis, while

desperoxyoxanthromicin (59) and decarboxydesperoxyoxanthromicin (60) were byproducts that showed an interesting dimerization pattern.

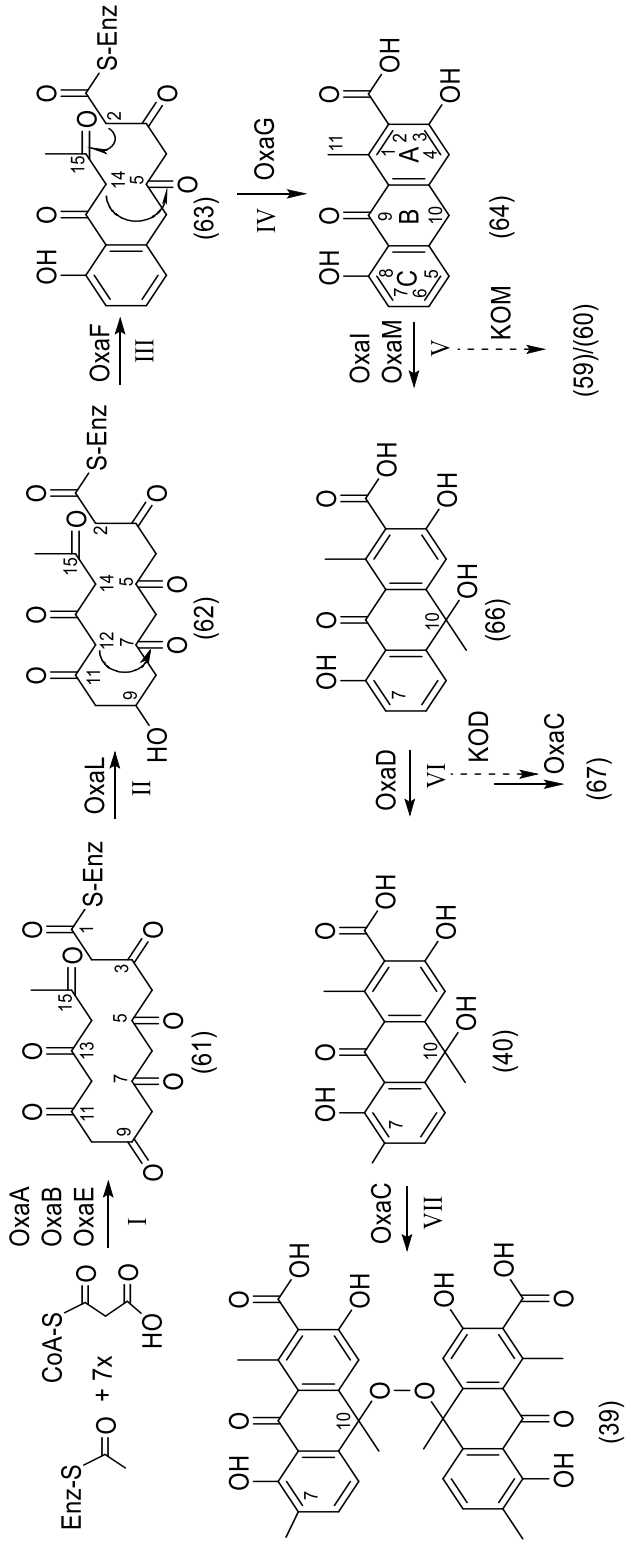

Figure 61. Proposed oxanthromicin biosynthesis by *S. acidiscabies* LU19992.

5 Conclusion

Within this work heterologous expression was used for the discovery and analysis of biosynthetic gene clusters found in Actinomycetes.

In the first project the cyclohuinilsopeptin A (34) BGC was heterologously expressed successfully in ten new host strains. Out of the new strains the strain LV1-22 2D19 produced cyclohuinilsopeptin A (34) the same way as *S. albus* Del14. This strengthened the point that cyclohuinilsopeptin A (34) is a metabolite of *K. albida* DSM43870. Full verification was not achieved since conjugation of neither plasmids nor BACs in *K. albida* DSM43870 was successful and so wildtype knockouts were not performed. Production of cyclohuinilsopeptin A (34) in *K. albida* DSM43870 might be inducible in an experimental line with different cultivation conditions.

In the second project four T2PKS clusters were discovered in the genome of *S. acidiscabies* LU19992 and analyzed in the process. All four clusters were heterologously expressed in *S. albus* Del14. The resulting strains were cultivated and their butanol extracts were analyzed. The clusters covered by both the cosmids 2D04 and 9H08 were not analyzed further after heterologous expression in *S. albus* Del14. The cosmid 18F05 harbors the BGC for desmethylmensacarcin B (44) a new mensacarcin derivative and the cosmid 1D11 harbors the BGC for oxanthromicin (39).

The biosynthesis of the new mensacarcin derivate desmethylmensacarcin B (44) was solved through sequence analysis and comparison with the mensacarcin biosynthesis. Further analysis of desmethylmensacarcin B (44) in regards of its activity in comparison with mensacarcin (41) and desmethylmensacarcin (42) will help to understand why *S. acidiscabies* LU19992 produces this mensacarcin derivative and what function desmethylmensacarcin B (42) serves for *S. acidiscabies* LU19992.

The biosynthetic pathway of oxanthromicin (39) production was solved through sequence analysis and gene deletion experiments. During these experiments four new and two known oxanthromicin derivatives were discovered and analyzed. The dimerization reaction is a crucial factor in the oxanthromicin (39) biosynthesis. The understanding of the underlying mechanism of this peroxide bridge production may be an interesting key factor in the modification of other anthrone polyketides. The production of new dimeric anthrone

polyketides in turn are potentially interesting for pharmaceutical, medical and chemical uses, by providing new agents with novel chemical features. They may alsoincrease the bioavailability of currently used agents.

Supplementary Information

SI.1: Cyclohuinilsopeptin A project

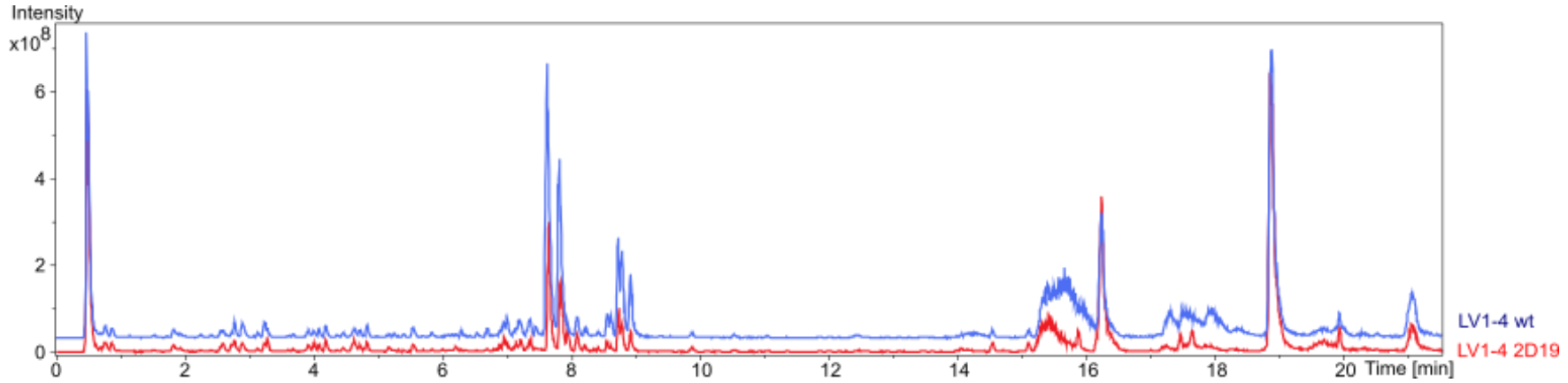

Figure 62. LC-MS base peak chromatograms of butanol extract from LV1-4 (blue) and LV1-4 2D19 (red) after cultivation for 7 days at 28°C and 180 rpm in 100 mL DNPM.

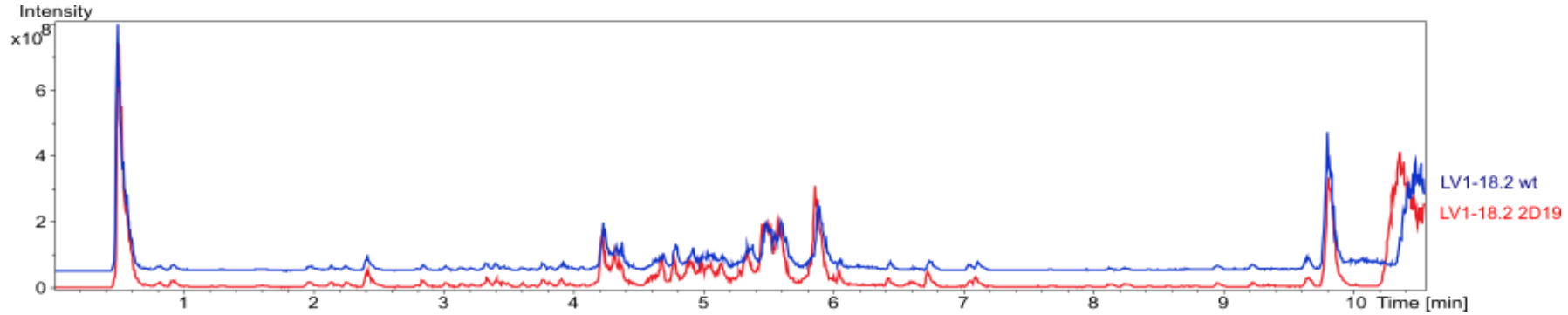

Figure 63. LC-MS base peak chromatograms of butanol extract from LV1-18.2 (blue) and LV1-18.2 2D19 (red) after cultivation for 7 days at 28°C and 180 rpm in 100 mL DNPM.

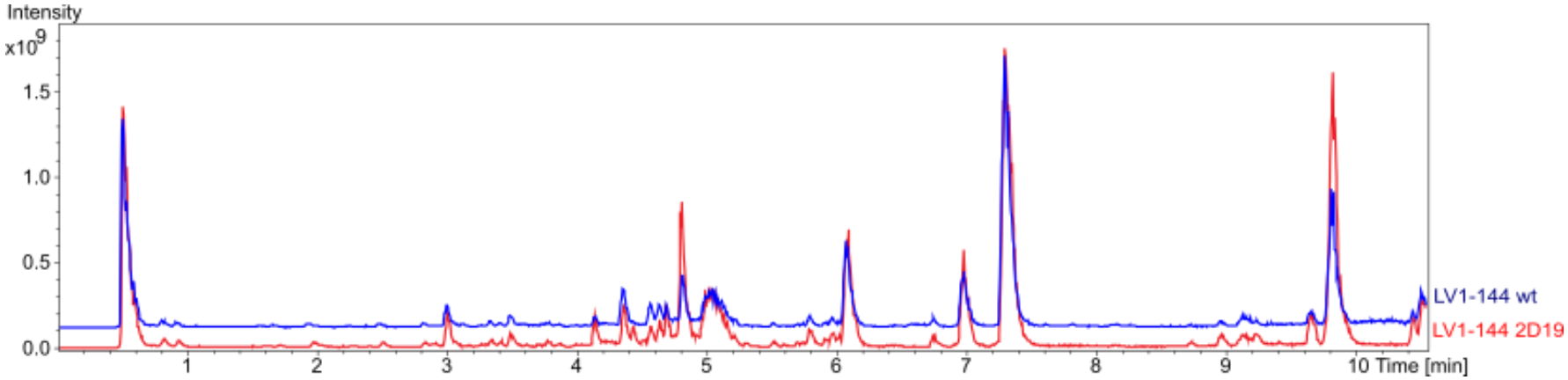

Figure 64. LC-MS base peak chromatograms of butanol extract from LV1-144 (blue) and LV1-144 2D19 (red) after cultivation for 7 days at 28°C and 180 rpm in 100 mL DNPM.

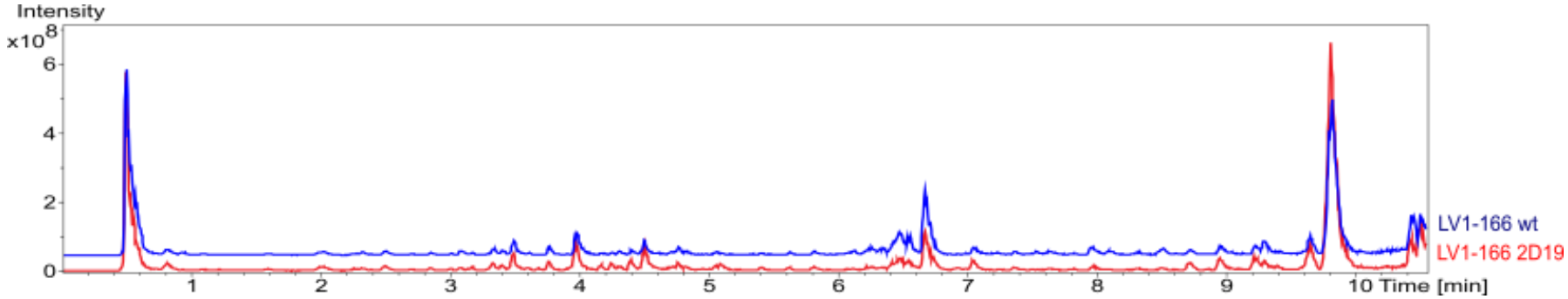

Figure 65. LC-MS base peak chromatograms of butanol extract from LV1-166 (blue) and LV1-166 2D19 (red) after cultivation for 7 days at 28°C and 180 rpm in 100 mL DNPM.

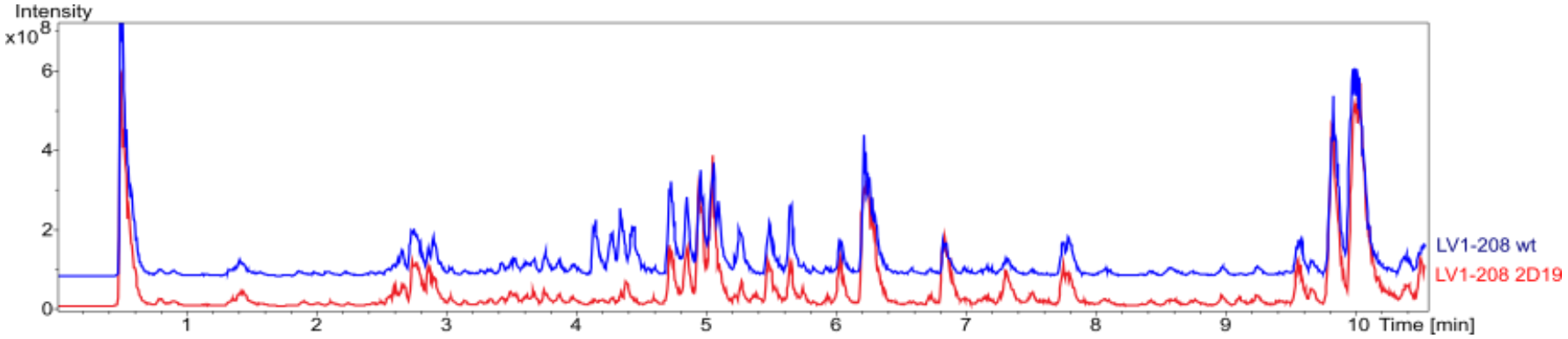

Figure 66. LC-MS base peak chromatograms of butanol extract from LV1-208 (blue) and LV1-208 2D19 (red) after cultivation for 7 days at 28°C and 180 rpm in 100 mL DNPM.

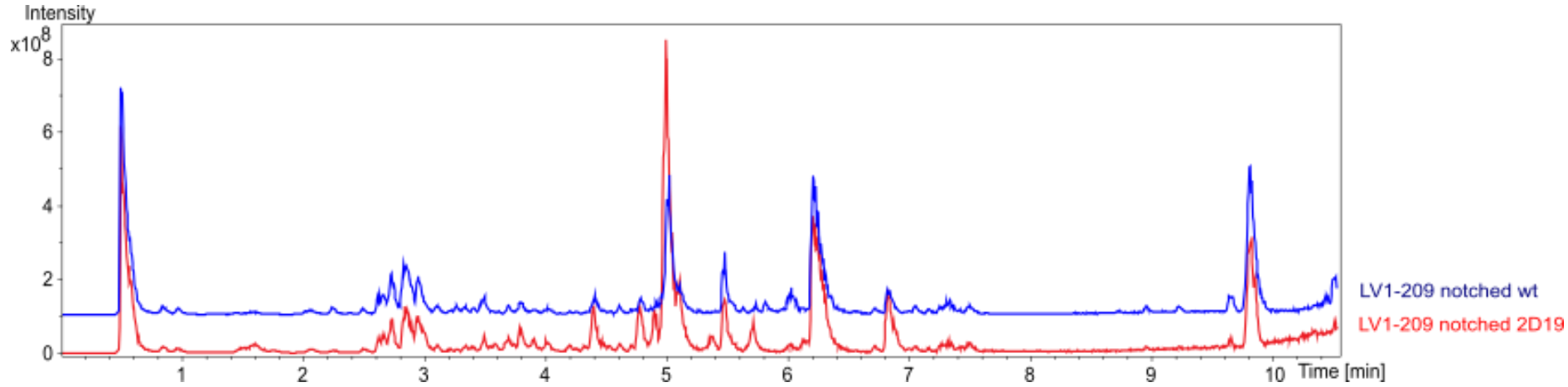

Figure 67. . LC-MS chromatograms of butanol extract from LV1-209 notched (blue) and LV1-209 notched 2D19 (red) after cultivation for 7 days at 28°C and 180 rpm in 100 mL DNPM.

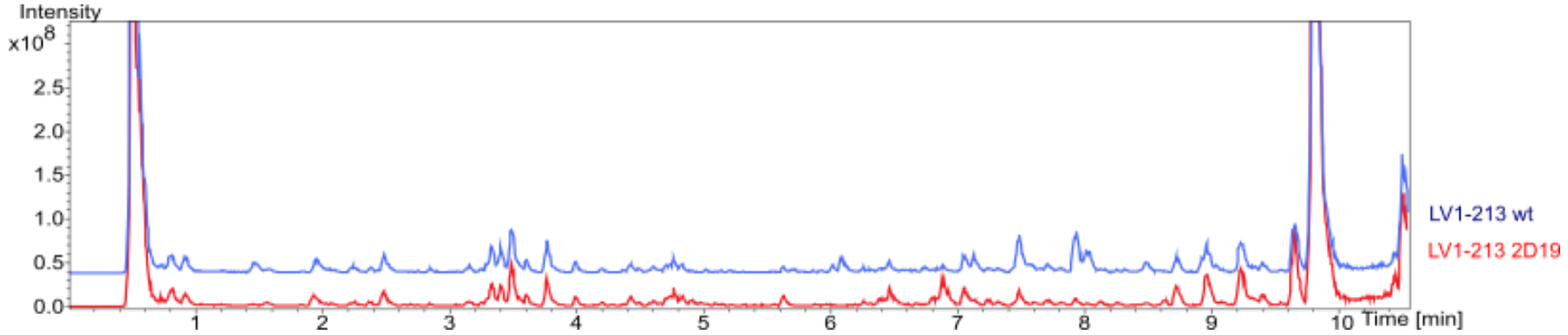

Figure 68. LC-MS base peak chromatograms of butanol extract from LV1-213 (blue) and LV1-213 2D19 (red) after cultivation for 7 days at 28°C and 180 rpm in 100 mL DNPM.

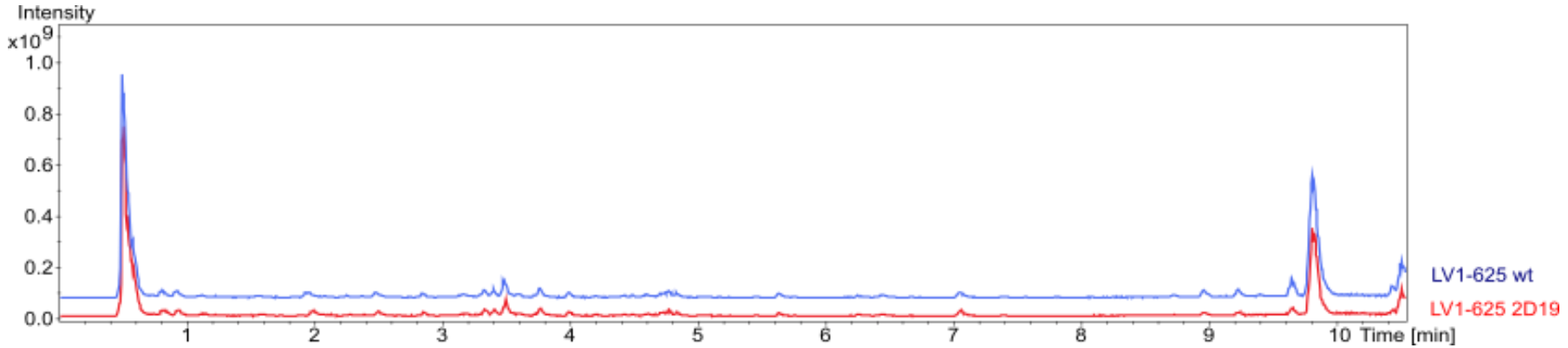

Figure 69. LC-MS base peak chromatograms of butanol extract from LV1-625 (blue) and LV1-625 2D19 (red) after cultivation for 7 days at 28°C and 180 rpm in 100 mL DNPM.

SI.2: *Streptomyces acidiscabies* LU19992 project

Table 16. NMR spectroscopic data of oxanthromicin (39) and comparison with literature [158].

#	H Shift	C Shift	XHn	H Shift Literature [158]	C Shift Literature [158]
1		135.2	C		124.8
2		139.6	C		127.1
3		162.2	C		159.5
4	6.79	115.8	CH	6.7	112.1
4a		148.6	C		148.9
5	6.69	118.2	CH	6.55	116.7
6	7.34	135.6	CH	7.25	135.8
7		126.0	C		119.9
8		160.8	C		158.2
8a		116.4	C		114.5
9		191.0	C		189.3
9a		119.9	C		141.1
10		80.4	C		79.7
10a		143.9	C		139.4
11	2.84	21.6	CH_3	2.85	20.5
12		177.0	C		168.7
13	2.29	15.38	CH_3	2.24	15.1
14	1.23	33.7	CH_3	1.2	32.9

Table 17. Secondary metabolism gene clusters within the genome of *Streptomyces acidiscabies* LU19992 identified with antiSMASH software [132]. T2PKS gene cluster are marked in blue.

BGC	Type	Most similar known cluster
1	NRPS	cysteoamide
2	terpene	albaflavenone
3	NRPS	thaxtomin A
4	lanthipeptide	phthoxazolin
5	lanthipeptide	foxicin A-C
6	NRPS	thaxtomin A
7	terpene	albaflavenone
8	NRPS	cysteoamide
9	terpene	cyphomycin (polyketide)
10	T1PKS – phosphonate – transAT-PKS – NRPS	phthoxazolin
11	terpene	ebelactone
12	T1PKS – T3PKS – terpene	furaquinocin B
13	NRPS	coelichelin
14	terpene	
15	T1PKS – furan	saprolmycin E
16	butyrolactone	streptovaricin
17	T1PKS - aminoglycoside/aminocyclitol	divergolide A-D
18	indole	5-isoprenylindole-3-carboxylate β-D-glycosyl ester
19	NRPS – betalactone	malacidin A-B
20	siderophore	grincamycin
21	NRPS-like – betalactone – nucleoside	neopolyoxin C
22	terpene – butyrolactone	γ-butyrolactone
23	bacteriocin	
24	siderophore	kinamycin
25	non-alpha poly-amino acids like ε-polylysin	ε-poly-L-lysine
26	redox cofactor	dutomycin
27	T2PKS	WS-5995 B-D/SEK 43
28	terpene	
29	terpene – RiPP-like	legonindolizidine A6
30	phophonate – PKS-like – T1PKS - arylpolyene	pactamycin
31	NRPS-like – T1PKS – betalactone	meridamycin
32	T1PKS	monesin
33	ectoine	ectoine
34	siderophore – lanthipeptide	Peucechelin
35	T2PKS – PKS-like	SF2575
36	siderophore	FW0622
37	melanin	istamycin
38	RRE-element containing cluster	
39	lanthiopeptide	
40	T3PKS	herboxidiene
41	NRPS-like – T1PKS – T2PKS – NRPS	kedarcidin
42	T2PKS	mensacarcin
43	bacteriocin	informatipeptin
44	nucleoside	huimycin
45	terpene	hopene
46	NRPS	ohmyungsamycin A/B
47	hydrogen-cyanide	
48	T1PKS	auroramycin
49	lanthipeptide	
50	hglE-KS – T1PSK	hexacosalactone A
51	T1PKS	J1-001-2
52	T1PKS	

SI.3: Desmethylmensacarcin project

Table 18. NMR spectroscopic data of desmethylmensacarcin (42) and comparison with literature data [193].

experimental data in MeOD				literature data in MeOD			
No	C Shift	H Shift	H Multiplicity	No	C Shift	H Shift	H Multiplicity
1	72,4	4.33, s	s	1	70,8	4.35	s
2	85,4			2	83,8		
3	33,3	2.14	dq (7.4, 3.3)	3	31,8	2.16	dq (7.1, 3.3)
4	68,6	4.65	d (2.9)	4	67,1	4.67	d (3.1)
4a	65,6			4a	64,1		
5	191,5			5	189,9		
5a	130,9			5a	129,3		
6	120,0	7.66	dd (7.9, 0.9)	6	118,5	7.68	dd (7.9, 0.9)
7	130,6	7.46	t (8.1)	7	129	7.48	dd (8.1, 7.9)
8	117,8	7.35	dd (8.2, 0.9)	8	116,2	7.36	dd (8.2, 0.9)
9	160,1			9	158,5		
9a	131,1			9a	129,6		
10	61,6	5.85	s	10	60,1	5.87	s
10a	68,1			10a	66,5		
11	212,2			11	210,6		
12	59,8	4.06	d (1.9)	12	58,2	4.08	d (1.9)
13	58,0	2.99	dq (5.1, 1,9)	13	56,5	3.02	dq (5.1, 1,9)
14	18,0	1.42	d (5.1)	14	16,5	1.44	d (5.1)
15	11,7	1.04	d (7.1)	15	10,2	1.06	d (7.1)
9-OMe	56,7	3.96	s	9-OMe	55,1	3.98	s

Table 19. NMR spectroscopic data of desmethylmensacarcin B (44).

No	C Shift	H Shift	H Multiplicity	COSY	HMBC	NOESY
1	70,7	4.76	s			
2	87,9					
3	43,6	3.34	q (6.9)	15	4	
4	204,4					
4a	64,2					
5	66,7	5.29			4a, 5a, 6, 9a, 10a	6
5a	136,9					
6	123,7	6.98	d (7.6)	7	5	5
7	130,5	7.33	t (7.9)	8, 6		
8	112,5	7.05	dd (8.3, 0.7)	7		
9	159,9					
9a	124,5					
10	65,8	5.75	s			
10a	70,0					
11	209,3					
12	59,2	4.05	d (1.8)	13		
13	58,1	3.03	dq (5.1, 1.9)	12, 14		
14	17,9	1.44	d (5.2)	13		
15	8,4	0.97	d (6.9)	3	4	
9-OMe	56,4	3.92	s			

SI.4: Oxanthromicin project

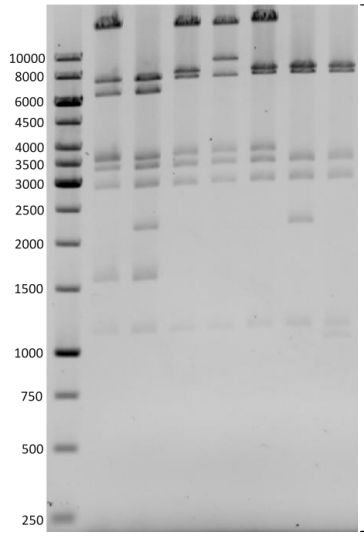

1	2	3	4	5	6	7
1D11	1D11_LS	1D11_RS2	1D11_RS1	1D11_RS1-delHyg	1D11_RS/LS	1D11_RS/LS-delHyg 1D11-KO0
17819		17819	17819	17819		
			8850			
		7819				
				7743	7743	7743
7382	7382	7382	7382	7382	7382	7382
6356	6356					
3574		3574	3574	3574		
3522	3522					
3271	3271	3271	3271	3271	3271	3271
2847	2847	2847	2847	2847	2847	2847
	2140				2140	
1552	1552					
1549	1549					
1115	1115	1115	1115	1115	1115	1115
						1033
198	198					
147	147					
76	76	76	76	76	76	76

Figure 70. Restriction mapping after digestion with *Kpn*I of the cosmid 1D11 and the knockout cosmids leading to the cosmid 1D11 KO0 and prediction of size of bands in base pairs generated with Geneious software.

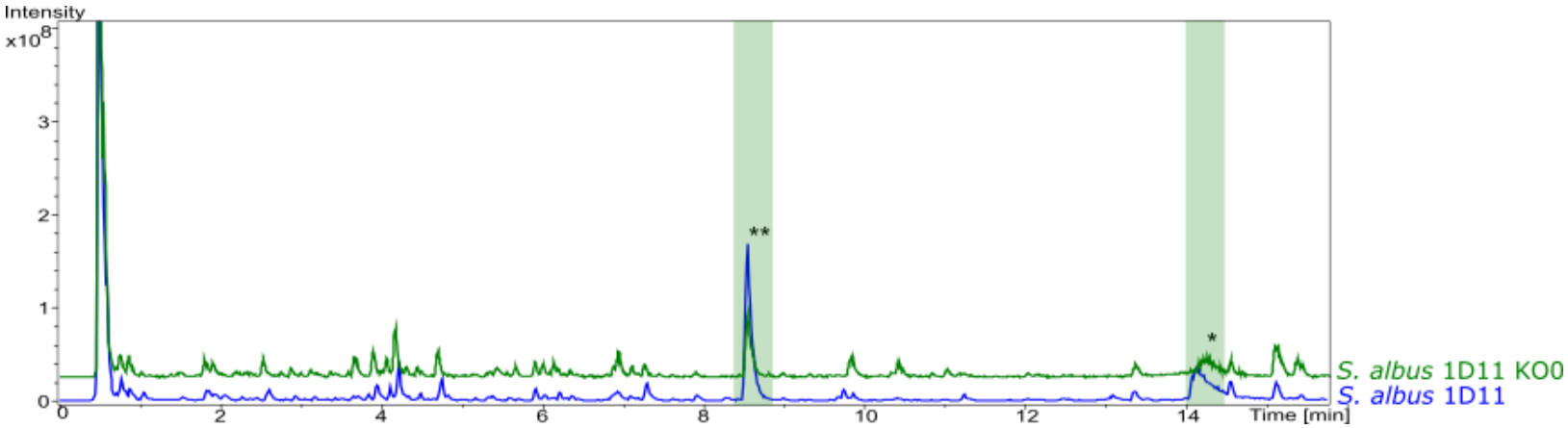

Figure 71. LC-MS chromatograms of butanol extract from *S. albus* 1D11 (blue) and *S. albus* 1D11 KO0 (green) after cultivation for 7 days at 28°C and 180 rpm in 100 mL DNPM. The oxanthromicin (39) peak is indicated by an asterisk (*). The *hemi*-oxanthromicin (40) peak is indicated by two asterisks (**). Both oxanthromicin (39) and *hemi*-oxanthromicin (40) were detected in the butanol extract from *S. albus* 1D11 (blue) and *S. albus* 1D11 KO0 (green).

OxaL

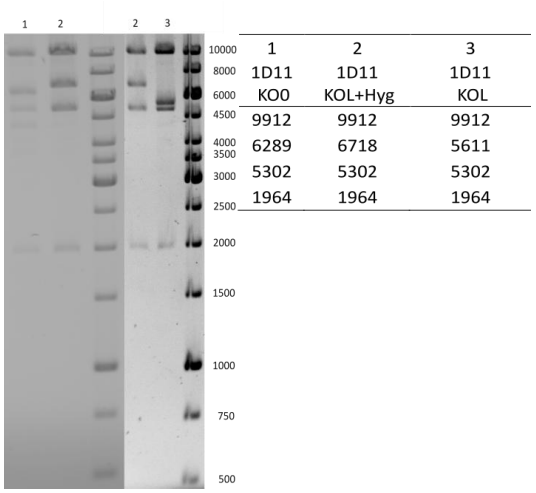

1	2	3
1D11 KO0	1D11 KOL+Hyg	1D11 KOL
9912	9912	9912
6289	6718	5611
5302	5302	5302
1964	1964	1964

Figure 72. Restriction mapping after digestion with *Bam*HI of generation of the cosmid 1D11 KOL compared to the prediction of size of bands in base pairs generated with Geneious software.

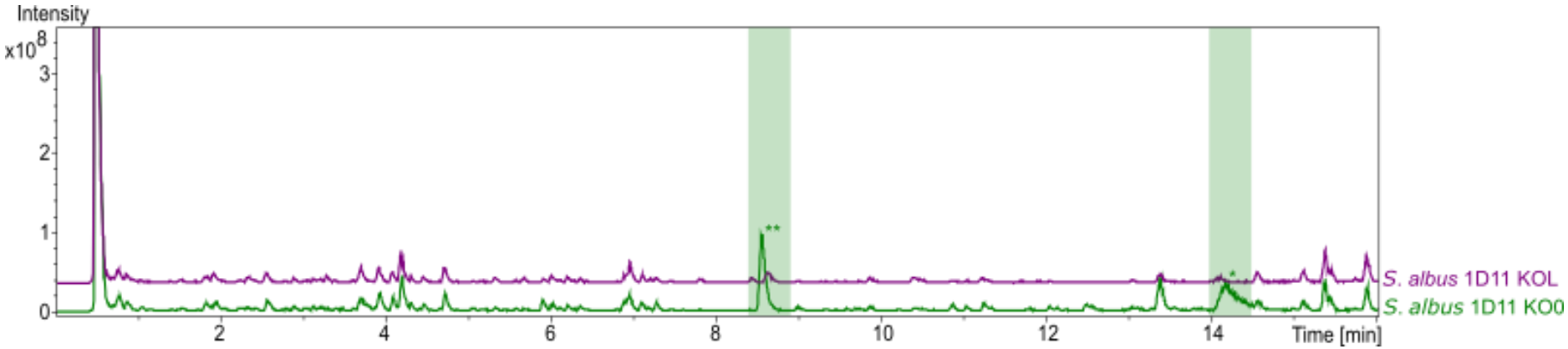

Figure 73. LC-MS base peak chromatograms of butanol extract from *S. albus* 1D11 (green) and *S. albus* 1D11 KOL (purple) after cultivation for 7 days at 28°C and 180 rpm in 100 mL DNPM. In green the oxanthromicin (39) peak is indicated by one asterisk (*) and *hemi*-oxanthromicin (40) by two asterisks (**).

OxaF and OxaG

1	2	3	4	5
1D11 KO0	1D11 KOF+Hyg	1D11 KOG+Hyg	1D11 KOF	1D11 KOG
9912	9912	11876	9912	10769
6289	6289	9912	6289	9912
5302	5563	1964	4456	1964
1964	1964		1964	

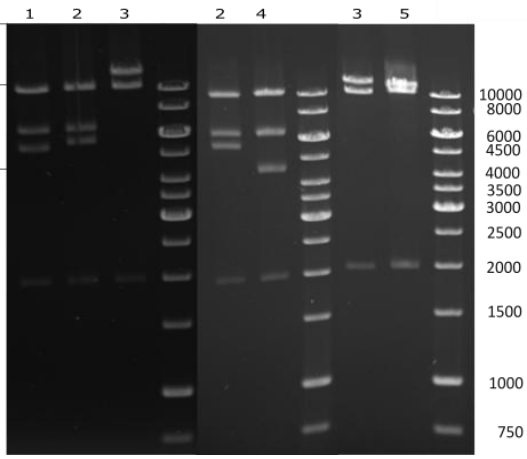

Figure 74. Restriction mapping after digestion with *Bam*HI of generation of the cosmid 1D11 KOF and 1D11 KOG compared to the prediction of size of bands in base pairs generated with Geneious software.

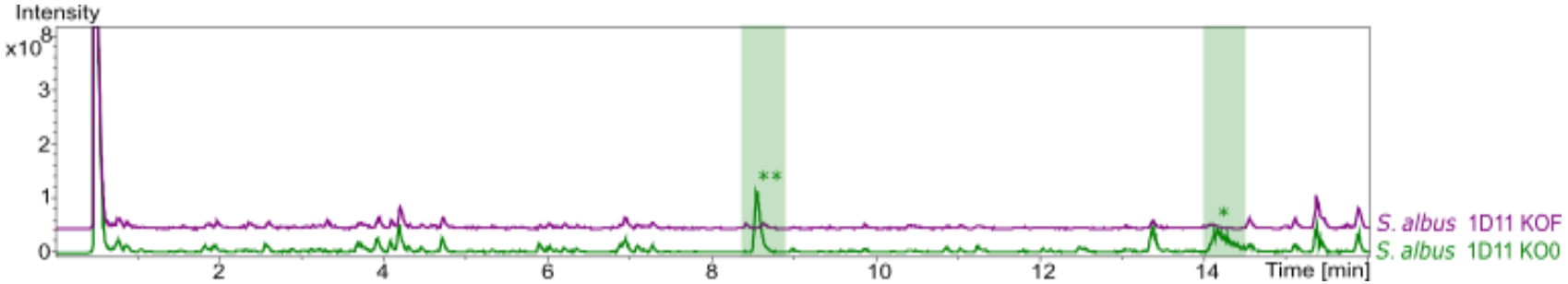

Figure 75. LC-MS base peak chromatograms of butanol extract from *S. albus* 1D11 (green) and *S. albus* 1D11 KOF (purple) after cultivation for 7 days at 28°C and 180 rpm in 100 mL DNPM. In green the oxanthromicin (39) peak is indicated by one asterisk (*) and *hemi*-oxanthromicin (40) by two asterisks (**).

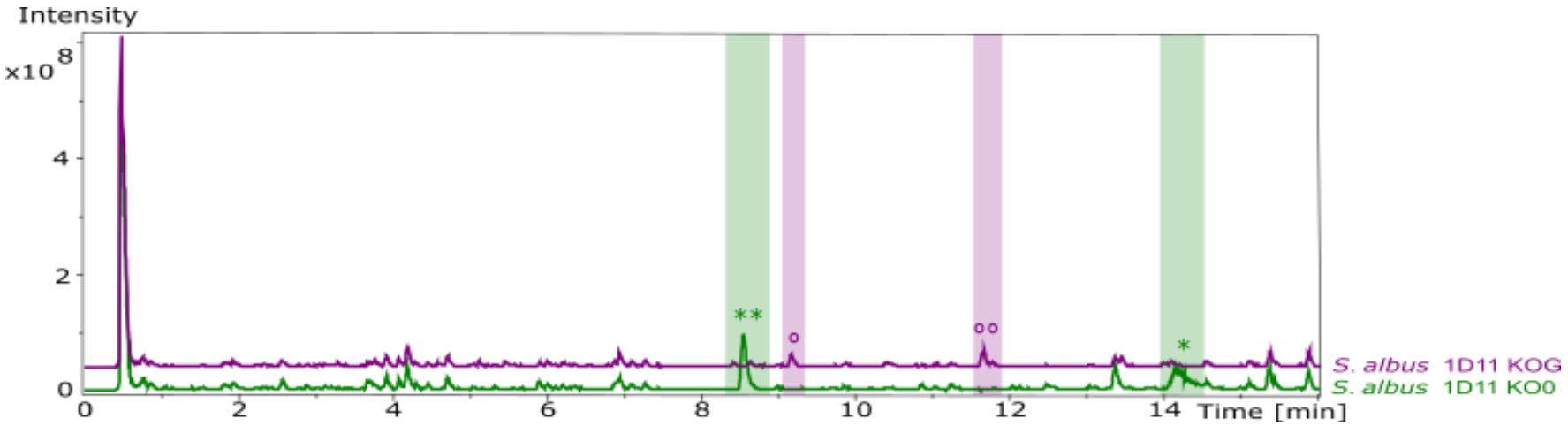

Figure 76. LC-MS base peak chromatograms of butanol extract from *S. albus* 1D11 (green) and *S. albus* 1D11 KOG (purple) after cultivation for 7 days at 28°C and 180 rpm in 100 mL DNPM. In green the oxanthromicin (39) peak is indicated by one asterisk (*) and *hemi*-oxanthromicin (40) by two asterisks (**). In purple the two new occurring compounds are indicated by circles. The compound with the mass 719.1965 Da with one circle (°) and the one with the mass 597.1664 Da with two circles (°°).

OxaI and OxaJ

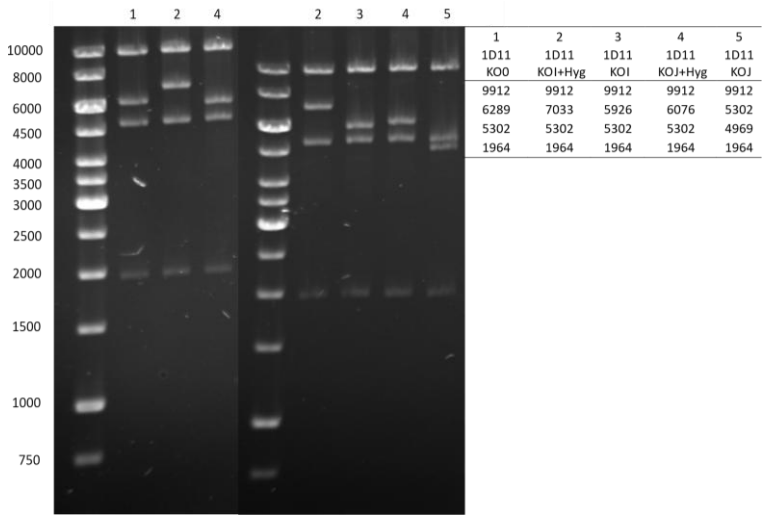

1	2	3	4	5
1D11 KO0	1D11 KOI+Hyg	1D11 KOI	1D11 KOJ+Hyg	1D11 KOJ
9912	9912	9912	9912	9912
6289	7033	5926	6076	5302
5302	5302	5302	5302	4969
1964	1964	1964	1964	1964

Figure 77. Restriction mapping after digestion with *Bam*HI of generation of the cosmids 1D11 KOI and 1D11 KOJ compared to the prediction of size of bands in base pairs generated with Geneious software.

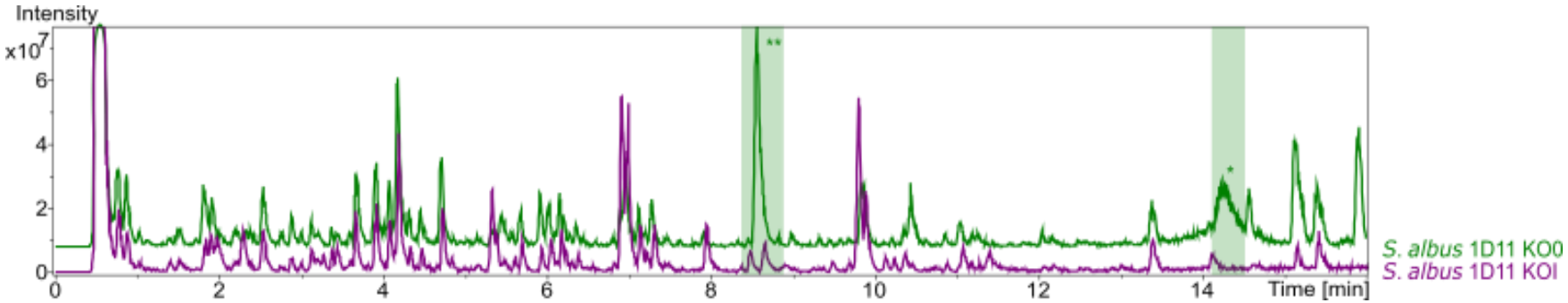

Figure 78. LC-MS chromatograms of butanol extract from *S. albus* 1D11 (green) and *S. albus* 1D11 KOI (purple) after cultivation for 7 days at 28°C and 180 rpm in 100 mL DNPM. Base peak chromatograms of *S. albus* 1D11 and *S. albus* 1D11 KOI. In green the oxanthromicin (39) peak is indicated by one asterisk (*) and *hemi*-oxanthromicin (40) by two asterisks (**).

Table 20. NMR spectroscopic data of *spiro*-oxanthromicin (70) and comparison with literature [168].

experimental data in MeOD				literature data in DMSO-d6			
No	C Shift	H Shift	H Multiplicity	No	C Shift	H Shift	H Multiplicity
1	144,79			1	140,2		
1'	143,18			1'	139,8		
2	121,96			2	119		
2'	121,96			2'	119		
3	161,82			3	158,6		
3'	161,31			3'			
4	108,25	7.34	s	4	106,8	7.38	s
4'	115,53	6.63	s	4'	113,9	6.64	s
4a	141,34			4a	139,4		
4a'	156,80			4a'	154,6		
5	130,12			5	128,3		
5'	119,89	6.51	d (7.9)	5'	118,6	6.48	d (7.9)
6	139,22	6.78	s	6	137,8	6.83	s
6'	137,18	7.20	d (7.9)	6'	136,4	7.29	d (7.9)
7	127,91			7	126,1		
7'	125,47			7'	123,5		
8	161,54			8	159,7		
8'	161,81			8'	159,9		
8a	114,33			8a	112,4		
8'a	116,51			8'a	114,7		
9	192,49			9	190,3		
9'	191,87			9'	189,7		
9a	128,33			9a	127,2		
9a'	127,61			9'a	126,2		
10	128,82			10	126,1		
10'	47,55			10'	45,5		
10a	131,77			10a	129,9		
10a'	149,73			10a'	148,2		
11	21,97	2.98	s	11	20,8	2.77	s
11'	21,72	2.91	s	11'	20,7	2.71	s
12	174,27			12	168,6		
12'	173,97			12'	168,8		
13	15,87	2.08	s	13	15,2	2.04	s
13'	15,48	2.21	s	13'	15	2.16	s
14	128,95	6.98	t (4.54)	14	128,8	6.96	d (7.9)
14'	48,72	3.15	m	14'	47,1	3.13	m

OxaM

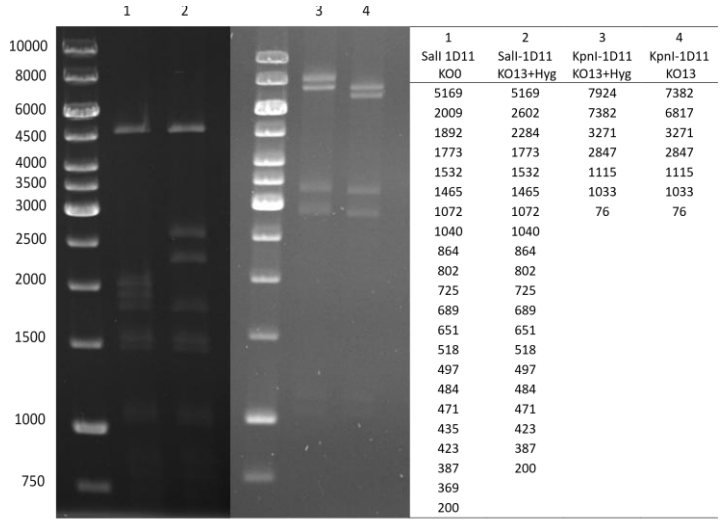

1 SalI 1D11 KO0	2 SalI-1D11 KO13+Hyg	3 KpnI-1D11 KO13+Hyg	4 KpnI-1D11 KO13
5169	5169	7924	7382
2009	2602	7382	6817
1892	2284	3271	3271
1773	1773	2847	2847
1532	1532	1115	1115
1465	1465	1033	1033
1072	1072	76	76
1040	1040		
864	864		
802	802		
725	725		
689	689		
651	651		
518	518		
497	497		
484	484		
471	471		
435	423		
423	387		
387	200		
369			
200			

Figure 79. Restriction mapping after digestion with *Sal*I and *Kpn*I of generation of the cosmid 1D11 KOM compared to the prediction of size of bands in base pairs generated with Geneious software.

Table 21. NMR spectroscopic data of desperoxyoxanthromicin (59).

#	H Shift	C Shift	H Multiplicity	XHn	COSY	C to H HMBC
1		142.3		C		
2		124.8				
3		159.8		C		
4a		147.4		C		
4	6.48	114.7	s, br	CH		-
5	5.78	119.5	d, 5.04	CH	6.93	57.3, 118.9, 126.4
6	6.93	135.4	d, 6.41	CH	5.78	15.4, 137.0, 160.4
7		126.4		C		
8		160.4		C		
8a		118.9				
9		190.4		C		
9a		125.1		C		
10a		137.0		C		
10	4.16	57.3	s	CH		57.3, 114.7, 118.9, 125.1, 137.0, 147.4,
11	2.52	20.4	s	CH3		125.1, 142.3, 147.4
12		172.6		C		
13	2.11	15.4	s	CH3		57.3, 126.4, 135.4, 137.0, 160.4, 164.5

Table 22. NMR spectroscopic data of decarboxydesperoxyoxanthromicin (60).

#	H Shift	C Shift	H Multiplicity	XHn	COSY	H to C HMBC	C to H HMBC
1		143.6		C			
1′		145.129		C		2,51	
2′	6.499	114.707	br s	CH	2.51, 6.61	4.35, 6.61	57.77, 125.26
3		161.5		C			
3′		162.306		C		6,61	
4	6,58	115.058	br s	CH			57.97, 125.26
4′	6.613	119.729	br s	CH	2.51, 6.50		24.26, 114.71, 125.26, 162.31
4a		147.6		C			
4a′		147.3		C		5.86, 6.96	
5	5.856	119.561	br d (7.32)	CH	6,96	2,51	57.77, 119.51, 126.20, 160.55, 190.88
5′	5.948	119.729	br d (7.32)	CH	6,99		57.77, 118.97, 126.20, 160.87, 190.88
6	6.956	135.334	br d (7.48)	CH	2.15, 5.86	2,15	119.51, 137.67, 160.55
6′	6.990	135.545	s	CH	5,95		118.97, 138.03, 160.87
7		126.198		C		2.15, 5.86, 5.95	
7′		126.241		C			
8		160.5		C			
8′		160.866		C		2.15, 5.95, 6.99	
8a		119.510		CH		5.86, 6.96	
8a′		118.969		CH		5.95, 6.99	
9		190.951		C		2,51	
9′		190.878		C		2.65, 5.86, 5.95	
9a		125.554		C			
9a′		125.262		C		2.51, 2.65, 4.35, 6.50, 6.58, 6.61	
10	4.354	57.965	br s	CH		6,58	57.77, 114.71, 119.16, 125.26, 137.67, 147.26
10′	4.375	57.768	br s	CH		2.15, 4.35, 5.86, 5.95, 6.50	
10a		137.673		C		2.15, 4.35, 6.96	
10a′		138.031		C		6,99	
11	2.654	20.756	s	CH			125.26, 147.57, 190.88
11′	2.513	24.262	s	CH	6.50, 6.61	0.90, 6.61	119.56, 125.26, 145.13, 147.26, 190.95
13/13′	2.149	15.606	m	CH	6.96, 6.97	6,97	57.77, 119.16, 126.20, 135.33, 137.67, 160.87

OxaD

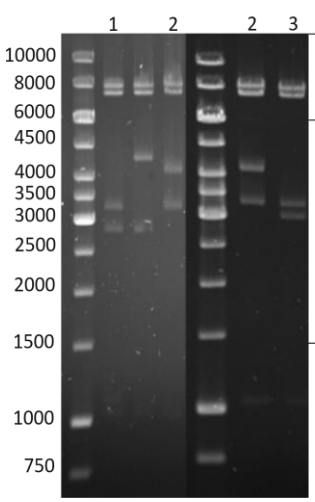

1	2	3
1D11 KO0	1D11 KOD+Hyg	1D11 KOD
7743	7743	7743
7382	7382	7382
3271	4127	3271
2847	3271	3020
1115	1033	1033
1033	76	76
76		

Figure 80. Restriction mapping with *Kpn*I of generation of the cosmid 1D11 KOD.

Table 23. NMR spectroscopic data of (±)-*hemi*-7-desmethyloxanthromicin (66)

#	H Shift	C Shift	H Multiplicity	XHn	COSY	H to C HMBC	C to H HMBC
1		142.894		C		2.78, 7.40	
2		121.310		C		2.78, 7.40	
3		160.831		C		2.78, 7.40	
4	7.39	111.610	s	CH	2.78	2.78	39.45, 71.69, 121.31, 126.35, 142.89, 156.87, 160.83, 172.66, 191.15
4a		156.869		C		1.55, 2.78, 7.40	
5	7.34	116.683	dd (7.71, 0.99)	CH	6.86, 7.51	6.86, 7.51, 117.18	39.45, 71.69, 117.18, 136.59, 163.38, 191.15
6	7.50	136.593	t	CH	6.86, 7.35	6.86, 7.35	71.69, 116.68, 151.41, 163.38
7	6.85	117.180	dd (8.24, 1.07)	CH	7.35, 7.51	7.35, 116.68	116.68, 136.59, 151.41, 163.38, 191.15
8		163.382		C		6.86, 7.35, 7.51	
8a		116,7		C		6.86, 7.35, 7.51	
9		191.150		C		2.78, 6.86, 7.35, 7.40	
9a		126.346		C		2.78, 7.40	
10		71.687		C		1.55, 7.35, 7.40, 7.51	
10a		151.409		C		1.55, 6.86, 7.51	
11	2.78	20.960	s	CH_3	7.40		111.61, 121.31, 126.35, 142.89, 156.87, 160.83, 172.66, 191.15
12		172.658		C		2.78, 7.40	
13	1.55	39.452	s	CH_3		7.35, 7.40	71.69, 151.41, 156.87

Table 24. NMR spectroscopic data of 7,7'-didesmethyloxanthromicin (67)

#	H Shift	C Shift	H Multiplicity	XHn	COSY	H to C HMBC	C to H HMBC
1		140.90		C		2.86, 6.76	
2		120.71		C		2.86, 6.76	
3		158.83		C		6.76	
4	6.765	112.02	s	CH	2.86	2.86	79.44, 120.71, 126.49, 140.91, 149.86, 158.84, 171.75, 189.46
4a		149.86		C		1.36, 2.86, 6.76	
5	6.951	116.36	dd (8.24, 0.76)	CH	6.74, 7.49	115.87	115.87, 118.17, 144.28, 162.05, 189.46
6	7.492	134.62	t (8.01, 8.01)	CH	6.74, 6.95	6.74	79.44, 115.87, 118.17, 144.28, 162.05
7	6.735	118.16	dd (7.78, 0.92)	CH	6.95, 7.49	6.95, 7.49	79.44, 115.87, 134.63, 162.05, 189.46
8		162.04		C		6.74, 6.95, 7.49	
8a		115.87		C		6.74, 6.95, 7.49	
9		189.46		C		2.86, 6.74, 6.76, 6.95	
9a		126.48		C		2.86, 6.76	
10		79.443		C		1.36, 6.74, 6.76, 7.49	
10a		144.28		C		1.36, 6.95, 7.49	
11	2.860	19.937	s	CH_3	6.76		112.03, 120.71, 126.49, 140.91, 149.86, 158.8, 171.75, 189.46
12		171.75		C		2.86, 6.76	
13	1.360	32.297	s	CH_3			79.44, 144.28, 149.86

OxaC

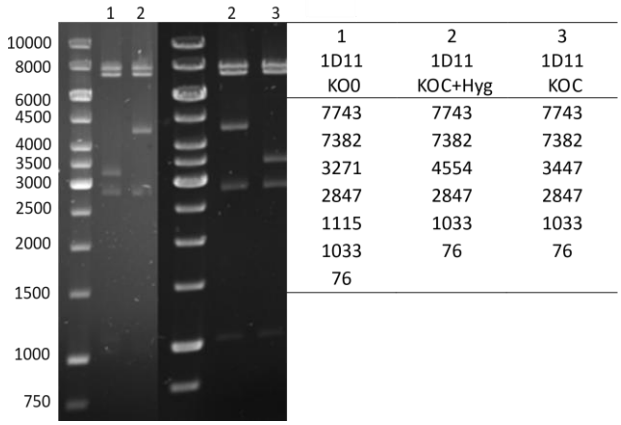

Figure 81. Restriction mapping with *Kpn*I of generation of the cosmid 1D11 KOC.

Table 25. NMR spectroscopic data of (±)-*hemi*-oxanthromicin A (40)

Peak	H shift	C shift	H Multiplicity	XHn	COSY	HMBC
1		142,6		C		
2		121,3		C		
3		160,4		C		
4	7,38	111,4	S	CH_3	2,77	71,5-121,3-125,9-142,6-156,7-160,4-172,5-191,2
4a		156,7		C		
5	7,2	115,7	Dd	CH	2,21-1,52-7,35	15,4-39,3-71,5-115,7-125,9-137,2-148,3-156,7-161,3-191,2
6	7,35	137,2	T	CH	2,21-7,2	15,4-115,7-148,3-161,3
7		125,9	Dd	CH		
8		161,3		C		
8a		115,7		C		
9		191,2		C		
9a		125,9		C		
10a		71,5		C		
10		148,3		C		
11	2,77	20,8	S	CH_3	2,21-3,35-7,38	111,4-121,3-125,9-142,6-156,7-160,4-172,5-191,2
12		172,5		C		
13		15,4	S	CH_3	2,77-7,20-7,35	125,9-137,2-161,3
14	1,52	39,3		C	7,20	71,5-148,3-156,7

OxaH

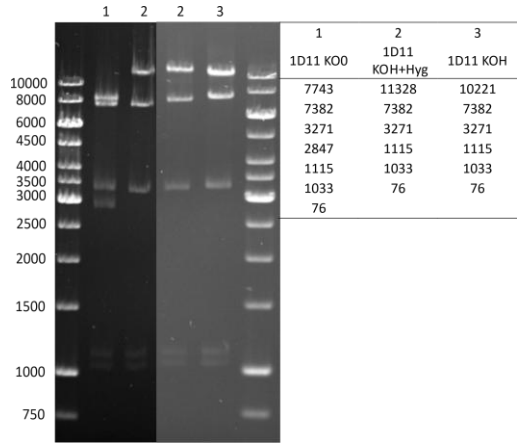

1	2	3
1D11 KO0	1D11 KOH+Hyg	1D11 KOH
7743	11328	10221
7382	7382	7382
3271	3271	3271
2847	1115	1115
1115	1033	1033
1033	76	76
76		

Figure 82. Restriction mapping with *Kpn*I of generation of the cosmid 1D11 KOH.

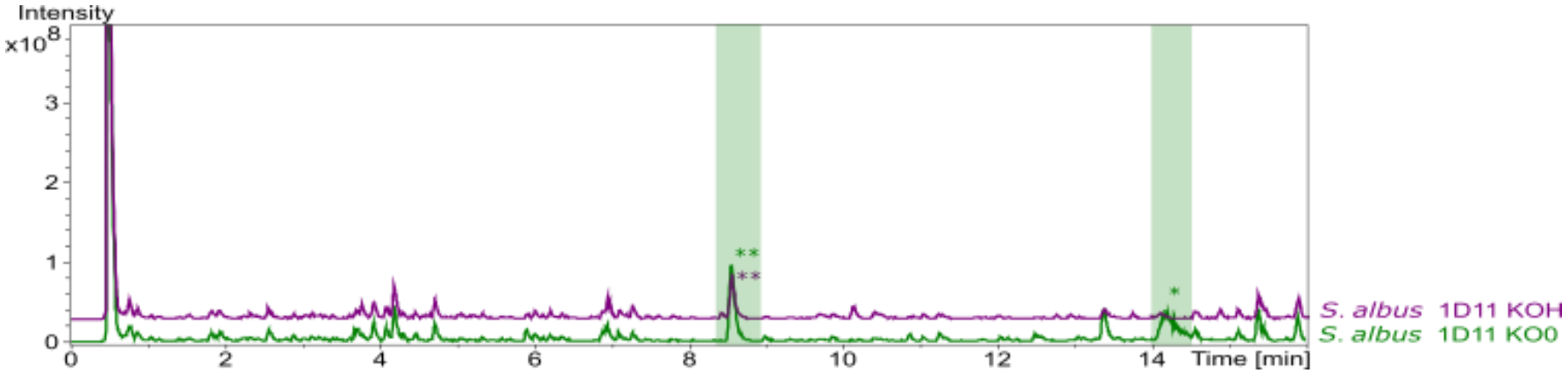

Figure 83. LC-MS chromatograms of butanol extract from *S. albus* 1D11 (green) and *S. albus* 1D11 KOH (purple) after cultivation for 7 days at 28°C and 180 rpm in 100 mL DNPM. Base peak chromatograms of *S. albus* 1D11 and S. albus 1D11 KOH. In green the oxanthromicin (39) peak is indicated by one asterisk (*) and *hemi*-oxanthromicin (40) by two asterisks (**).

OxaK

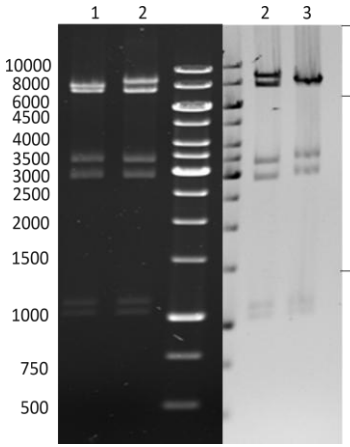

1 1D11 KO0	2 1D11 KOK+Hyg	3 1D11 KOK
7743	8163	7382
7382	7382	7056
3271	3271	3271
2847	2847	2847
1115	1115	1115
1033	1033	1033
76	76	76

Figure 84. Restriction mapping with *Kpn*I of generation of the cosmid 1D11 KOK.

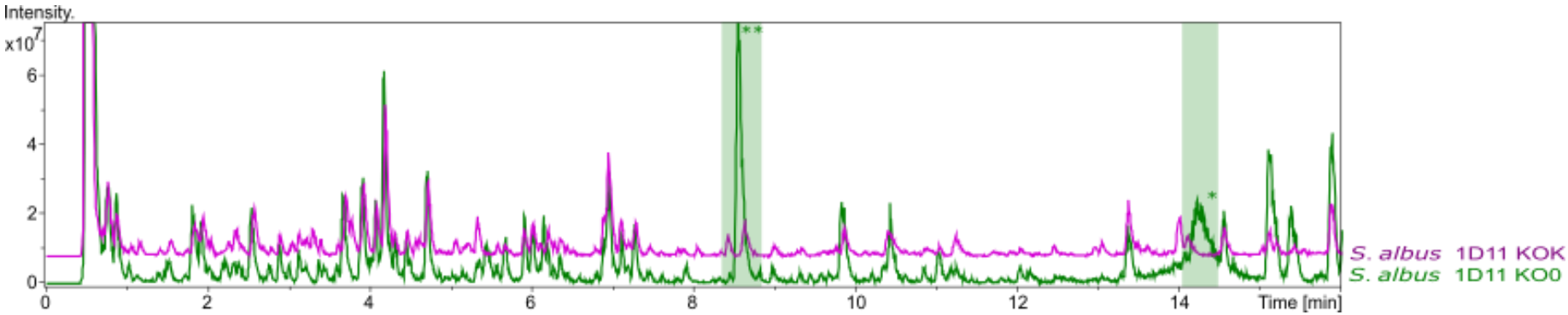

Figure 85. LC-MS base peak chromatograms of butanol extract from *S. albus* 1D11 (green) and *S. albus* 1D11 KOK (purple) after cultivation for 7 days at 28°C and 180 rpm in 100 mL DNPM. In green the oxanthromicin (39) peak is indicated by one asterisk (*) and *hemi*-oxanthromicin (40) asterisks (**).

References

1. Cragg, G.M. and D.J. Newman, *Biodiversity: A continuing source of novel drug leads.* Pure and applied chemistry, 2005. **77**(1): p. 7-24.
2. Dias, D.A., S. Urban, and U. Roessner, *A historical overview of natural products in drug discovery.* Metabolites, 2012. **2**(2): p. 303-336.
3. Zhan, J., *Biosynthesis of bacterial aromatic polyketides.* Current topics in medicinal chemistry, 2009. **9**(17): p. 1598-1610.
4. Berdy, J., *Bioactive microbial metabolites.* The Journal of antibiotics, 2005. **58**(1): p. 1-26.
5. Staunton, J. and K.J. Weissman, *Polyketide biosynthesis: a millennium review.* Natural product reports, 2001. **18**(4): p. 380-416.
6. Hertweck, C., et al., *Type II polyketide synthases: gaining a deeper insight into enzymatic teamwork.* Natural product reports, 2007. **24**(1): p. 162-190.
7. Finking, R. and M.A. Marahiel, *Biosynthesis of nonribosomal peptides.* Annu. Rev. Microbiol., 2004. **58**: p. 453-488.
8. Genilloud, O., *Actinomycetes: still a source of novel antibiotics.* Natural product reports, 2017. **34**(10): p. 1203-1232.
9. Aslam, B., et al., *Antibiotic resistance: a rundown of a global crisis.* Infection and drug resistance, 2018: p. 1645-1658.
10. Nathan, C. and O. Cars, *Antibiotic resistance—problems, progress, and prospects.* New England Journal of Medicine, 2014. **371**(19): p. 1761-1763.
11. Bode, H.B., et al., *Big effects from small changes: possible ways to explore nature's chemical diversity.* ChemBioChem, 2002. **3**(7): p. 619-627.
12. Fuchser, J. and A. Zeeck, *Secondary Metabolites by Chemical Screening, 34.–Aspinolides and Aspinonene/Aspyrone Co-Metabolites, New Pentaketides Produced by Aspergillus ochraceus.* Liebigs Annalen, 1997. **1997**(1): p. 87-95.
13. Myronovskyi, M. and A. Luzhetskyy, *Heterologous production of small molecules in the optimized Streptomyces hosts.* Natural product reports, 2019. **36**(9): p. 1281-1294.
14. Baltz, R.H., *Streptomyces and Saccharopolyspora hosts for heterologous expression of secondary metabolite gene clusters.* Journal of Industrial Microbiology and Biotechnology, 2010. **37**(8): p. 759-772.
15. Galm, U. and B. Shen, *Expression of biosynthetic gene clusters in heterologous hosts for natural product production and combinatorial biosynthesis.* Expert opinion on drug discovery, 2006. **1**(5): p. 409-437.
16. Myronovskyi, M., et al., *Generation of a cluster-free Streptomyces albus chassis strains for improved heterologous expression of secondary metabolite clusters.* Metabolic engineering, 2018. **49**: p. 316-324.
17. Ahmed, Y., et al., *Engineering of Streptomyces lividans for heterologous expression of secondary metabolite gene clusters.* Microbial cell factories, 2020. **19**: p. 1-16.
18. Zhou, M., et al., *Sequential deletion of all the polyketide synthase and nonribosomal peptide synthetase biosynthetic gene clusters and a 900-kb subtelomeric sequence of the linear chromosome of Streptomyces coelicolor.* FEMS microbiology letters, 2012. **333**(2): p. 169-179.
19. Bentley, S.D., et al., *Complete genome sequence of the model actinomycete Streptomyces coelicolor A3 (2).* nature, 2002. **417**(6885): p. 141-147.
20. Kang, H.-S. and E.-S. Kim, *Recent advances in heterologous expression of natural product biosynthetic gene clusters in Streptomyces hosts.* Current Opinion in Biotechnology, 2021. **69**: p. 118-127.
21. Chater, K.F. and L. Wilde, *Restriction of a bacteriophage of Streptomyces albus G involving endonuclease SalI.* Journal of bacteriology, 1976. **128**(2): p. 644-650.

22. Zaburannyi, N., et al., *Insights into naturally minimised Streptomyces albus J1074 genome.* BMC genomics, 2014. **15**: p. 1-11.
23. Lombó, F., et al., *Deciphering the biosynthesis pathway of the antitumor thiocoraline from a marine actinomycete and its expression in two Streptomyces species.* ChemBioChem, 2006. **7**(2): p. 366-376.
24. Schwarzer, D., R. Finking, and M.A. Marahiel, *Nonribosomal peptides: from genes to products.* Natural product reports, 2003. **20**(3): p. 275-287.
25. Strieker, M., A. Tanović, and M.A. Marahiel, *Nonribosomal peptide synthetases: structures and dynamics.* Current opinion in structural biology, 2010. **20**(2): p. 234-240.
26. Marahiel, M.A., *A structural model for multimodular NRPS assembly lines.* Natural Product Reports, 2016. **33**(2): p. 136-140.
27. Süssmuth, R.D. and A. Mainz, *Nonribosomal peptide synthesis—principles and prospects.* Angewandte Chemie International Edition, 2017. **56**(14): p. 3770-3821.
28. Miller, B.R. and A.M. Gulick, *Structural biology of nonribosomal peptide synthetases.* Nonribosomal Peptide and Polyketide Biosynthesis: Methods and Protocols, 2016: p. 3-29.
29. Shen, B., *Polyketide biosynthesis beyond the type I, II and III polyketide synthase paradigms.* Current opinion in chemical biology, 2003. **7**(2): p. 285-295.
30. Risdian, C., T. Mozef, and J. Wink, *Biosynthesis of polyketides in Streptomyces.* Microorganisms, 2019. **7**(5): p. 124.
31. Austin, M.B. and J.P. Noel, *The chalcone synthase superfamily of type III polyketide synthases.* Natural product reports, 2003. **20**(1): p. 79-110.
32. Shimizu, Y., H. Ogata, and S. Goto, *Type III polyketide synthases: functional classification and phylogenomics.* ChemBioChem, 2017. **18**(1): p. 50-65.
33. Hertweck, C., *The biosynthetic logic of polyketide diversity.* Angewandte Chemie International Edition, 2009. **48**(26): p. 4688-4716.
34. Hillenmeyer, M.E., et al., *Evolution of chemical diversity by coordinated gene swaps in type II polyketide gene clusters.* Proceedings of the National Academy of Sciences, 2015. **112**(45): p. 13952-13957.
35. Chen, S., C. Zhang, and L. Zhang, *Investigation of the molecular landscape of bacterial aromatic polyketides by global analysis of type II polyketide synthases.* Angewandte Chemie International Edition, 2022. **61**(24): p. e202202286.
36. McBride, C.M., E.L. Miller, and L.K. Charkoudian, *An updated catalogue of diverse type II polyketide synthase biosynthetic gene clusters captured from large-scale nucleotide databases.* Microbial Genomics, 2023. **9**(3).
37. Castaldo, G., et al., *Proposed arrangement of proteins forming a bacterial type II polyketide synthase.* Chemistry & biology, 2008. **15**(11): p. 1156-1165.
38. McDaniel, R., et al., *Engineered biosynthesis of novel polyketides.* Science, 1993. **262**(5139): p. 1546-1550.
39. Bräuer, A., et al., *Structural snapshots of the minimal PKS system responsible for octaketide biosynthesis.* Nature Chemistry, 2020. **12**(8): p. 755-763.
40. Ridley, C.P., H.Y. Lee, and C. Khosla, *Evolution of polyketide synthases in bacteria.* Proceedings of the National Academy of Sciences, 2008. **105**(12): p. 4595-4600.
41. Sayers, E.W., et al., *Database resources of the national center for biotechnology information.* Nucleic Acids Research, 2024. **52**(D1): p. D33-D43.
42. Sulpizio, A., et al., *Probing the structure and function of acyl carrier proteins to unlock the strategic redesign of type II polyketide biosynthetic pathways.* Journal of Biological Chemistry, 2021. **296**.
43. Lambalot, R.H. and C.T. Walsh, *Cloning, Overproduction, and Characterization of the Escherichia coli Holo-acyl Carrier Protein Synthase (∗).* Journal of Biological Chemistry, 1995. **270**(42): p. 24658-24661.

44. Pickens, L.B. and Y. Tang, *Oxytetracycline biosynthesis.* Journal of Biological Chemistry, 2010. **285**(36): p. 27509-27515.
45. Wang, J., et al., *Biosynthesis of aromatic polyketides in microorganisms using type II polyketide synthases.* Microbial cell factories, 2020. **19**: p. 1-11.
46. Schwarzer, P., et al., *Biosynthesis of rishirilide B.* Antibiotics, 2018. **7**(1): p. 20.
47. Waldman, A.J. and E.P. Balskus, *Lomaiviticin biosynthesis employs a new strategy for starter unit generation.* Organic letters, 2014. **16**(2): p. 640-643.
48. Tong, L., *Acetyl-coenzyme A carboxylase: crucial metabolic enzyme and attractive target for drug discovery.* Cellular and Molecular Life Sciences CMLS, 2005. **62**: p. 1784-1803.
49. Molnos, J., et al., *A continuous coupled enzyme assay for bacterial malonyl–CoA: acyl carrier protein transacylase (FabD).* Analytical biochemistry, 2003. **319**(1): p. 171-176.
50. Dreier, J. and C. Khosla, *Mechanistic analysis of a type II polyketide synthase. Role of conserved residues in the β-ketoacyl synthase− chain length factor heterodimer.* Biochemistry, 2000. **39**(8): p. 2088-2095.
51. Qian, Z., et al., *Discovery of the streptoketides by direct cloning and rapid heterologous expression of a cryptic PKS II gene cluster from Streptomyces sp. Tu 6314.* The Journal of organic chemistry, 2019. **85**(2): p. 664-673.
52. Deng, Z., et al., *An unusual type II polyketide synthase system involved in cinnamoyl lipid biosynthesis.* Angewandte Chemie, 2021. **133**(1): p. 155-160.
53. Zhang, J., et al., *Reconstitution of a highly reducing type II PKS system reveals 6π-electrocyclization is required for o-dialkylbenzene biosynthesis.* Journal of the American Chemical Society, 2021. **143**(7): p. 2962-2969.
54. Thong, W.L., et al., *Methylbenzene-containing polyketides from a Streptomyces that spontaneously acquired rifampicin resistance: structural elucidation and biosynthesis.* Journal of natural products, 2016. **79**(4): p. 857-864.
55. Hua, K., et al., *Offloading role of a discrete thioesterase in type II polyketide biosynthesis.* Mbio, 2020. **11**(5): p. 10.1128/mbio. 01334-20.
56. Tang, Y., A.T. Koppisch, and C. Khosla, *The acyltransferase homologue from the initiation module of the R1128 polyketide synthase is an acyl-ACP thioesterase that edits acetyl primer units.* Biochemistry, 2004. **43**(29): p. 9546-9555.
57. Kalaitzis, J.A., et al., *Policing starter unit selection of the enterocin type II polyketide synthase by the type II thioesterase EncL.* Bioorganic & medicinal chemistry, 2011. **19**(22): p. 6633-6638.
58. Taguchi, T., et al., *Bifunctionality of ActIV as a Cyclase-Thioesterase Revealed by in Vitro Reconstitution of Actinorhodin Biosynthesis in Streptomyces coelicolor A3 (2).* ChemBioChem, 2017. **18**(3): p. 316-323.
59. Das, A. and C. Khosla, *Biosynthesis of aromatic polyketides in bacteria.* Accounts of chemical research, 2009. **42**(5): p. 631-639.
60. Rao, S.T. and M.G. Rossmann, *Comparison of super-secondary structures in proteins.* Journal of molecular biology, 1973. **76**(2): p. 241-256.
61. Hanukoglu, I., *Proteopedia: Rossmann fold: A beta-alpha-beta fold at dinucleotide binding sites.* Biochemistry and Molecular Biology Education, 2015. **43**(3): p. 206-209.
62. Javidpour, P., et al., *Structural and biochemical studies of the hedamycin type II polyketide ketoreductase (Hed KR): molecular basis of stereo-and regiospecificities.* Biochemistry, 2011. **50**(34): p. 7426-7439.
63. Korman, T.P., et al., *Inhibition kinetics and emodin cocrystal structure of a type II polyketide ketoreductase.* Biochemistry, 2008. **47**(7): p. 1837-1847.
64. Lackner, G., et al., *Biosynthesis of pentangular polyphenols: deductions from the benastatin and griseorhodin pathways.* Journal of the American Chemical Society, 2007. **129**(30): p. 9306-9312.

65. Zhao, S., et al., *Molecular basis for polyketide ketoreductase–substrate interactions.* International journal of molecular sciences, 2020. **21**(20): p. 7562.
66. Husain, S.M., et al., *Insights into the role of ketoreductases in the biosynthesis of partially reduced bacterial aromatic polyketides.* ChemBioChem, 2020. **21**(6): p. 780-784.
67. Caldara-Festin, G., et al., *Structural and functional analysis of two di-domain aromatase/cyclases from type II polyketide synthases.* Proceedings of the National Academy of Sciences, 2015. **112**(50): p. E6844-E6851.
68. Zhang, M., et al., *Biosynthesis of trioxacarcin revealing a different starter unit and complex tailoring steps for type II polyketide synthase.* Chemical science, 2015. **6**(6): p. 3440-3447.
69. Ichinose, K., et al., *The granaticin biosynthetic gene cluster of Streptomyces violaceoruber Tü22: sequence analysis and expression in a heterologous host.* Chemistry & biology, 1998. **5**(11): p. 647-659.
70. Xu, R., et al., *Six Sets of Aromatic Polyketides Differing in Size and Shape Derive from a Single Biosynthetic Gene Cluster.* Journal of Natural Products, 2023.
71. Ishida, K., K. Fritzsche, and C. Hertweck, *Geminal tandem C-methylation in the discoid resistomycin pathway.* Journal of the American Chemical Society, 2007. **129**(42): p. 12648-12649.
72. Rix, U., et al., *Modification of post-PKS tailoring steps through combinatorial biosynthesis.* Natural product reports, 2002. **19**(5): p. 542-580.
73. Beinker, P., et al., *Crystal structures of SnoaL2 and AclR: two putative hydroxylases in the biosynthesis of aromatic polyketide antibiotics.* Journal of molecular biology, 2006. **359**(3): p. 728-740.
74. Shen, B. and C.R. Hutchinson, *Tetracenomycin F1 monooxygenase: oxidation of a naphthacenone to a naphthacenequinone in the biosynthesis of tetracenomycin C in Streptomyces glaucescens.* Biochemistry, 1993. **32**(26): p. 6656-6663.
75. Fetzner, S., *Oxygenases without requirement for cofactors or metal ions.* Applied Microbiology and Biotechnology, 2002. **60**: p. 243-257.
76. Fetzner, S. and R.A. Steiner, *Cofactor-independent oxidases and oxygenases.* Applied Microbiology and Biotechnology, 2010. **86**: p. 791-804.
77. Kamerbeek, N.M., et al., *Baeyer–Villiger monooxygenases, an emerging family of flavin-dependent biocatalysts.* Advanced Synthesis & Catalysis, 2003. **345**(6-7): p. 667-678.
78. Fürst, M.J., et al., *Baeyer–Villiger monooxygenases: tunable oxidative biocatalysts.* ACS Catalysis, 2019. **9**(12): p. 11207-11241.
79. Urlacher, V.B. and M. Girhard, *Cytochrome P450 monooxygenases: an update on perspectives for synthetic application.* Trends in biotechnology, 2012. **30**(1): p. 26-36.
80. Fessner, N.D., *P450 monooxygenases enable rapid late-stage diversification of natural products via C− H bond activation.* ChemCatChem, 2019. **11**(9): p. 2226-2242.
81. Präg, A., et al., *Regio-and stereoselective intermolecular oxidative phenol coupling in Streptomyces.* Journal of the American Chemical Society, 2014. **136**(17): p. 6195-6198.
82. Ji, X., et al., *Elucidation of the tailoring steps in Julichrome biosynthesis by marine gastropod mollusk-associated Streptomyces sampsonii SCSIO 054.* Organic Letters, 2020. **22**(17): p. 6927-6931.
83. Tian, Q., et al., *Insights into the Multisymmetric Tailoring of Julichrome Compounds by the Oxygenases JuiN and JuiO: Enzymatic Processing around the Biaryl C–C Axis.* ACS Catalysis, 2023. **13**: p. 7544-7556.
84. Agarwal, V., et al., *Enzymatic halogenation and dehalogenation reactions: pervasive and mechanistically diverse.* Chemical reviews, 2017. **117**(8): p. 5619-5674.
85. Dorrestein, P.C., et al., *Dichlorination of a pyrrolyl-S-carrier protein by FADH2-dependent halogenase PltA during pyoluteorin biosynthesis.* Proceedings of the National Academy of Sciences, 2005. **102**(39): p. 13843-13848.

86. Neumann, C.S., D.G. Fujimori, and C.T. Walsh, *Halogenation strategies in natural product biosynthesis.* Chemistry & biology, 2008. **15**(2): p. 99-109.
87. Gao, P. and Y. Huang, *Detection, distribution, and organohalogen compound discovery implications of the reduced flavin adenine dinucleotide-dependent halogenase gene in major filamentous actinomycete taxonomic groups.* Applied and environmental microbiology, 2009. **75**(14): p. 4813-4820.
88. Kong, L., et al., *Flavin adenine dinucleotide-dependent halogenase XanH and engineering of multifunctional fusion halogenases.* Applied and Environmental Microbiology, 2020. **86**(18): p. e01225-20.
89. Buedenbender, S., et al., *Structure and action of the myxobacterial chondrochloren halogenase CndH: a new variant of FAD-dependent halogenases.* Journal of molecular biology, 2009. **385**(2): p. 520-530.
90. Yeh, E., et al., *Chlorination by a long-lived intermediate in the mechanism of flavin-dependent halogenases.* Biochemistry, 2007. **46**(5): p. 1284-1292.
91. Dong, C., et al., *Tryptophan 7-halogenase (PrnA) structure suggests a mechanism for regioselective chlorination.* Science, 2005. **309**(5744): p. 2216-2219.
92. Kong, L., et al., *A multifunctional monooxygenase XanO4 catalyzes xanthone formation in xantholipin biosynthesis via a cryptic demethoxylation.* Cell Chemical Biology, 2016. **23**(4): p. 508-516.
93. Zhang, W., et al., *Unveiling the post-PKS redox tailoring steps in biosynthesis of the type II polyketide antitumor antibiotic xantholipin.* Chemistry & biology, 2012. **19**(3): p. 422-432.
94. Hu, Y. and S. Walker, *Remarkable structural similarities between diverse glycosyltransferases.* Chemistry & biology, 2002. **9**(12): p. 1287-1296.
95. Gutmann, A. and B. Nidetzky, *Switching between O-and C-glycosyltransferase through exchange of active-site motifs.* Angewandte Chemie International Edition, 2012. **51**(51): p. 12879-12883.
96. Cai, X., et al., *Identification of a C-glycosyltransferase involved in medermycin biosynthesis.* ACS Chemical Biology, 2021. **16**(6): p. 1059-1069.
97. Bililign, T., et al., *The hedamycin locus implicates a novel aromatic PKS priming mechanism.* Chemistry & biology, 2004. **11**(7): p. 959-969.
98. Thibodeaux, C.J., C.E. Melançon, and H.-w. Liu, *Unusual sugar biosynthesis and natural product glycodiversification.* Nature, 2007. **446**(7139): p. 1008-1016.
99. Toral-Barza, L., et al., *Discovery of lactoquinomycin and related pyranonaphthoquinones as potent and allosteric inhibitors of AKT/PKB: mechanistic involvement of AKT catalytic activation loop cysteines.* Molecular cancer therapeutics, 2007. **6**(11): p. 3028-3038.
100. Gutacker, F., et al., *Identification and Characterization of a Novel N-and O-Glycosyltransferase from Saccharopolyspora erythraea.* Molecules, 2020. **25**(15): p. 3400.
101. Eida, A.A., et al., *Glycosylation of acyl carrier protein-bound polyketides during pactamycin biosynthesis.* Nature chemical biology, 2019. **15**(8): p. 795-802.
102. Mao, Y., M. Varoglu, and D.H. Sherman, *Molecular characterization and analysis of the biosynthetic gene cluster for the antitumor antibiotic mitomycin C from Streptomyces lavendulae NRRL 2564.* Chemistry & biology, 1999. **6**(4): p. 251-263.
103. Kudo, F., et al., *Cloning of the pactamycin biosynthetic gene cluster and characterization of a crucial glycosyltransferase prior to a unique cyclopentane ring formation.* The Journal of Antibiotics, 2007. **60**(8): p. 492-503.
104. Ito, T., et al., *Deciphering pactamycin biosynthesis and engineered production of new pactamycin analogues.* ChemBioChem, 2009. **10**(13): p. 2253-2265.
105. Shapiro, S.K., *Adenosylmethionine-homocysteine transmethylase.* Biochimica et Biophysica Acta, 1958. **29**(2): p. 405-409.

106. Liscombe, D.K., G.V. Louie, and J.P. Noel, *Architectures, mechanisms and molecular evolution of natural product methyltransferases.* Natural product reports, 2012. **29**(10): p. 1238-1250.
107. Miller, D.J., et al., *Crystal complexes of a predicted S-adenosylmethionine-dependent methyltransferase reveal a typical AdoMet binding domain and a substrate recognition domain.* Protein science, 2003. **12**(7): p. 1432-1442.
108. Louie, G.V., et al., *Structure-function analyses of a caffeic acid O-methyltransferase from perennial ryegrass reveal the molecular basis for substrate preference.* The Plant Cell, 2010. **22**(12): p. 4114-4127.
109. O'Hagan, D. and J.W. Schmidberger, *Enzymes that catalyse SN 2 reaction mechanisms.* Natural product reports, 2010. **27**(6): p. 900-918.
110. Grove, T.L., et al., *A radically different mechanism for S-adenosylmethionine–dependent methyltransferases.* Science, 2011. **332**(6029): p. 604-607.
111. Gummerlich, N., et al., *Targeted Genome Mining-From Compound Discovery to Biosynthetic Pathway Elucidation.* Microorganisms, 2020. **8**(12).
112. Matroodi, S., et al., *Genotyping-guided discovery of persiamycin A from sponge-associated halophilic Streptomonospora sp. PA3.* Frontiers in Microbiology, 2020. **11**: p. 1237.
113. Huang, R., et al., *Discovery and Biosynthesis of the Amodesmycins, Aromatic Polyketide-Siderophore Hybrid Conjugates.* Organic Letters, 2022. **24**(51): p. 9408-9412.
114. Brachmann, A.O., et al., *A type II polyketide synthase is responsible for anthraquinone biosynthesis in Photorhabdus luminescens.* ChemBioChem, 2007. **8**(14): p. 1721-1728.
115. Sandmann, A., et al., *A Type II Polyketide Synthase from the Gram-Negative Bacterium Stigmatella aurantiaca Is Involved in Aurachin Alkaloid Biosynthesis.* Angewandte Chemie International Edition, 2007. **46**(15): p. 2712-2716.
116. Panter, F., et al., *Self-resistance guided genome mining uncovers new topoisomerase inhibitors from myxobacteria.* Chemical science, 2018. **9**(21): p. 4898-4908.
117. Zhou, Q., et al., *Molecular mechanism of polyketide shortening in anthraquinone biosynthesis of Photorhabdus luminescens.* Chemical science, 2019. **10**(25): p. 6341-6349.
118. Huber, E.M., et al., *A set of closely related methyltransferases for site-specific tailoring of anthraquinone pigments.* Structure, 2023. **31**(5): p. 573-583. e5.
119. Feng, Z., *O-methyltransferases selectively modify anthraquinone natural products.* Structure, 2023. **31**(5): p. 507-508.
120. Cummings, M., et al., *Assembling a plug-and-play production line for combinatorial biosynthesis of aromatic polyketides in Escherichia coli.* PLoS biology, 2019. **17**(7): p. e3000347.
121. Dinis, P., et al., *Evolution-inspired engineering of anthracycline methyltransferases.* PNAS nexus, 2023. **2**(2): p. pgad009.
122. Grocholski, T., et al., *Divergent evolution of an atypical S-adenosyl-l-methionine–dependent monooxygenase involved in anthracycline biosynthesis.* Proceedings of the National Academy of Sciences, 2015. **112**(32): p. 9866-9871.
123. R. Tormo, J., et al., *A method for the selection of production media for actinomycete strains based on their metabolite HPLC profiles.* Journal of Industrial Microbiology and Biotechnology, 2003. **30**(10): p. 582-588.
124. Kieser, T., et al., *Practical streptomyces genetics*. Vol. 291. 2000: John Innes Foundation Norwich.
125. Hanahan, D., *Studies on transformation of Escherichia coli with plasmids.* Journal of molecular biology, 1983. **166**(4): p. 557-580.
126. Green, M.R. and J. Sambrook, *Molecular cloning.* A Laboratory Manual 4th, 2012.
127. Grant, S.G., et al., *Differential plasmid rescue from transgenic mouse DNAs into Escherichia coli methylation-restriction mutants.* Proceedings of the National Academy of Sciences, 1990. **87**(12): p. 4645-4649.

128. Flett F, M.V., and Smith CP, *High efficiency intergeneric conjugal transfer of plasmid DNA from Escherichia coli to methyl DNA-restricting streptomycetes.* FEMS Microbiol. Lett, 1997. **155**: p. 223-229.
129. Fu, J., et al., *Full-length RecE enhances linear-linear homologous recombination and facilitates direct cloning for bioprospecting.* Nature biotechnology, 2012. **30**(5): p. 440-446.
130. Rebets, Y., et al., *Complete genome sequence of producer of the glycopeptide antibiotic Aculeximycin Kutzneria albida DSM 43870 T, a representative of minor genus of Pseudonocardiaceae.* Bmc Genomics, 2014. **15**: p. 1-15.
131. Paulus, C., J. Zapp, and A. Luzhetskyy, *New Scabimycins A-C Isolated from Streptomyces acidiscabies (Lu19992).* Molecules, 2021. **26**(19).
132. Blin, K., et al., *antiSMASH 7.0: New and improved predictions for detection, regulation, chemical structures and visualisation.* Nucleic acids research, 2023: p. gkad344.
133. Altschul, S.F., et al., *Protein database searches using compositionally adjusted substitution matrices.* The FEBS journal, 2005. **272**(20): p. 5101-5109.
134. Kearse, M., et al., *Geneious Basic: an integrated and extendable desktop software platform for the organization and analysis of sequence data.* Bioinformatics, 2012. **28**(12): p. 1647-1649.
135. Myronovskyi, M., et al., *Generation of new compounds through unbalanced transcription of landomycin A cluster.* Applied microbiology and biotechnology, 2016. **100**: p. 9175-9186.
136. Yanisch-Perron, C., J. Vieira, and J. Messing, *Improved M13 phage cloning vectors and host strains: nucleotide sequences of the M13mpl8 and pUC19 vectors.* Gene, 1985. **33**(1): p. 103-119.
137. Bierman, M., et al., *Plasmid cloning vectors for the conjugal transfer of DNA from Escherichia coli to Streptomyces spp.* Gene, 1992. **116**(1): p. 43-49.
138. Paulus, C., et al., *Miramides A–D: Identification of Detoxin-like Depsipeptides after Heterologous Expression of a Hybrid NRPS-PKS Gene Cluster from Streptomyces mirabilis Lu17588.* Microorganisms, 2022. **10**(9): p. 1752.
139. Gregory, M.A., R. Till, and M.C. Smith, *Integration site for Streptomyces phage φBT1 and development of site-specific integrating vectors.* Journal of bacteriology, 2003. **185**(17): p. 5320-5323.
140. Shuai, H., *Discovery of natural products through heterologous expression of biosynthetic gene clusters in Streptomyces albus.* 2020.
141. Zhang, Y., et al., *A new logic for DNA engineering using recombination in Escherichia coli.* Nature genetics, 1998. **20**(2): p. 123-128.
142. Muyrers, J.P., Y. Zhang, and A.F. Stewart, *Techniques: recombinogenic engineering–new options for cloning and manipulating DNA.* Trends in biochemical sciences, 2001. **26**(5): p. 325-331.
143. Muyrers, J.P., et al., *ET recombination: DNA engineering using homologous recombination in E. coli.* Bacterial Artificial Chromosomes: Volume 2 Functional Studies, 2004: p. 107-121.
144. Kaster, K.R., et al., *Analysis of a bacterial hygromycin B resistance gene by transcriptional and translational fusions and by DNA sequencing.* Nucleic acids research, 1983. **11**(19): p. 6895-6911.
145. Plttengbr, R., et al., *Hygromycin. I. Preliminary studies on the production and biologic activity of a new antibiotic.* 1953.
146. Fincham, J., *Genetic complementation.* Science Progress (1933-), 1968: p. 165-177.
147. Furumai, T., H. OGAWA, and T. OKUDA, *Taxonomic study on Streptosporangium albidum nov. sp.* The Journal of Antibiotics, 1968. **21**(3): p. 179-181.
148. Kolling, D., *Natural Product Discovery in Actinobacteria through biosynthetic engineering*, in *Pharmazeutische Biotechnologie*. 2021, Universitaet des Saarlandes.

149. Kontou, E.E., et al., *Discovery and characterization of epemicins A and B, new 30-membered macrolides from Kutzneria sp. CA-103260.* ACS chemical biology, 2021. **16**(8): p. 1456-1468.
150. Ullrich, G., *Activation of cryptic biosynthetic gene clusters in actinobacteria*, in *Pharmazeutische Biotechnologie*. 2020, Universitaet des Saarlandes.
151. Oberhäuser, P., et al., *Algremapamycine, a non-ribosomally synthesized cyclopeptide from the non-categorized Streptomyces LV1-209GEK biosynthesized by two interfering NRPS gene cluster*. 2024: unpublished.
152. Mitousis, L., Y. Thoma, and E.M. Musiol-Kroll, *An update on molecular tools for genetic engineering of actinomycetes—the source of important antibiotics and other valuable compounds.* Antibiotics, 2020. **9**(8): p. 494.
153. Seghezzi, N., et al., *The construction of a library of synthetic promoters revealed some specific features of strong Streptomyces promoters.* Applied microbiology and biotechnology, 2011. **90**: p. 615-623.
154. Lambert, D. and R. Loria, *Streptomyces acidiscabies sp. nov.* International Journal of Systematic and Evolutionary Microbiology, 1989. **39**(4): p. 393-396.
155. Loria, R., J. Kers, and M. Joshi, *Evolution of plant pathogenicity in Streptomyces.* Annu. Rev. Phytopathol., 2006. **44**: p. 469-487.
156. Huguet-Tapia, J.C. and R. Loria, *Draft genome sequence of Streptomyces acidiscabies 84-104, an emergent plant pathogen*. 2012, Am Soc Microbiol.
157. Patel, M., et al., *Oxanthromicin, a novel antibiotic from Actinomadura.* The Journal of Antibiotics, 1984. **37**(4): p. 413-415.
158. Wright, J.K., et al., *Structure of oxanthromicin (antibiotic 16–550), a novel dimeric anthrone peroxide.* Journal of the Chemical Society, Chemical Communications, 1984(7): p. 473-474.
159. Puar, M., et al., *Biosynthesis of oxanthromicin.* The Journal of Antibiotics, 1985. **38**(7): p. 952-954.
160. Rebets, Y., et al., *Characterization of sigma factor genes in Streptomyces lividans TK24 using a genomic library-based approach for multiple gene deletions.* Frontiers in microbiology, 2018. **9**: p. 3033.
161. Tietze, L.F., K.M. Gericke, and I. Schuberth, *Synthesis of highly functionalized anthraquinones and evaluation of their antitumor activity*. 2007, Wiley Online Library.
162. Probst, K., *Untersuchungen zur Biosynthese von Didesmethylmensacarcin*. 2011, Dissertation, Albert-Ludwigs-Universität Freiburg, 2011.
163. Maier, S., et al., *Insights into the bioactivity of mensacarcin and epoxide formation by MsnO8.* ChemBioChem, 2014. **15**(5): p. 749-756.
164. Yan, X., et al., *Cloning and heterologous expression of three type II PKS gene clusters from Streptomyces bottropensis.* ChemBioChem, 2012. **13**(2): p. 224-230.
165. Maier, S., et al., *Functional Characterization of Different ORFs Including Luciferase-Like Monooxygenase Genes from the Mensacarcin Gene Cluster.* ChemBioChem, 2015. **16**(8): p. 1175-1182.
166. Jansson, A., et al., *Crystallization and preliminary X-ray diffraction studies of aclacinomycin-10-methyl esterase and aclacinomycin-10-hydroxylase from Streptomyces purpurascens.* Acta Crystallographica Section D: Biological Crystallography, 2003. **59**(9): p. 1637-1639.
167. Ding, T., et al., *The secondary metabolites of rare actinomycetes: chemistry and bioactivity.* RSC advances, 2019. **9**(38): p. 21964-21988.
168. Salim, A.A., et al., *Rare Streptomyces sp. polyketides as modulators of K-Ras localisation.* Organic & biomolecular chemistry, 2014. **12**(27): p. 4872-4878.
169. Li, H.-M., et al., *A new dimeric neolignan from Magnolia grandiflora L. seeds.* Archives of pharmacal research, 2015. **38**: p. 1066-1071.

170. Hallam, S.E., F. Malpartida, and D.A. Hopwood, *Nucleotide sequence, transcription and deduced function of a gene involved in polyketide antibiotic synthesis in Streptomyces coelicolor.* Gene, 1988. **74**(2): p. 305-320.
171. Fernández-Moreno, M.A., et al., *Nucleotide sequence and deduced functions of a set of cotranscribed genes of Streptomyces coelicolor A3 (2) including the polyketide synthase for the antibiotic actinorhodin.* Journal of Biological Chemistry, 1992. **267**(27): p. 19278-19290.
172. Xie, S. and L. Zhang, *Type II Polyketide Synthases: A Bioinformatics-Driven Approach.* ChemBioChem, 2023. **24**(9): p. e202200775.
173. Sherman, D.H., et al., *Molecular genetic analysis reveals a putative bifunctional polyketide cyclase/dehydrase gene from Streptomycea coelicolor and Streptomyces violoceoruber, and a cyclase/O-methyltransferase from Streptomyces glaucescens.* Tetrahedron, 1991. **47**(31): p. 6029-6043.
174. Metsä-Ketelä, M., et al., *Biosynthesis of pyranonaphthoquinone polyketides reveals diverse strategies for enzymatic carbon–carbon bond formation.* Current Opinion in Chemical Biology, 2013. **17**(4): p. 562-570.
175. Valentic, T.R., et al., *Comprehensive analysis of a novel ketoreductase for pentangular polyphenol biosynthesis.* ACS Chemical Biology, 2016. **11**(12): p. 3421-3430.
176. August, P.R., M.C. Flickinger, and D.H. Sherman, *Cloning and analysis of a locus (mcr) involved in mitomycin C resistance in Streptomyces lavendulae.* Journal of bacteriology, 1994. **176**(14): p. 4448-4454.
177. Penketh, P.G., et al., *Inhibition of DNA cross-linking by mitomycin C by peroxidase-mediated oxidation of mitomycin C hydroquinone.* Journal of Biological Chemistry, 2001. **276**(37): p. 34445-34452.
178. Becker, H.D. and D. Sanchez, *Acid-catalyzed dimerization of 10-methyleneanthrone. Synthesis of spiro-substituted benz [de] anthracenes.* The Journal of Organic Chemistry, 1979. **44**(11): p. 1787-1792.
179. Romero-Hernández, L.L., et al., *Syntheses and medicinal chemistry of spiro heterocyclic steroids.* Beilstein Journal of Organic Chemistry, 2024. **20**(1): p. 1713-1745.
180. Zhang, W., et al., *Engineered biosynthesis of a novel amidated polyketide, using the malonamyl-specific initiation module from the oxytetracycline polyketide synthase.* Applied and environmental microbiology, 2006. **72**(4): p. 2573-2580.
181. Wang, P., et al., *Heterologous expression and manipulation of three tetracycline biosynthetic pathways.* Angewandte Chemie (International ed. in English), 2012. **51**(44): p. 11136.
182. Pickens, L.B., et al., *Biochemical analysis of the biosynthetic pathway of an anticancer tetracycline SF2575.* Journal of the American Chemical Society, 2009. **131**(48): p. 17677-17689.
183. Blanco, G., et al., *Deciphering the biosynthetic origin of the aglycone of the aureolic acid group of anti-tumor agents.* Chemistry & Biology, 1996. **3**(3): p. 193-196.
184. Rohr, J., C. Méndez, and J.A. Salas, *The biosynthesis of aureolic acid group antibiotics.* Bioorganic Chemistry, 1999. **27**(1): p. 41-54.
185. Madduri, K., et al., *Cloning and sequencing of a gene encoding carminomycin 4-O-methyltransferase from Streptomyces peucetius and its expression in Escherichia coli.* Journal of bacteriology, 1993. **175**(12): p. 3900-3904.
186. Grocholski, T.e., et al., *Evolutionary trajectories for the functional diversification of anthracycline methyltransferases.* ACS chemical biology, 2019. **14**(5): p. 850-856.
187. Quimby, B.B., et al., *Functional Analysis of the Hydrophobic Patch on Nuclear Transport Factor 2 Involved in Interactions with the Nuclear Porein Vivo.* Journal of Biological Chemistry, 2001. **276**(42): p. 38820-38829.

188. Stewart, M., H.M. Kent, and A.J. McCoy, *Structural basis for molecular recognition between nuclear transport factor 2 (NTF2) and the GDP-bound form of the Ras-family GTPase Ran.* Journal of molecular biology, 1998. **277**(3): p. 635-646.
189. Eberhardt, R.Y., et al., *Filling out the structural map of the NTF2-like superfamily.* Bmc Bioinformatics, 2013. **14**: p. 1-11.
190. Huang, T., et al., *Crystal structure of SgcJ, an NTF2-like superfamily protein involved in biosynthesis of the nine-membered enediyne antitumor antibiotic C-1027.* The Journal of antibiotics, 2016. **69**(10): p. 731-740.
191. Fernández-Moreno, M.A., et al., *The act cluster contains regulatory and antibiotic export genes, direct targets for translational control by the bldA tRNA gene of Streptomyces.* Cell, 1991. **66**(4): p. 769-780.
192. Stutzman-Engwall, K.J., S. Otten, and C.R. Hutchinson, *Regulation of secondary metabolism in Streptomyces spp. and overproduction of daunorubicin in Streptomyces peucetius.* Journal of bacteriology, 1992. **174**(1): p. 144-154.
193. Lapaz, M.I., et al., *Isolation and structural characterization of a non-diketopiperazine phytotoxin from a potato pathogenic Streptomyces strain.* Natural product research, 2019. **33**(20): p. 2951-2957.